

**HALDANE PHASE IN THE
BOND-ALTERNATING SPIN-1/2 XXZ
CHAIN: DMRG AND FERMIONIZATION
STUDIES**

A THESIS SUBMITTED TO
THE GRADUATE SCHOOL OF ENGINEERING AND SCIENCE
OF BILKENT UNIVERSITY
IN PARTIAL FULFILLMENT OF THE REQUIREMENTS FOR
THE DEGREE OF
MASTER OF SCIENCE
IN
PHYSICS

By
Murod Bahovadinov
December 2018

Haldane phase in the bond-alternating spin-1/2 XXZ chain: DMRG
and fermionization studies

By Murod Bahovadinov

December 2018

We certify that we have read this thesis and that in our opinion it is fully adequate,
in scope and in quality, as a thesis for the degree of Master of Science.

Prof. Dr. Oğuz Gülseren(Advisor)

Prof.Dr. Bilal Tanatar

Prof.Dr. Sadi Turgut

Approved for the Graduate School of Engineering and Science:

Ezhan Karaşan
Director of the Graduate School

ABSTRACT

HALDANE PHASE IN THE BOND-ALTERNATING SPIN-1/2 XXZ CHAIN: DMRG AND FERMIONIZATION STUDIES

Murod Bahovadinov

M.S. in Physics

Advisor: Prof. Dr. Oğuz Gülseren

December 2018

In this thesis, the subject of study is the Haldane phase in bond - alternating XXZ chain with $S = \frac{1}{2}$. We firstly mapped our model to the fermionic chain by the use of standard Jordan-Wigner Transformation, which leads to the famous interacting spinless Su-Schrieffer-Heeger (SSH) fermionic model with modifications. Firstly, we studied trivial quantum phase transition (QPT) under the magnetic field in exactly soluble non-interacting limit, which corresponds to the bond-alternating XX chain . Excitation spectrum, magnetization, magnetic susceptibility are used to characterize QPT and compared with the numerical results. Correlation functions for all components of spins are calculated exactly.

Secondly, we studied symmetry - protected topological phase transition in the given non-interacting SSH model and characterized it by calculating topological winding number. Fermionized string order parameter as a function of spin couplings is obtained and the Haldane phase diagram in the XX limit is confirmed. The correspondence of the Haldane phase in the spin chain in XX limit and topological insulating phase of fermionic non-interacting SSH model is shown. Finally, by the use of entanglement spectrum as an order parameter, we numerically obtained Haldane phase diagram for XXZ model with bond-alternation.

For numerical investigation, we used density matrix renormalization group theory in matrix product states formulation (MPS-DMRG) for a system with open boundary conditions (OBC) .

Keywords: Quantum phase transitions, Density Matrix Renormalization Group theory, Matrix Product States, bond-alternating XXZ chain, Haldane phases, SSH model, String order parameter .

ÖZET

HALDANE FAZINDA BAĞ DEĞİŞTİREN SPIN-1/2 XXZ ZİNCİRİ: DMRG VE FERMIYONLAŞTIRMA ÇALIŞMASI

Murod Bahovadinov

Fizik, Yüksek Lisans

Tez Danışmanı: Prof. Dr. Oğuz Gülseren

Aralık 2018

Haldane fazında bağ değiştiren spin-1/2 XXZ zincirleri konusu işlenmiştir. Öncelikle modelimizi standart Jordan-Wigner Dönüşümü kullanarak fermiyonik zincire dönüştürdük; bu dönüşüm bize modifiye edilmiş etkileşim halindeki spinsiz Su-Schrieffer-Heeger (SSH) fermiyonik modeli verdi. İlk olarak bize bağ değiştiren XX zinciri veren manyetik alan altındaki basit kuantum faz geçişini (QPT) çözülebilir etkileşimsizlik limitinde çalıştık. QPTyi karakterize etmek için uyarılma tayfı, manyetizasyon, ve manyetik duyarlılık kullanıldı ve hesaplanmış sonuçlar ile karşılaştırıldı. Her spin bileşeni için korelasyon fonksiyonu tam olarak hesaplandı. Bundan sonra, bulunan etkileşimsiz SSH modeli üzerinde simetrik olarak korunan topolojik faz geçişi çalışıldı ve topolojik sarma sayısı hesaplanarak tanımlandı. Spin eşleşme, Fermiyonlaşmış yay düzeni değişkenine bağlı bir fonksiyon olarak elde edildi ve XX limitindeki Haldane faz diyagramı onaylandı. Spin zincirinde XX limiti Haldane fazı ve etkileşimsiz Fermiyonik SSH topolojik yalıtkanlık fazı modelinin uyumluluğu gösterildi. Son olarak, dolaşıklık tayfını düzen değişkeni olarak kullanarak, hesaplamalı olarak bağ değişimli XXZ modeli için Haldane faz diyagramı elde edildi. Hesaplamalı çalışmada açık sınır koşullu sistemler için, matris çarpım evresi formüllendirmesindeki renormalizasyon yoğunluk matrisi grup teorisi (MPS-DMRG) kullanıldı.

Anahtar sözcükler: Kuantum faz geçişleri, DMRG, iDMRG, Matris çarpım Evresi, Bağ Değiştiren XXZ Zinciri, Haldane Fazları, SSH Modeli, Sicim Düzen Değişkenleri .

Dedicated to my parents,

=====

Modar-e hushnazaram, her nazaram hadyae tust,
Asar-e daaram agar, on asaram hadyae tust.

=====

Acknowledgement

Firstly, I would like to thank Prof. Oğuz Gülseren for provided resources to do research here in Bilkent and for his help during my studies.

Special thanks to my friend Dr. Firat Yilmaz for valuable discussions on the diverse topics of condensed matter physics.

I would also like to thank Prof. Ceyhun Bulutay and Prof. Cemal Yalabık for valuable delivered courses.

Secondly, I'm very lucky to make new friends like Jamoliddin Khanifaev, Ahmed Ouf, Muhamet Ibrahim, Mujahid Aliyu, M. Ali Saberi, Mustafa Kahraman, Umutcan Güler, Enes Aybar and others who made my social life in Bilkent more diverse and interesting .

Finally, I must express my very profound gratitude to my parents, sisters and my soulmate Saida for emotional support during my studies.

Murod Bahovadinov

Contents

1	Introduction	1
1.1	Introduction to the problem	1
1.2	Introduction to theoretical part of the thesis	4
1.2.1	Spontaneous Symmetry Breaking and Landau theory	4
1.2.2	Symmetry - protected topological states	6
1.2.3	Antiferromagnetic Heisenberg S=1 Chain	6
1.2.4	Order parameters to identify the Haldane phase	9
2	Density Matrix Renormalization Group Theory	11
2.1	Numerical Renormalization Group	12
2.2	Density Matrix Renormalization Group	14
2.2.1	Reduced density matrix	14
2.2.2	Singular Value Decomposition	17
2.2.3	Infinite-size DMRG algorithm	18

2.2.4	Finite-size DMRG algorithm	26
2.2.5	Measurement	29
3	Matrix Product States and Matrix Product Operators	31
3.1	Matrix Product States	32
3.1.1	Tensor networks notation	33
3.1.2	Tensor contraction	35
3.1.3	Tensor notations for MPS	35
3.2	Canonical MPS representations	36
3.2.1	Left-Canonical MPS	37
3.2.2	Right-Canonical MPS	38
3.2.3	Mixed-Canonical MPS	40
3.2.4	Calculation of overlaps and expectation values	41
3.3	Matrix Product Operators	43
3.3.1	Explicit form of MPO	44
3.4	Variational MPS DMRG	45
3.4.1	Variational MPS for XXX Heisenberg chain	51
3.5	Infinite-size MPS DMRG	52
4	Bond-Alternating Heisenberg Chain	59

4.1	Fermionization approach for quantum spin chains	59
4.1.1	Jordan-Wigner transformation	60
4.1.2	Jordan-Wigner Transformation for XXZ model	62
4.1.3	Jordan-Wigner Transformation of BAHC	63
4.2	Zero-temperature properties of XX BAHC model	67
4.2.1	Spectrum and ground state energy	68
4.2.2	Zero - temperature quantum phase transition under the magnetic field	71
4.2.3	Spin-Spin correlation functions	74
5	Haldane phase in the BAHC	83
5.1	Winding number	83
5.2	String order parameter	85
5.3	Edge states as an order parameter	89
5.4	Entanglement spectrum as an order parameter	90
5.5	When does the order parameters work?	91
5.6	Haldane phase of bond-alternating XXZ model	92
6	Conclusions	95
A	Szegö theorem	101

List of Figures

1.1	Gap closure in 1D Ising model	5
2.1	Numerical Renormalization Group algorithm	13
2.2	Bipartited Universe Block	15
2.3	White's Infinite-size DMRG algorithm	20
2.4	Ground state energy per site calculation for AFHC with S=1 . . .	26
2.5	Density matrix eigenvalues in descending order and truncation error $\epsilon_r = 1 - \sum_{\alpha} \omega_{\alpha}$ for $L = 124$	27
2.6	Finite - Size sweeping process	28
2.7	Comparison of bond strength expectation value for two DMRG algorithms	30
3.1	Diagrammatic tensor notations	33
3.2	Diagrammatic notations of operations with tensors	34
3.3	Diagrammatic notations for tensor contractions: (a) vector - vector multiplication; (b) vector - matrix multiplication (c) General tensor contraction	35

3.4	Diagrammatic notations of MPS $ \Psi\rangle$: (a) single-site tensor (b) MPS representation for $\langle\Psi $ and (c) for $ \Psi\rangle$	36
3.5	Diagrammatic representation of L-MPS generation process	37
3.6	Diagrammatic representation of R-MPS generation process	39
3.7	Diagrammatic M-MPS representation of a chain with $L = 6$ sites	40
3.8	Diagrammatic representation of overlap calculation	41
3.9	An example of MPS diagram for expectation value calculation	42
3.10	Diagrammatic representation of MPO	43
3.11	Diagrammatic representation of $\langle\psi \hat{O} \psi\rangle$	43
3.12	Righ-Block R_2 tensor for $L = 4$	46
3.13	Tensor contractions to obtain Hamiltonian	48
3.14	Variational MPS algorithm	50
3.15	Ground state energy per site calculated using VMPS algorithm	51
3.16	Ground state energy per site calculated using VMPS algorithm	52
3.17	General iDMRG procedure: L-W-W-R contractions	54
3.18	VMPS sweeping process	55
3.19	General iDMRG procedure: L-W-W-R contractions	56
3.20	VMPS calculation followed after iDMRG procedure	57
3.21	Two point correlators behavior in different XXZ chain phases	58

4.1	Bond-alternating Heisenberg chain	63
4.2	Energy spectrum of the model for $t' = 1$	69
4.3	Gap closure in QPT points	70
4.4	Energy per site calculated via i-DMRG for $N = 100$	71
4.5	Spectrum in F-AF limit under the magnetic field $B=[0,3]$ for $t =$ -4 and $t' = 2$	72
4.6	Magnetization curve for F-AF limit	74
4.7	Comparison of analytical and numerical i-DMRG results of $C_{1,n}^{xx(a,b)}$	80
4.8	Comparison of analytical and numerical i-DMRG results of $C_{1,n}^{zz(a,b)}$	81
4.9	The behavior of $C^{xx(a)}$ (a) and it's absolute value (b) for all $\frac{t}{t'}$ range	82
5.1	Graphical representation of winding number	84
5.2	Calculation of string order parameter	88
5.3	O^S in the trivial insulating phase $t/t' = 1.5$	88
5.4	O^S based phase diagram of non-interacting model	89
5.5	Topological Edge states in the Haldane phase	89
5.6	Entanglement Spectrum in the XX limit	91
5.7	Entanglement spectrum character for XXZ model	92
5.8	Local magnetization in two different phases of the model	93
5.9	Phase diagram of bond-alternating XXZ model	94

Chapter 1

Introduction

We start introductory section by formulating the problems to be solved in the thesis, discuss the actuality of these problems from an experimental and also theoretical point of views. Then we briefly introduce theoretical prerequisite necessary for this thesis.

1.1 Statement of the problem

The **object of the study** in the current thesis is bond-alternating Heisenberg XXZ chain (BAHC) with $S = -\frac{1}{2}$ defined as:

$$H = J \sum_{i=1}^N \vec{S}_{2i-1} \cdot \vec{S}_{2i}(\Delta) + J' \sum_{i=1}^N \vec{S}_{2i} \cdot \vec{S}_{2i+1}(\Delta') \quad (1.1)$$

where J, J' are coupling constant which can be ferromagnetic(< 0) or antiferromagnetic (> 0) types. Δ, Δ' are z -component anisotropies of the model , such that for $\Delta = \Delta' = 1$ one has bond-alternating XXX Heisenberg chain.

The **subject of the study** is analytical fermionization and numerical Density Matrix Renormalization group (DMRG) study approaches for zero- temperature properties and Haldane phase diagram of generalized model (1.1).

In the scope of the theses, we consider the following **tasks** :

I. Analytically:

- By the use of the Jordan - Wigner transformation, to obtain an analytically exact form of ground state energy, two-point correlators for all components of spins in the XX limit of the model (1.1).
- By fermionization of string order parameter and calculating topological winding number, to identify the Haldane phase and to get corresponding phase diagram in XX limit.

II. Numerically:

- By the use of matrix product states based DMRG to show the existence of edge states in corresponding Haldane phase of XX limit with open boundary conditions and to show the consistency of analytically obtained phase diagram by the calculating the bipartite entanglement spectrum.
- To obtain the Haldane phase diagram of XXZ model in antiferromagnetic couplings regime $J, J' > 0$.

Actuality of the study

Theoretical perspectives

Phase characterization in quantum many-body systems is one of the most important topics in condensed matter physics. While Landau-Ginsburg (LG) theory has been describing phase transition quite successfully, it is unable to identify topological orders of quantum systems due to the lack of local order parameter in these phases. Thus, one of the actual problems of modern condensed matter physics of one dimension is the classification of newly discovered symmetry-protected topological (SPT) phases. While the main features of SPT phases

are: the existence of finite-gap to the first excited state in a system with periodic boundary condition and the formation of localized edge states in a system with open boundary conditions, these are ambiguous order parameters to fully characterize these systems. Nevertheless, using group theoretical approaches classification of fermionic and bosonic systems in interacting and the non-interacting limit was performed [1, 2, 3].

When we are dealing with spin systems, the most famous SPT phase is the Haldane phase. This phase is the ground state phase of the Heisenberg model with $S = 1$. Although the gapped nature of the ground state and the existence of edge states were predicted long time ago [4, 5, 6], the full understanding of the phase emergence came much later [7]. For a long time, the only condition for the existence of the Haldane phase in spin systems was a non-zero value of non-local string order parameter (SOP). In this respect, in early 1990's the Haldane phase was detected in modified Heisenberg spin chains with $S = 1$ and Heisenberg ladders with $S = \frac{1}{2}$ both numerically and analytically [8, 9]. In particular, the Haldane phase of bond-alternating model (1.1) was also studied numerically using SOP via exact diagonalization method [10, 11].

While nontrivial topological phases like Haldane phase were under study using SOP in spin systems, in fermionic and bosonic systems advanced and versatile tools like Berry phase has been used, so the question about a generalization of fermionic order parameters for spins has arisen. Hastings et al. [12] has introduced local spin twist as a generic parameter of Berry phase for gapped spin systems, which has been used extensively [13]. Rosch and Anfuso [14] has used reconstructed SOP for identification of topological phase in band insulators. In this thesis, we obtained a fermionic version of SOP which can be used as order parameter of the topological phase for dimerized fermionic chain even in a certain interacting limit. However, even if SOP has been widely used, this is not a robust order parameter. We will discuss this issue in the last Chapter of this thesis. A more general order parameter-doubly degeneracy of whole entanglement spectrum has emerged after deep group theoretical study of symmetries of matrix product states [15, 7]. In these studies, the authors have shown that there are certain symmetries which stabilize the Haldane phase and this reflects on the

degenerate character of entanglement in the bipartited chain. We will use this order parameter to identify the Haldane phase in the XXZ chain of (1.1).

Experimental perspectives

Just after the prediction of Haldane about the gapped nature of integer Heisenberg chain, there has been an excessive number of experiments which has proved Haldane's conjecture with finding the finite gap and predicted edge states[16, 17, 18].

From an experimental point of view, model (1.1) is a relevant theoretical model to describe numerous compounds [19, 20] and the list is progressively updating [21]. Thus, a theoretical study of the current model with possible extensions is an important topic to consider.

1.2 Theoretical Background

1.2.1 Spontaneous Symmetry Breaking and Landau theory

We call a system gapped if there is a finite excitation gap between ground state and the first excited state. In fermionic systems, this property characterizes insulating phases. Thus, in analogy to fermionic systems, one may call gapped phase of spin chains also 'insulating' phase. In spin chains, except a finite gap, the local correlators of all spin components exponentially decay in a gapped phase.

We consider 1D quantum Ising model in a transverse magnetic field in x -direction:

$$H_I = -J \sum_{i=1}^N S_i^z S_{i+1}^z - \Gamma \sum_{i=1}^N S_i^x \quad (1.2)$$

where $J > 0$ and S - operators obey $SU(2)$ algebra. For the moment, we set

$\Gamma = 0$.

The system has discrete Z_2 symmetry, which is a physical 'spin-reversal' symmetry. When Hamiltonian diagonalized, due to double degeneracy of ground states, we have all spins in the 'up' states with $\langle S_i^z \rangle = \frac{1}{2}$, or all are in the 'down' states with $\langle S_i^z \rangle = -\frac{1}{2}$. This means that there is a spontaneous breaking of Z_2 symmetry and we have a ferromagnetic phase. Thus, one can detect this spontaneous symmetry breaking (SSB) by measuring local magnetization $m_i^z = \langle S_i^z \rangle$ and here it plays a role of order parameter in the system.

In the limit of $\Gamma \gg J$, we have paramagnetic phase, where all spins are polarized to the direction of a magnetic field and more importantly there is no any SSB. One can calculate long-range correlation functions $\langle S_i^\alpha S_{i+r}^\alpha \rangle$ and see that it decays exponentially so that there is a finite correlation length. From this, particularly, one can conclude that the system in this regime also is gapped.

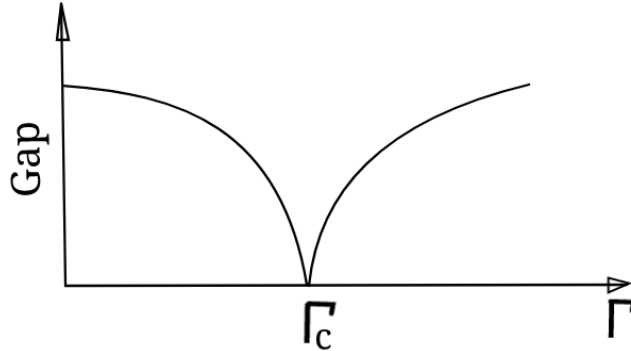


Figure 1.1: Gap closure in 1D Ising model

From schematic representation (Fig.1.1) we see that in two extreme limits of Γ the system is gapped. In one of them, one has SSB, while on the other there is no SSB. Thus, there is a quantum phase transition (QPT) with a quantum critical point (QCP) Γ_c , where gap-closure occurs. From explanations above one can conclude that QPT of the model under considerations can be identified by measuring local order parameter m_i^z .

In conclusion, SSB causes the existence of a local order parameter while in the absence of it, local order parameter vanishes. Thus, using this local order parameter

one can identify QPT. This is a fundamental idea behind Landau theory.

1.2.2 Symmetry - protected topological states

It has been believed that Landau theory is able to fully classify quantum phases in terms of symmetry - breaking. However, from recent time new phases of matter - topological phases, have been discovered and their classification is beyond the ability of the Landau theory.

Here, we consider only a subgroup of topological phases - symmetry-protected topological (SPT) phases. SPT phases are gapped phases of matter that have no any symmetry-breaking and one cannot distinguish two different SPT phases using local order parameter.

1.2.3 Antiferromagnetic Heisenberg S=1 Chain

Let us consider Antiferromagnetic Heisenberg Chain (AHC) with uniaxial anisotropy in z -direction D :

$$H = J \sum_{i=1}^N \vec{S}_i \cdot \vec{S}_{i+1} + D \sum_{i=1}^N (S_i^z)^2 \quad (1.3)$$

with $J > 0$. AHC with $S = 1$ ($D = 0$) is known to be gapped [4] [5]. As it was mentioned, if it is gapped, spin component correlation functions should exponentially decay. However, the same model with $S = \frac{1}{2}$ is gapless and was solved exactly by Bethe [22]. In fact, the AHC with general integer S is gapped, while with half-integer S is gapless.

If we consider model (1.3) in two extreme D limits, we have two different gapped phases: when $D \ll J$ we have gapped 'Haldane phase', while for $D \gg J$ we have gapped D -phase. Gapped D - phase is just a direct product of $|0\rangle$'s:

$$|\Psi\rangle = |00000\dots 0\rangle \quad (1.4)$$

As one can notice, this example is very similar to one from the previous section. In fact, there is gap closure with a critical D_c in which we have QPT. However,

there is not any SSB in the current model in both phases. Therefore, there is no any local order parameter which can separate these two phases. The question to ask is what makes these phases to differ from each other?

Den Nijs and Rommelse [23] have shown that the Haldane phase has hidden non-local antiferromagnetic (Neel) order and proposed so-called String Order Parameter (SOP) which is defined as:

$$O_S^\alpha(H) = - \lim_{|i-j| \rightarrow \infty} \left\langle S_i^\alpha e^{i\pi \sum_{l=i+1}^{j-1} S_l^\alpha} S_j^\alpha \right\rangle \quad (1.5)$$

where $\alpha = x, y, z$. It should be noted that SOP is non-local order parameter. Obviously, SOP for D -phase vanishes. The hidden non-local Neel order supposes a state in which if all set of sites g with $S_g^z = 0$ are deleted, one has rigid Neel order, e.g

$$|\Psi\rangle = |\uparrow\downarrow 00 \uparrow 0 \downarrow 000 \uparrow \dots\rangle \quad (1.6)$$

The 'clearness' of hidden Neel order determines the value of O_S^α .

Except non-zero SOP, Haldane phase also has a localized edge states. In a finite chain with Hamiltonian (1.3) and $D \ll J$, one has 4-fold degenerate ground state with free spin $-\frac{1}{2}$ at the edges. These edge states cause 4-fold degeneracy of the ground state.

Later on, Affleck, Kennedy, Lieb and Tasaki [6] has proposed an exactly solvable model which has the Haldane phase as a ground state:

$$H_{AKLT} = \sum_{i=1}^N (\vec{S}_i \cdot \vec{S}_{i+1}) + \frac{1}{3} (\vec{S}_i \vec{S}_{i+1})^2 \quad (1.7)$$

Similar to Majumdar-Ghosh Hamiltonian [24], H_{AKLT} is projection operator onto the sector of $S_{Tot} = 2$:

$$H_{AKLT} = 2 \sum_{i=1}^N (P_2(i, i+1) - \frac{1}{3}) \quad (1.8)$$

where $P_2(i, i+1)$ is projection operator onto the sector with $S_{Tot} = 2$. Thus, two neighboring spins in the ground state lie on $S_{Tot} = 1$ or $S_{Tot} = 0$. This suggests that any given two spins are antiparallel if both of they don't have non-zero z component. This proposes the existence of hidden Neel order in the ground states of the Hamiltonian.

While SOP was identifying Haldane phase successfully, the question about why AHC is gapped was open for a while. Kennedy and Tasaki [9] (and parallelly Oshikawa [25]) has proposed a non-local unitary transformation which explains the existence of the gap by hidden $Z_2 \otimes Z_2$ (or D_2) symmetry breaking. Rigorously speaking, one can formulate following unitary transformation: The first non-zero spin is left unchanged, the second non-zero spin is flipped, the third is unchanged, the fourth is flipped and so on. As a result of the transformation, non-zero spins are 'ferromagnetized' in the hidden Neel order. Mathematically, this transformation has the following form[25]:

$$V = V^{-1} = \prod_{j < k} e^{i\pi S_j^z S_k^x} \quad (1.9)$$

Then, applying this to Hamiltonian (1.3) ($J = 1$) leads to:

$$\tilde{H} = V H V^{-1} = \sum_i S_j^x e^{i\pi S_{j+1}^x} S_{j+1}^x + S_j^y e^{i\pi(S_{j+1}^x + S_j^z)} S_{j+1}^y + S_j^z e^{i\pi S_j^z} S_{j+1}^z + D(S_j^z)^2 \quad (1.10)$$

One can see that Hamiltonian (1.10) has $Z_2 \otimes Z_2$ symmetry, π rotations of all sites about x, y or z doesn't change the energy. Then, the formation of the gap can be explained in terms of breaking this symmetry like in the 1D Ising model. More interestingly, SOP transforms by V to a ferromagnetic correlation function, i.e

$$O_S^\alpha(H) = O_F^\alpha(\tilde{H}) \quad (1.11)$$

with

$$O_F^\alpha(\tilde{H}) = \lim_{|i-j| \rightarrow \infty} \langle S_i^\alpha S_j^\alpha \rangle \quad (1.12)$$

Thus, non-local SOP transforms into the local order parameter.

At this point, everything is similar to the 1D Ising model . For $D \gg 1$ we have a paramagnetic phase without any SSB, while for $D \ll 1$ we have SSB of D_2 symmetry .

In a first glance, it seems that the problem of gapped nature of the Haldane phase is solved by unitary transformation and can be explained by SSB. However, this is partially true. Particularly, these results suggest that if one adds terms which break D_2 symmetry in original Hamiltonian (1.3) , Haldane phase should

disappear. However, this is not true. Haldane phase in the model (1.3) is not only 'protected' by D_2 symmetry but also by time reversal, bond-centered inversion symmetries [15]. Thus to eliminate the Haldane phase, one should break all these symmetries in the original Hamiltonian. Discussed Haldane phase is an example of symmetry-protected topological phase.

In the current thesis, we consider the model (1.1) with $S = \frac{1}{2}$. Using symmetry fractionalization technique, it was shown [26] that the Haldane phase of the model is protected by the same symmetries of $S = 1$ AFH.

1.2.4 Order parameters to identify the Haldane phase

To identify the Haldane phase in the model (1.1) we use the following order parameters:

- XX limit of (1.1): In this limit, one has full $SU(2)$ symmetry. Thus modified SOP [8] should be able to identify the Haldane phase in the model.
- XXZ model: due to the broken $SU(2)$ symmetry, SOP cannot identify the Haldane phase. Thus, we will use the degeneracy of Entanglement Spectrum (ES) as an order parameter of the model in the XXZ limit.

Degeneracy of Entanglement Spectrum as an order parameter

Since there is not generalized non-local correlation function (like SOP) to identify the Haldane phase of a generic Hamiltonian, we will use so called Entanglement spectrum to identify the Haldane phase in XXZ model.

Consider a ground state $|\Psi\rangle$ of gapped 1D system with a tuning parameter G in a Schmidt decomposition:

$$|\Psi\rangle = \sum_{\alpha} \Lambda_{\alpha}(G) |\alpha_L\rangle \otimes |\alpha_R\rangle \quad (1.13)$$

where $\Lambda_{\alpha}(G)$ matrix of Schmidt values and has only non-zero positive diagonal elements. Entanglement Spectrum (ES) is defined as $\epsilon_S = -\log(\Lambda(G))^2$. The

claim is that in the SPT phase the whole ES is doubly degenerate [15] [7]. When G is varied and crosses QPT (it may be any type of QPT) , the ES degeneracy character changes. Thus, one can use it as an order parameter to identify the Haldane phase in 1D spin systems.

Chapter 2

Density Matrix Renormalization Group Theory

In this chapter, we briefly discuss a central and important numerical method for this thesis, namely Density Matrix Renormalization Group Theory (DMRG). However, we will start this chapter by discussing Numerical Renormalization Group method, which is the historical father of the DMRG. The idea of the chapter is delivering the idea behind DMRG rather than an expanded pedagogical explanation of the numerical method since the main numerical tool of this thesis is matrix product state based DMRG (MPS-DMRG) algorithm, which will be discussed in next chapter. However, introducing standard White's DMRG methods makes MPS-DMRG clearer. Thereafter, we introduce concepts of Reduced Density Matrix and Singular Value Decomposition which clarify the fundamental idea behind DMRG. Infinite Size and Finite Size algorithms of DMRG for open boundary conditions with implementation details also will be presented. Periodic Boundary condition DMRG algorithms together with all computational aspects of algorithms like the implementation of symmetries, diagonalization methods which will not be discussed.

2.1 Numerical Renormalization Group

The problem of studying quantum many-body phenomena in lattices leads to numerical diagonalization of large matrices. This is bound to the fact that Hilbert space dimension grows exponentially with the lattice size. While modern exact diagonalization algorithms are advanced, they can be applied to the restricted number of lattice sites, which excludes their usage on the investigation of thermodynamic limit properties. Furthermore, for a big number of lattice sites usually, numerical instabilities appear which are leading to wrong calculated energy spectrum. In any case, the solution of the problem is related to the fact that in strongly correlated quantum systems, zero temperature properties are mainly defined by the low energy spectrum. It means that even if the dimension of Hilbert space of the quantum system is exponentially large, only a small sector of the Hilbert space states define the quantum systems' properties. Thus, the problem reduces to finding those important states. The first successful approach was done by Wilson to solve Kondo impurity problem [27]. It turns out, that for quantum impurity problem the recipe of solving the problem is easy, as shown in the algorithm below.

Algorithm 1 Numerical Renormalization Group algorithm

- 1: Consider a block B of a length L . A superblock S of size $2*L$ should be diagonalizable.
 - 2: Diagonalize a Superblock S Hamiltonian H_S and keep only m lowest states
 - 3: From the m lowest states, form transformation matrix O
 - 4: 'Rotate' all necessary matrices of the Superblock S and call new block as B' (i.e $H'_B = O^\dagger H_S O$)
 - 5: Repeat procedure
-

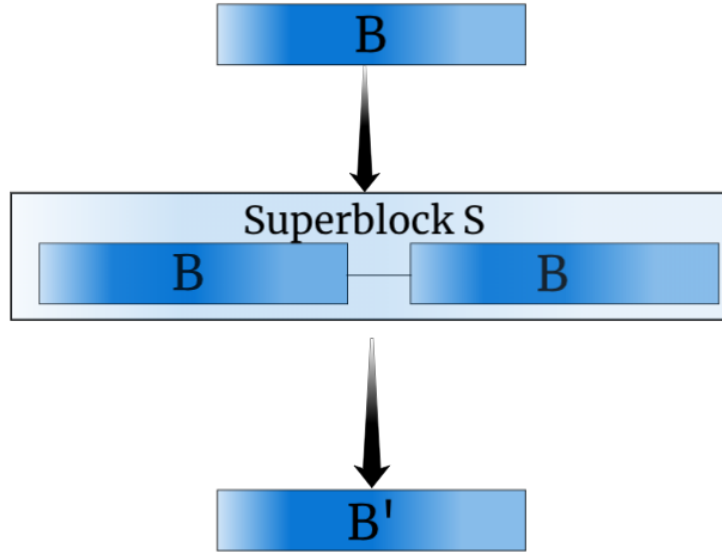


Figure 2.1: Numerical Renormalization Group algorithm

So, one starts with a chain of size L , which conditionally we call block B . Then 2 blocks are joined to form new superblock S , which is diagonalizable. After diagonalization, only m - lowest energy states are kept and transformation matrix O formed out of these m lowest states. One should rotate the all superblock S operators. This rotated Superblock S is called now Block B' . Obviously, after rotation, the dimension of Hilbert space is reduced and depends on the number of states kept. The procedure should be repeated until the desired chain length is obtained.

Despite the accuracy on solving quantum impurity problems, NRG algorithm is failing for a lattice systems. The reason is the choice of the optimal basis set: low-lying states of two blocks B are not a good choice of the states for Superblock S of quantum chains since it treats the system as if all blocks are independent of each other. The success of NRG in solving the Kondo model is due to the fact that the coupling between blocks is small, so the assumption is true.

Summing up, the main idea of NRG algorithm was to enlarge block keeping the Hilbert space manageable by consequent basis 'rotations'. So, for quantum spin models, in particular, it is important to find optimal basis set out of the states

of the given Block B, such that only they contribute in the full spin chain.

2.2 Density Matrix Renormalization Group

In the previous section, we emphasized the main idea of NRG and its crucial problem in treating lattice systems. The problem of choosing an optimal basis set out of exponentially large Hilbert space for the lattice systems was solved by S. White in 1992 [28, 29]. Since the low lying eigenstates kept in NRG don't contain any information about the rest of the lattice system, it fails to treat lattice systems. White has noticed that in order to treat the system correctly, one needs to include information about the rest of the system when deciding which states to keep. This has led to the concept of Density Matrix Renormalization Group (DMRG) theory. In contrast to the NRG, DMRG is focused in a chosen target state of interest, while NRG gives the full spectrum of the system. Mainly the state of the focus in the DMRG calculation is the ground state of the quantum system. So, one needs to choose which optimal states to keep based on the density matrix of the target states. We start introduction of DMRG method with the concept of density matrix in order to explain this powerful numerical method.

2.2.1 Reduced density matrix

Before going to the direct algorithm of DMRG, here we repeat the basic concepts behind DMRG method. Particular importance carries the concept of Reduced density matrix.

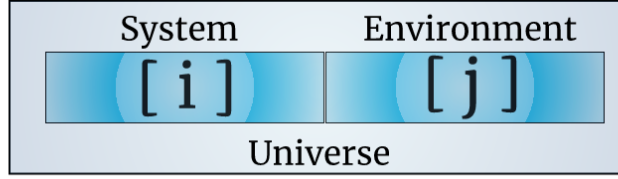


Figure 2.2: Bipartited Universe Block

In the beginning we define a universe , a chain of finite number of sites L . Every site has local degree of freedom d , so that the dimension of Hilbert space is $D_u = \dim(H_u) = d^L$. We divide our chain in two parts of the lengths L_1 and L_2 and call them system with the orthonormal set of states $|i\rangle$ and environment with the orthonormal set of states $|j\rangle$ respectively, as shown in the scheme above. It is clear that the dimension of Hilbert spaces are $D_s = \dim(H_s) = d^{L_1}$ and $D_e = \dim(H_e) = d^{L_2}$ so that $H_u = H_s \otimes H_e$ with $D_u = D_s \cdot D_e$. For a given Hamiltonian of the universe, one can write the full universe wavefunction as a direct tensor product:

$$|\Psi\rangle = \sum_{i,j} \psi_{i,j} |i\rangle \otimes |j\rangle \quad (2.1)$$

where summation runs over all states of aforementioned orthonormal sets. For convenience, we further drop the sign \otimes .

Example: Matrix form of $\psi_{i,j}$

Suppose we have a universe state with three spin-1/2 spins with the local degree of freedom $d=2$: $|\psi\rangle = a_{11} |\uparrow\uparrow\uparrow\rangle + a_{12} |\uparrow\uparrow\downarrow\rangle + \dots$. Next, if we define our system as the first spin, and environment as the rest of the universe, the coefficient $\psi_{i,j}$ can be written as the matrix of dimension 2×4 :

$$\psi = \begin{bmatrix} a_{11} & a_{12} & a_{13} & a_{14} \\ a_{21} & a_{22} & a_{23} & a_{24} \end{bmatrix}$$

From above example, one can see that the size of the ψ matrix depends on the definition of the system and environment lengths and equal to $D_s \times D_e$, where $D_{s,e}$ are Hilbert space dimensions of the corresponding parts.

Next, to get reduced density matrix of the system, we consider operator R acting only on the system space:

$$R = \sum_{i,j,i'} R_{i,i'} |i\rangle |j\rangle \langle i'| \langle j| \quad (2.2)$$

Then, one can calculate expectation value of the operator R :

$$\langle \Psi | R | \Psi \rangle = \sum_{i,j,i'} \psi_{i,j} \psi_{i',j}^\dagger \langle i | R | i' \rangle \quad (2.3)$$

which is obtained using the orthogonality property of the $|j\rangle$ set.

The equation above can be rearranged as:

$$\langle \Psi | R | \Psi \rangle = \sum_{i,i'} \rho_{i,i'}^S \langle i | R | i' \rangle = \text{Tr}(\rho R) \quad (2.4)$$

where reduced density matrix is defined as

$$\rho_{i,i'}^S = \sum_j \psi_{i,j} \psi_{i',j}^\dagger \quad (2.5)$$

From this equation one can easily figure out how to form ρ matrix if the universe wavefunction is given, using the example above.

Also, from definition, we can trace out the environment states to get the system density matrix:

$$\rho^S = \text{Tr}_E(|\Psi\rangle\langle\Psi|) \quad (2.6)$$

which can be easily proven. Generally, the reduced density matrix ρ is not diagonal in the basis of $|i\rangle$ states. If diagonalized, ρ can be represented as:

$$\rho = \sum_\alpha \omega_\alpha |u_\alpha\rangle\langle u_\alpha| \quad (2.7)$$

where ω_α and $|u_\alpha\rangle$ are the corresponding eigenvalues and eigenstates.

At this point, we mention several important properties of the reduced density matrix:

1. Hermiticity: $\rho^\dagger = \rho$
2. Positivity of eigenvalues: $\omega_\alpha \geq 0$
3. Probabilistic interpretation: $\sum_\alpha \omega_\alpha = 1$

All these three important properties can be derived using equations above. The most important property for us is the last one: it means that the system is in a state $|u_\alpha\rangle$ with the probability ω_α .

Summing up, if a universe wavefunction Ψ is given, one can define the reduced density matrix for a given 'system'. The values of ω_α show the contribution percentage of states $|u_\alpha\rangle$ in the system to the total universe wavefunction Ψ , or how much system it is 'entangled' with the environment. If sorted ω_α falls exponentially, it means, only a very few states in the system can be kept. And more importantly, it means that we have a new criterion for cutting our big Hilbert space: based on the reduced density matrix eigenvalues.

If m states $|u_\alpha\rangle$ with lowest eigenvalues are kept, there will an error due to the full Hilbert space truncation, which can be defined as $\epsilon_r = 1 - \sum_{\alpha=1}^m \omega_\alpha$. At this point, the concept of Singular-Value Decomposition and its' connection with the reduced density matrix needs to be discussed.

2.2.2 Singular Value Decomposition

Singular Value Decomposition (SVD) which is well-known from linear algebra, will be used extensively in the thesis, thus the main idea behind the concept should be introduced. SVD of any rectangular matrix M of the dimensions $D_A \times D_B$ is defined as follows:

$$M = USV^\dagger \tag{2.8}$$

where:

1. U is the matrix which has dimensions $D_A \times \min(D_A, D_B)$ and left normalized so that $U^\dagger U = I$. If $D_A < D_B$, U is a diagonal matrix of dimensions $D_A \times D_A$.
2. S is diagonal matrix with the dimensions $\min(D_A, D_B) \times \min(D_A, D_B)$ with positive entries. The elements are called singular values. The number of non-zero

entries define the rank of M .

V is the unitary matrix which is right - normalized, so that $VV^\dagger = I$ with the dimensions $\min(D_A, D_B) \times D_B$.

From definitions above, it is clear that if only several biggest values of S are kept and others are set to 0, one gets approximate matrix \tilde{M} .

Our interest in using of this linear algebra tool is so-called Schmidt decomposition of our bipartited universe $|\Psi\rangle$, which is defined as:

$$\begin{aligned} |\Psi\rangle &= \sum_{i,j} \psi_{i,j} |i\rangle |j\rangle = \sum_{i,j} \sum_{a=1}^{\min(D_S, D_E)} U_{ia} S_{aa} V_{aj}^\dagger |i\rangle |j\rangle = \\ &= \sum_{a=1}^{\min(D_S, D_E)} \left[\sum_i U_{ia} |i\rangle \right] s_a \left[\sum_j V_{aj}^\dagger |j\rangle \right] = \sum_{a=1}^{\min(D_S, D_E)} s_a |a\rangle_S |a\rangle_E \end{aligned} \quad (2.9)$$

where new basis sets are defined by rotating the previous system and environment basis sets. This is guaranteed by orthonormality of U and V^\dagger . In fact, one can keep only a few states of $|a\rangle$ based on s_a , so that the quantum state can be approximated. Schmidt decomposition allows us to show that density matrices have the following form:

$$\rho^{S,E} = \sum_{a=1}^{a=m} s_a^2 |a_{S,E}\rangle \langle a_{S,E}| \quad (2.10)$$

where m is the maximum number of states which are included in approximation. Now, one can easily see that the basis set $|a\rangle_S$ in fact is the previously mentioned basis set $|u_\alpha\rangle$ with $\omega_\alpha = s_a^2$. Thus, it follows that U and V^\dagger matrices are transformation matrices which are mapping $|i, j\rangle$ to $|a_{S,E}\rangle$.

In summary, SVD decomposition of ψ_{ij} transforms standard basis sets to orthonormal basis sets of $\rho_{S,E}$. Thus, the decision which states to keep to truncate the Hilbert space should be done according to the eigenvalues of the density matrix.

2.2.3 Infinite-size DMRG algorithm

There are two types of standard White algorithms [28, 29] which have been widely used in the 1990s: Infinite-size DMRG algorithm and Finite - size algorithm.

Infinite - size algorithm is invented to get the thermodynamic properties of the 1D quantum systems. Here, for simplicity, we consider a symmetric algorithm, where system block and environmental block are supposed to be symmetric. The algorithm is presented below:

Algorithm 2 Infinite-size DMRG algorithm

- 1: Consider Initial system and Environment blocks of a length l each (e.g $l=2$), with Hamiltonians $H_{init}^{S,E}$ respectively.
- 2: Enlarge every block by one site, so that now, each block will have $l+1$ sites. Hamiltonians of every enlarged blocks are: $H_{enl}^{S,E}$ should be calculated.
- 3: Form a superblock (universe in our previous notation) Hamiltonian H_{2l+2}^{SB} out of these two blocks, so that superblock will have $2l+2$ sites.
- 4: Diagonalize H_{2l+2}^{SB} and get ground state $|\Psi\rangle$.
- 5: Obtain density matrix using: $\rho^S = \sum_j \psi_{i,j} \psi_{i',j}^\dagger$ and diagonalize it. If the universe is symmetric $\rho^S = \rho^E$.
- 6: Form out of m given eigenvectors V of ρ with the largest eigenvalues a transformation matrix:

$$O = \begin{bmatrix} \vdots & \vdots & \vdots & \vdots \\ V_1 & V_2 & \dots & V_m \\ \vdots & \vdots & \vdots & \vdots \end{bmatrix}$$

- 7: 'Rotate' all necessary operators of Enlarged System and Environment Blocks and treat them as new Initial System and Environment Blocks (i.e $\tilde{H}_{init}^S = O^\dagger H_{enl}^S O$)
 - 8: Repeat procedure, i.e enlarge new Initial System and Environment Blocks and form new Superblock and continue the process until the desired chain length is reached.
-

As shown in the algorithm below, one should start with the finite length symmetric blocks, so that $2l+2$ superblock Hamiltonian should be computational ease to diagonalize it. Of course, this condition depends on the local degree of freedom of sites, because of the dimension of $H_{2l+2}^{SB} = d^{2l+2}$. Since diagonalization has the biggest contribution to the computational cost of the algorithm, one should balance with the accuracy of the results and initial block sizes. In any case, in practice, even small size of initial blocks give very accurate results. For diagonalization procedure one can use standard diagonalization algorithms (i.e Davidson) and should exploit symmetries of a given Hamiltonian.

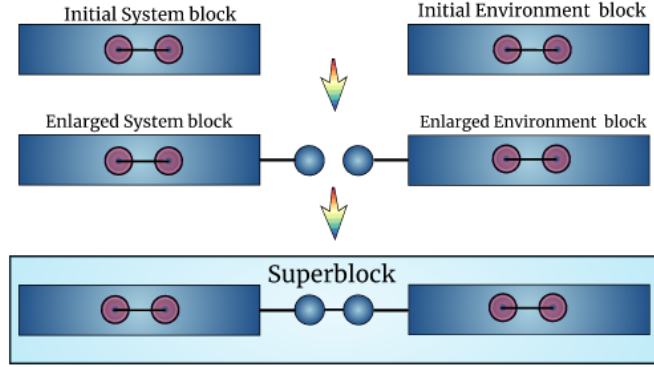


Figure 2.3: White's Infinite-size DMRG algorithm

2.2.3.1 Numerical implementation details of DMRG

Model definition

At this section we elucidate the algorithm above in a more formal and mathematical representation for a given Hamiltonian. Suppose, a given Hamiltonian for a chain of N sites is:

$$H = \sum_{i=1}^N J(S_i^z S_{i+1}^z + \frac{1}{2} (S_i^- S_{i+1}^+ + S_i^+ S_{i+1}^-)) \quad (2.11)$$

Here we assume $S = 1$ so that the local degree of freedom is $d = 3$. The matrix representations of corresponding operators are:

$$S^z = \begin{bmatrix} 1 & 0 & 0 \\ 0 & 0 & 0 \\ 0 & 0 & -1 \end{bmatrix} \quad (2.12)$$

$$S^+ = \sqrt{2} \begin{bmatrix} 0 & 1 & 0 \\ 0 & 0 & 1 \\ 0 & 0 & 0 \end{bmatrix} \quad (2.13)$$

$$S^- = \sqrt{2} \begin{bmatrix} 0 & 0 & 0 \\ 1 & 0 & 0 \\ 0 & 1 & 0 \end{bmatrix} \quad (2.14)$$

Initial Blocks settlement

We define Initial System and Environment blocks with 2 sites:

$$H_{init}^S = S^z \otimes S^z + \frac{1}{2} (S^- \otimes S^+ + S^+ \otimes S^-) \quad (2.15)$$

which has the following matrix representation:

$$H_{init}^S = \begin{bmatrix} 1.0000 & 0 & 0 & 0 & 0 & 0 & 0 & 0 & 0 \\ 0 & 0 & 0 & 1.0000 & 0 & 0 & 0 & 0 & 0 \\ 0 & 0 & -1.0000 & 0 & 1.0000 & 0 & 0 & 0 & 0 \\ 0 & 1.0000 & 0 & 0 & 0 & 0 & 0 & 0 & 0 \\ 0 & 0 & 1.0000 & 0 & 0 & 0 & 1.0000 & 0 & 0 \\ 0 & 0 & 0 & 0 & 0 & 0 & 0 & 1.0000 & 0 \\ 0 & 0 & 0 & 0 & 1.0000 & 0 & -1.0000 & 0 & 0 \\ 0 & 0 & 0 & 0 & 0 & 1.0000 & 0 & 0 & 0 \\ 0 & 0 & 0 & 0 & 0 & 0 & 0 & 0 & 1.0000 \end{bmatrix} \quad (2.16)$$

Also, one should keep left-most site operators for system and right-most for environment, since one needs them when making Hamiltonian for enlarged blocks:

$$\begin{aligned} S_{sysRight}^+ &= \mathbb{I}_3 \otimes S^+ \\ S_{sysRight}^z &= \mathbb{I}_3 \otimes S^z \end{aligned} \quad (2.17)$$

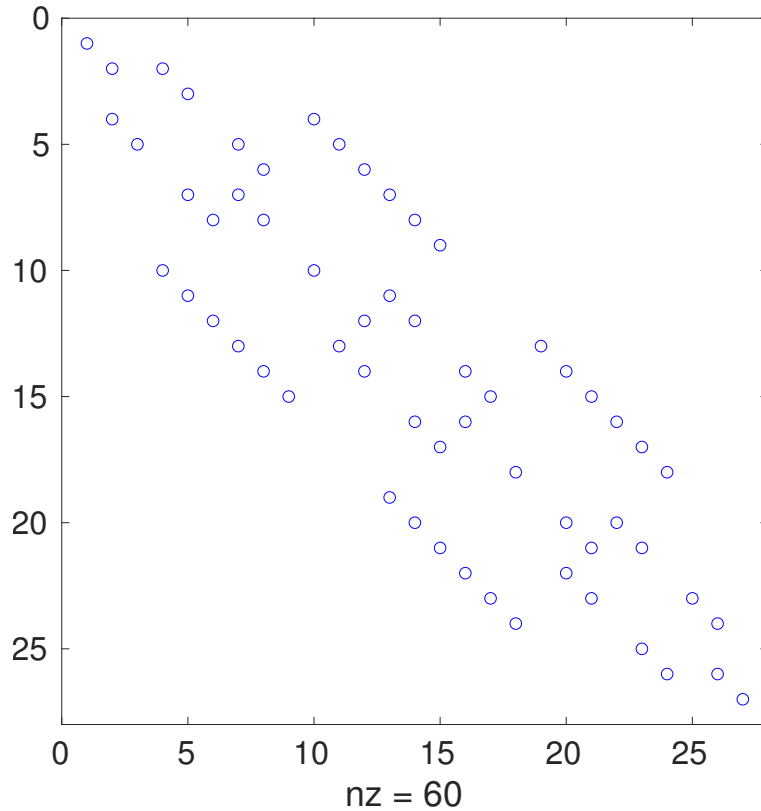
One can easily get the matrix representation of operators. Similarly, right-most operators for initial environment block should be saved.

Blocks Enlargement

Next, one should enlarge the initial blocks: the system block from the right side, the environment from left. Hamiltonian can be written in the following form:

$$H_{enl}^S = H_{init}^S \otimes \mathbb{I}_3 + S_{sysRight}^z \otimes S^z + \frac{1}{2} (S_{sysRight}^+ \otimes S^- + S_{sysRight}^- \otimes S^+) \quad (2.18)$$

The corresponding H_{enl}^S matrix has the dimensions $3^3 \times 3^3$ and it's sparsity portrait is shown in the figure below.



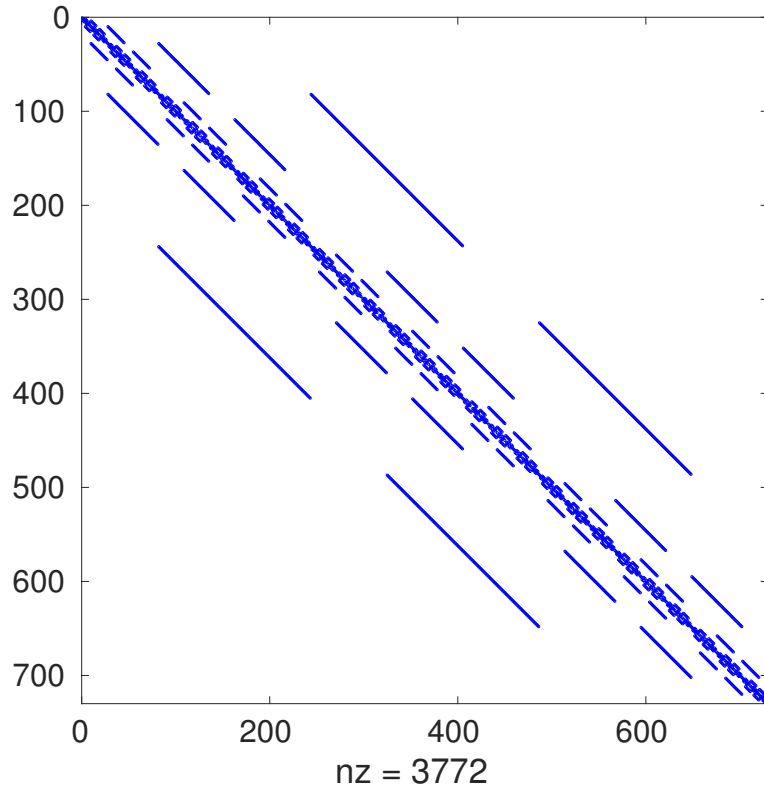
Enlarged Environment Block's Hamiltonian can be obtained by the following the logical path of the equations above. One should also upgrade leftmost and rightmost operators for enlarged environment and system blocks respectively.

Superblock H^{SB} diagonalization

The next step is obtaining the superblock Hamiltonian $H_{l=6}^{SB}$ with the dimensions $3^6 \times 3^6$:

$$\begin{aligned}
 H_{l=6}^{SB} = & H_{enl}^S \otimes \mathbb{I}_{\dim(H_{enl}^E)} + H_{enl}^E \otimes \mathbb{I}_{\dim(H_{enl}^S)} + \\
 & + S_{enlsysRight}^z \otimes S_{enlenvLeft}^z + \frac{1}{2} (S_{enlsysRight}^+ \otimes S_{enlenvLeft}^- + S_{enlsysRight}^- \otimes S_{enlenvLeft}^+)
 \end{aligned}
 \tag{2.19}$$

The sparsity portrait is shown in the figure below. The ground state energy of $E_{GS}^{SB} = -7.3703J$ and it's corresponding eigenstate can be found when $H_{l=6}^{SB}$ is diagonalized.



Density matrix formation and it's diagonalization

To form system density matrix, one should firstly define ψ_{ij} matrix and use $\rho^S = \sum_j \psi_{i,j} \psi_{i,j}^\dagger$, so that it leads to numerical matrix reshaping and summation

operations.

In our model, the corresponding ground state wavefunction has the dimension of 1×3^6 . Correct matrix manipulation leads to $3^3 \times 3^3$ matrix of ρ^s with the following non-zero eigenvalues:

$$\rho = \begin{bmatrix} 0.3281 & 0 & 0 & 0 & 0 & 0 \\ 0 & 0.3281 & 0 & 0 & 0 & 0 \\ 0 & 0 & 0.3281 & 0 & 0 & 0 \\ 0 & 0 & 0 & 0.0113 & 0 & 0 \\ 0 & 0 & 0 & 0 & 0.0007 & 0 \\ 0 & 0 & 0 & 0 & 0 & 0.0007 \end{bmatrix} \quad (2.20)$$

The exponential decay of eigenvalues can be observed, since out of 27 eigenvalues only 6 states have non-zero values up to fifth digit. This is true for gapped spin chains, and as we now from previous sections, AFH spin-1 chain ground state is in Haldane phase and gapped. Particularly this result means that if only $m=6$ states are kept, truncation error will be exponentially small.

Transformation matrix formation

To work in ρ basis, one need transformation matrix which can be formed as:

$$O = \begin{bmatrix} \vdots & \vdots & \vdots & \vdots \\ V_1 & V_2 & \dots & V_6 \\ \vdots & \vdots & \vdots & \vdots \end{bmatrix} \quad (2.21)$$

where $V_1, V_2 \dots V_6$ are eigenvectors with non-zero eigenvalues. One can easily check that $O^\dagger O = \mathbb{I}_{6 \times 6}$

Operator rotations

At this stage, one should 'rotate' all operators of enlarged system and environment blocks to a new basis. Their dimension will be reduced and rotated Hamiltonian

H_{enl}^S has the following form:

$$H_{enl}^S == \begin{bmatrix} 0.0000 & -0.0000 & 0.0000 & -0.4344 & -0.0000 & -0.0000 \\ -0.0000 & -0.8501 & -0.0000 & -0.0000 & 0.0000 & 0.2439 \\ 0.0000 & -0.0000 & 0.8501 & 0.0000 & -0.0000 & 0.0000 \\ -0.4344 & -0.0000 & 0.0000 & 0.0000 & 0.6562 & -0.0000 \\ -0.0000 & 0.0000 & -0.0000 & 0.6562 & 0.0000 & -0.0000 \\ -0.0000 & 0.2439 & 0.0000 & -0.0000 & -0.0000 & -0.5685 \end{bmatrix} \quad (2.22)$$

Similarly, other needed operators i.e S_{enl}^z should be rotated.

Repeat the procedure

When it is done, one should accept rotated operators as the operators of initial system and environment blocks and enlarge them. The procedure should be done until the chain of length N is reached.

Results

In this section we check results stability of the code which was realized as a part of numerical package 'BilkentDMRG'.

Ground state energy

Firstly, ground state energy per site $\epsilon = \frac{E_{GS}}{L}$ is calculated for a system with length $L = 124$. The number of kept states are $m = 4, 8, 10$.

As shown in Fig. 2.4 (a) ϵ decays algebraically from $\epsilon = -1.26J$ for the superblock of size $l = 6$ to $\epsilon = -1.388J$. The blue line corresponds to the most accurate numerical result available [9] which is equal to $\epsilon = -1.401484093J$. In Fig. 2.4 (b) the same trend can be observed in logarithmic scale for a different number of sites kept. Almost in all three cases, the absolute error starts $\approx 10^{-1}$ when the

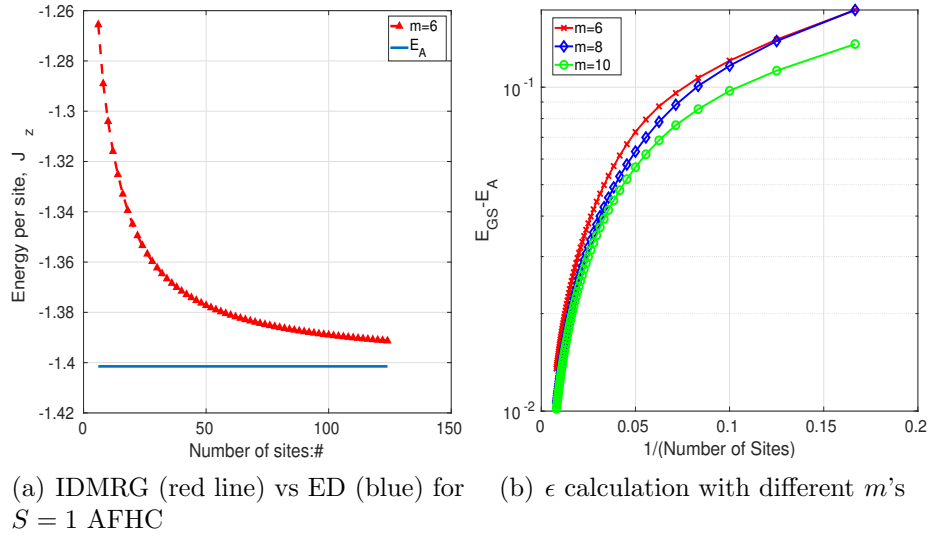


Figure 2.4: Ground state energy per site calculation for AFHC with $S=1$

superblock length is $l \approx 10$ and reach the error of $\approx 10^{-2}$ when the full chain length is achieved.

Truncation error

Next, to see the value distribution of density matrix eigenvalues ω_α , we plotted it when the full length of the chain is reached. From Fig. 2.5 (a) it is clear that keeping only $m=10$ states guarantees the truncation error of the order 10^{-6} . Indeed, from fig. b one can see that the truncation error gets closer to the 10^{-6} when the value of m is changing from $m = 8$ and $m = 10$.

2.2.4 Finite-size DMRG algorithm

Using the infinite size algorithm we cannot get wavefunction form with a good accuracy. The reason is the nature of the algorithm: in every iteration, we are cutting our basis, so that for the next iteration additional errors emerge with some information lost. To overcome this Finite Size DMRG (FS-DMRG) was introduced in the original paper of White [29]. The algorithm is shown below.

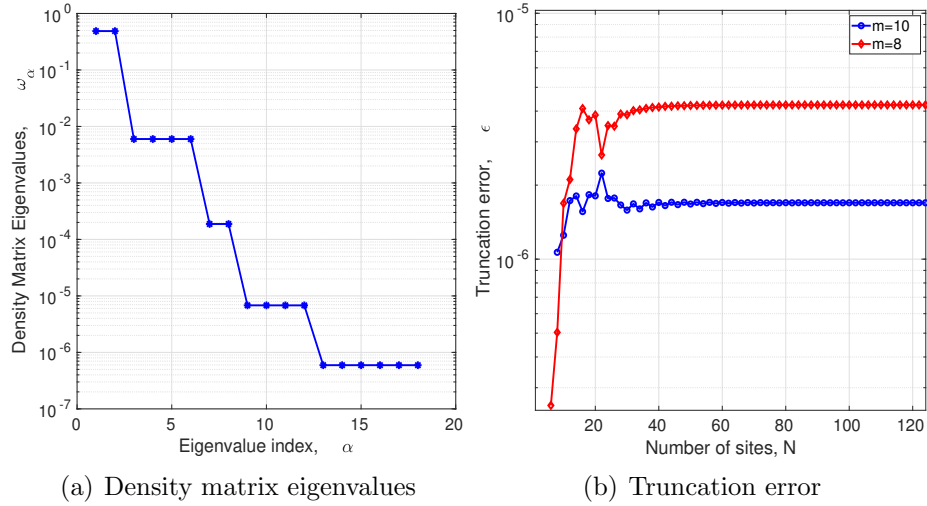


Figure 2.5: Density matrix eigenvalues in descending order and truncation error $\epsilon_r = 1 - \sum_{\alpha} \omega_{\alpha}$ for $L = 124$

Algorithm 3 Finite-size DMRG algorithm

- 1: Perform infinite - size DMRG to get the chain of the length L . In every iteration step, one should save all necessary operators. At this point, we have System Block of the size $L/2$ and symmetric Environment Block.
 - 2: LEFT SWEEP: Enlarge System and 'previous' Environment blocks by one site, while keeping the length of the total fixed, i.t System Block will have $l = L/2 + 1$, while Environment Block will have the length $L/2 - 1$. For this, one should enlarge not the last Environment block, but the previous one, so that the number of sites will be fixed.
 - 3: Do procedures explained in infinite size DMRG algorithm. Save new rotated operators.
 - 4: Repeat: Keep growing System Block until the Environment Block reaches Initial Environmental Block. At this stage, left sweeping is finished.
 - 5: RIGHT SWEEP: When the initial Environment Block is reached, the process should be reversed, i.e Environment Block should be grown when System Block is shrunk. The process should be repeated until the initial System Block is reached.
 - 6: Repeat left and right sweepings until the given criteria on energy convergence is reached.
-

The idea of the algorithm is based on the sweepings: expanding a system block while environment block is shrunk and reverse.

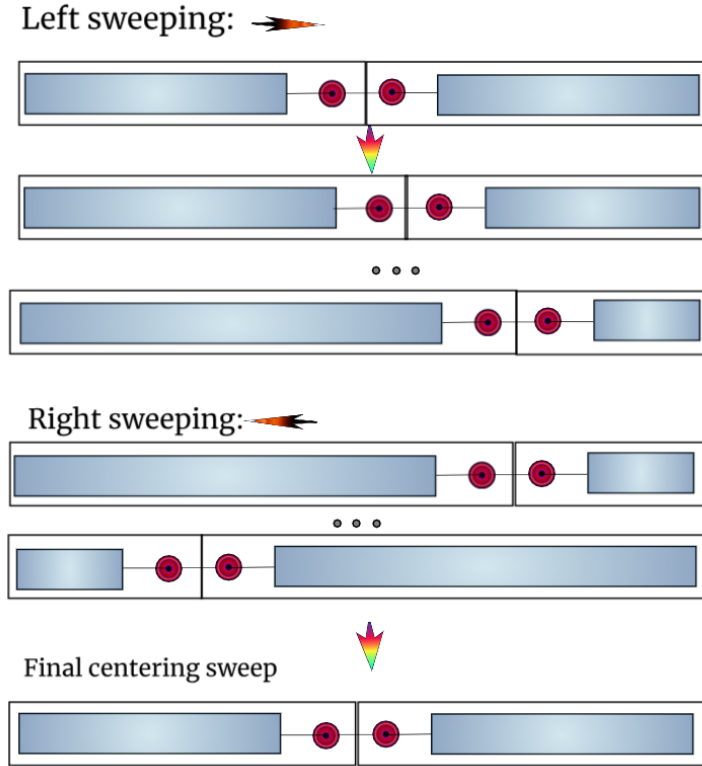


Figure 2.6: Finite - Size sweeping process

Initially, we do infinite size algorithm, until the desired chain length L is reached. For this, suppose M iterations were done. The corresponding environment and system blocks will have the same size $l = \frac{L}{2}$. At this point, one should have all operators saved in every iteration. Next, left sweeping should be done, which starts with enlarging System Block by 1 site. Enlarging environment block of $(M-2)^{th}$ iteration by 1 site leads to the Environment Block with a length of $l' = \frac{L}{2} - 1$. Thus, a total number of site L is kept. Next step is identical to the infinite size algorithm procedure from forming a superblock till rotating the basis set. By procedures described above, we grow our System Block while shrinking Environment Block. One should repeat this process until the last environment block to enlarge is the initial one.

For right sweeping, one repeats the same procedures, but in reverse direction. To be able to do that, one should save all operators in previous left-sweeping enlargements. The final point is reached when the last System Block to grow is the initial System Block.

One can repeat left and right sweepings until the desired accuracy for a given parameter is reached. Finally, one should sweep back to the center of the chain, to make the measurement process easy.

2.2.5 Measurement

Except calculating of ground state energy, DMRG also allows calculating expectation values of defined operators A : $\langle \Psi | A | \Psi \rangle$. However, the calculation of these quantities is not straightforward as calculating E_{GS} . For this, one needs to transform corresponding operators when blocks are enlarged and when the transformation matrix is applied.

Suppose one needs to calculate S_i^z on the i site, where the operator representation in the block B $\left[\tilde{S}_i^z \right]_{\alpha, \alpha'}^B$ is given. Here, $\{\alpha, \alpha'\}$ is the basis set of the block B. Block enlargement and further basis rotation leads to:

$$\left[\tilde{S}_i^z \right]_{\beta, \beta'}^{B'} = \sum_{\alpha, \alpha', z_d, z'_d} O_{\beta; \alpha, z_d} \left[\tilde{S}_i^z \right]_{\alpha, \alpha'}^B O_{\beta'; \alpha', z'_d}^\dagger \quad (2.23)$$

where $\{z_d, z'_d\}$ is the basis set of the single site. Now, when the operator represented in the new block B' , we can calculate expectation value:

$$\langle \Psi | S_i^z | \Psi \rangle = \sum_{\beta, \beta', z_d, z'_d, \gamma} \psi_{\beta, z_d, z'_d, \gamma}^\dagger \left[\tilde{S}_i^z \right]_{\beta, \beta'}^{B'} \psi_{\beta', z_d, z'_d, \gamma} \quad (2.24)$$

Similarly, one can calculate two-point correlators of the form: $\langle \Psi | S_i^z S_j^z | \Psi \rangle$. As one noticed, this is very inconvenient numerically to calculate long range correlators.

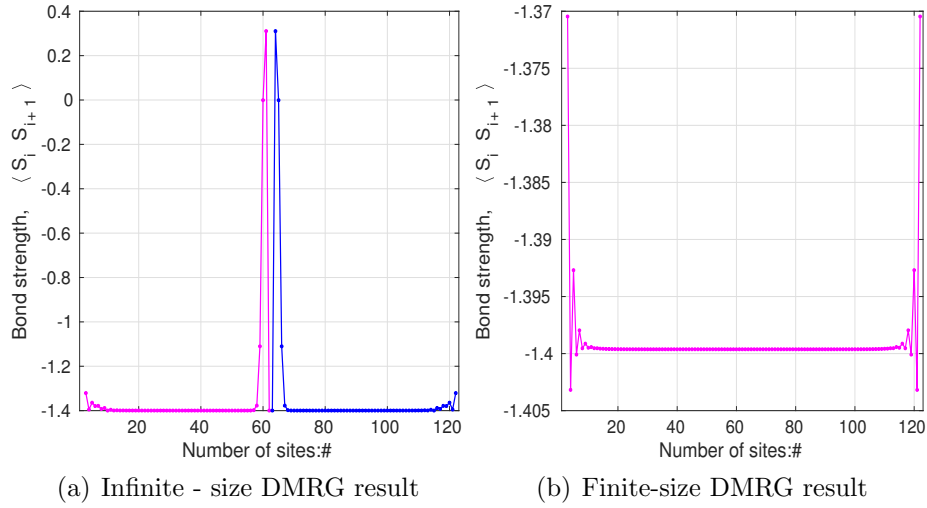


Figure 2.7: Comparison of bond strength expectation value for two DMRG algorithms

Bond strength and optimized wavefunction

Here we compared infinite size DMRG and finite size DMRG wavefunctions accuracy by calculating expectation values of the 'bond-strength' $\langle \Psi | \vec{S}_i \vec{S}_{i+1} | \Psi \rangle$, which is shown in the Fig.2.7 : From Fig. 2.7 it is clear, that even if the bond strength value saturates exponentially to the average value of E_{GS}/L from the edges of the chain, in Infinite-size calculations it has nonphysical peaks in the middle of the chain. When 2 full sweepings are completed in Finite size algorithm and wavefunction is optimized, these peaks disappear, as one can see in the Fig.(2.7 (b)).

Summary, in this chapter fundamental idea behind the DMRG method is discussed. We mainly highlighted the core points of DMRG and explained standard White's algorithms implementation details. In the next chapter, we are going to discuss the main aspects of Matrix Product States and MPS based DMRG.

Chapter 3

Matrix Product States and Matrix Product Operators

In the first part of this chapter, we introduce briefly the concept of Matrix Product States (MPS). For this, the basic diagrammatic notations of tensor networks will be discussed. Next, the canonical forms of MPS will be introduced. Also, calculation of overlaps and calculation of expectation values will be shown.

In the second part of the chapter, we introduce Matrix Product Operators (MPO) and show how to construct MPO for a given local Hamiltonian.

Lastly, we formulate two main MPS based DMRG algorithms which will be used as a numerical tool for this thesis. Throughout the chapter, we consider only chains with OBC.

One can find an extended review of MPS, MPO, and DMRG in Schollowck's review paper [30].

3.1 Matrix Product States

A general wavefunction of the system with a number of sites L can be represented as:

$$|\Psi\rangle = \sum_{\sigma_1, \sigma_2, \dots, \sigma_L} C_{\sigma_1; \sigma_2; \dots; \sigma_L} |\sigma_1, \sigma_2, \dots, \sigma_L\rangle \quad (3.1)$$

where

$$|\sigma_1, \sigma_2, \dots, \sigma_L\rangle = |\sigma_1\rangle \otimes |\sigma_2\rangle \otimes \dots \otimes |\sigma_L\rangle \quad (3.2)$$

and $C_{\sigma_1; \sigma_2; \dots; \sigma_L}$ is tensor of the rank L . The set $\{\sigma_i\}$ contain all possible site states, i.e d elements. As in the case of the example above, we can write a tensor element as the multiplication of local matrices such that:

$$|\Psi\rangle = \sum_{\sigma_1, \sigma_2, \dots, \sigma_L} \sum_{a_1, a_2, \dots, a_{L-1}} M_{1, a_1}^{\sigma_1} M_{a_1, a_2}^{\sigma_2} \dots M_{a_{L-1}, 1}^{\sigma_L} |\sigma_1, \sigma_2, \dots, \sigma_L\rangle \quad (3.3)$$

For any given site i , d matrices M_{a_{i-1}, a_i} of the dimensions $\dim(M) = a_{i-1} \times a_i$ are defined. Indexes $\{\sigma_i\}$ are called bond indexes or auxiliary indexes. In the first and the last sites they are just simple vectors of dimensions $\dim(M(1)) = 1 \times a_1$ and $\dim(M(L)) = a_{L-1} \times 1$ respectively. This guarantees of getting a number when all matrices are multiplied. One can compact these d matrices as the tensor of rank $R_M(i) = 3$, noting it as $M_{a_{i-1}, a_i}^{\sigma_i}$. Similarly, one can get the $\langle\Psi|$ state:

$$\langle\Psi| = \sum_{\sigma_1, \sigma_2, \dots, \sigma_L} \sum_{a_1, a_2, \dots, a_{L-1}} M_{1, a_1}^{*\sigma_1} M_{a_1, a_2}^{*\sigma_2} \dots M_{a_{L-1}, 1}^{*\sigma_L} \langle\sigma_1, \sigma_2, \dots, \sigma_L| \quad (3.4)$$

It should be noted that from the first edge of the chain the dimension of $M(i)$ will be getting exponentially large up to the center and then decrease symmetrically till the end, becoming vector at the edge.

Thus, one can put a restriction on the maximum auxiliary bond index as $\chi = \max(a_j)$, which allows us to approximate our $|\Psi\rangle$. It means we fix maximum the dimension $M(i)$ matrices, i.e they will have the dimension of $\chi \times \chi$ whenever it $a_{i-1} > \chi$. This is similar to the cutting out m states out of Hilbert space of ρ_S in standard DMRG algorithm.

3.1.1 Tensor networks notation

In this stage, it is useful to introduce a tensor network diagrammatic notations. These notations make operations with tensors very versatile and have demonstrative character.

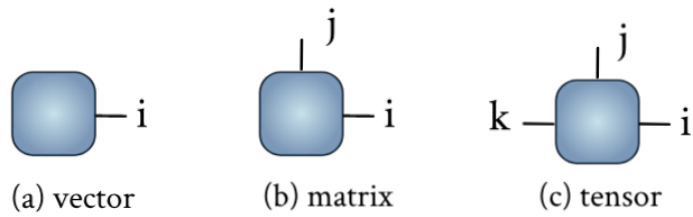


Figure 3.1: Diagrammatic tensor notations

A tensor of a rank n can be represented as geometric figure (rectangle in our case) with n legs. As it is clear from the graph, a general vector has 1 leg, when a matrix has 2 legs. Obviously, a scalar has no legs at all. Next, the following notations for operation with tensors will be useful:

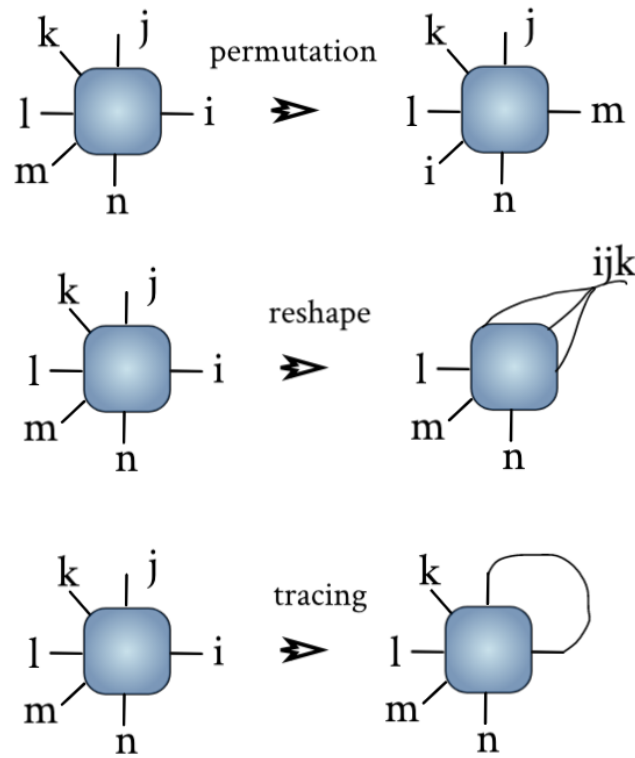


Figure 3.2: Diagrammatic notations of operations with tensors

- Permutation - in this operation the tensor legs will be interchanged. Symbolically, it means $A_{i;j;k} \rightarrow A_{j;i;k}$.
- Reshaping - if we have n legs, one can unify l out of n legs, so the number of legs will be decreased. In symbolic notation $A_{i;j;k} \rightarrow A_{ij;k}$. Similarly, one can reshape 1 leg with dimension q to 2 other legs r and t , so that $q = rt$.
- Tracing - this operation traces out two legs. For this, of course, the dimensions of the legs should be the same.

3.1.2 Tensor contraction

The most common operation while working with tensors is a contraction. Contraction is a generalized version of matrix multiplication in higher dimensions. However, matrix multiplication is very commonly used in real life, so that there are highly optimized packages like LAPACK, which do this operation fast. Thus, one needs to reshape high-rank tensors to the matrices perform matrix multiplication and reshape back.

The basic contraction operations are shown in the figure below:

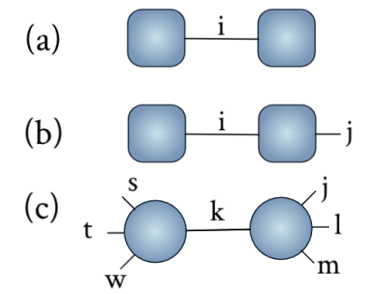


Figure 3.3: Diagrammatic notations for tensor contractions: (a) vector - vector multiplication; (b) vector - matrix multiplication (c) General tensor contraction

3.1.3 Tensor notations for MPS

Since MPS site unites are $M_{a_{i-1}, a_i}^{\sigma_i}$ tensors with rank 3, we can represent MPS as the contracting tensors:

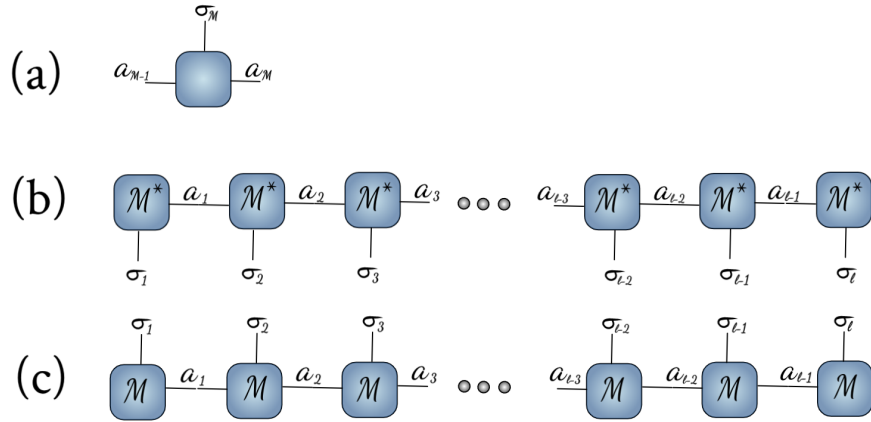


Figure 3.4: Diagrammatic notations of MPS $|\Psi\rangle$: (a) single-site tensor (b) MPS representation for $\langle\Psi|$ and (c) for $|\Psi\rangle$

In the figure above MPS representation for $\langle\Psi|$ and (c) for $|\Psi\rangle$ are shown. Auxiliary bond dimensions $a_m \times a_{m+1}$ also shown in every bond.

3.2 Canonical MPS representations

In this part we discuss 3 main MPS representations, namely:

- Left-canonical MPS
- Right-canonical MPS
- Mixed-canonical MPS

It should be mentioned that there is also common Vidal's $\Gamma - \Lambda$ notation which gives extensive information about symmetries of ground state wavefunction and entanglement for any bipartition [30]. We will not discuss it here, while realized in the BilkentDMRG.

3.2.1 Left-Canonical MPS

For a given wavefunction tensor $C_{\sigma_1; \sigma_2; \sigma_3 \dots \sigma_L}$ of equation (3.1) one can obtain canonical MPS. Here, we describe the procedure of obtaining Left-Canonical MPS (L-MPS).

Suppose $C_{\sigma_1; \sigma_2; \sigma_3 \dots \sigma_L}$ is given. In diagrammatic notations it has L legs, as it is shown in fig. One starts with converting this tensor to the matrix K of dimensions $\sigma_1 \times \prod_{j=2}^L \sigma_j$ where L is the total number of sites: $K_{\sigma_1; \sigma_2 * \sigma_3 * \sigma_4 \dots \sigma_L}$

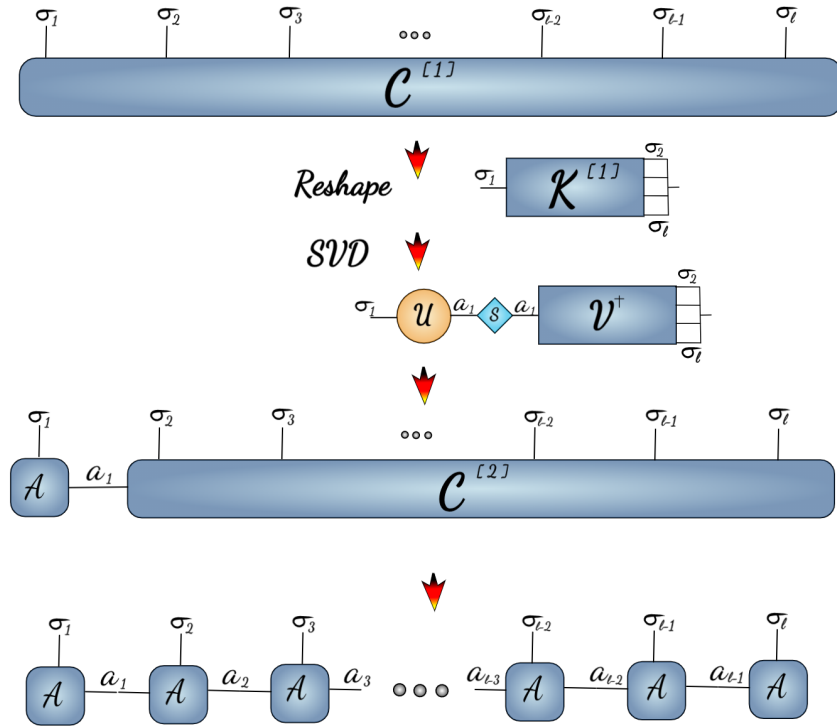


Figure 3.5: Diagrammatic representation of L-MPS generation process

Next, performing SVD of K gives:

$$K_{\sigma_1; \sigma_2 * \sigma_3 * \sigma_4 \dots \sigma_L} = \sum_{a_1} U_{\sigma_1; a_1} S_{a_1; a_1} V_{a_1; \sigma_2 * \sigma_3 * \sigma_4 \dots \sigma_L}^\dagger = \sum_{a_1} U_{\sigma_1; a_1} C_{a_1; \sigma_2 * \sigma_3 * \sigma_4 \dots \sigma_L}^{[2]} \quad (3.5)$$

where $C^{[2]}$ is obtained by multiplying $S * V^\dagger$. At this point, we reshape $U_{\sigma_1; a_1}$ to $A_{1; a_1}^{\sigma_1}$. Next iteration starts with reshaping $C_{a_1; \sigma_2 * \sigma_3 * \sigma_4 \dots \sigma_L}^{[2]}$ to $K_{a_1 * \sigma_2; \sigma_3 * \sigma_4 \dots \sigma_L}$ and

following SVD:

$$C_{\sigma_1; \sigma_2; \sigma_3 \dots \sigma_L} = \sum_{a_1, a_2} A_{1; a_1}^{\sigma_1} * U_{a_1 * \sigma_2; a_2} S_{a_2; a_2} V_{a_2; \sigma_3 * \sigma_4 \dots \sigma_L}^\dagger = \sum_{a_1, a_2} A_{1; a_1}^{\sigma_1} A_{a_1; a_2}^{\sigma_2} C_{a_2; \sigma_3 * \sigma_4 \dots \sigma_L}^{[3]} \quad (3.6)$$

One needs to repeat the process until A matrices are obtained for all sites. At the end of the procedure one has:

$$C_{\sigma_1; \sigma_2; \sigma_3 \dots \sigma_L} = \sum_{a_1, a_2, a_3 \dots a_L} A_{1; a_1}^{\sigma_1} A_{a_1; a_2}^{\sigma_2} A_{a_2; a_3}^{\sigma_3} \dots A_{a_{L-1}; 1}^{\sigma_L} \quad (3.7)$$

so that one can write wavefunction $|\Psi\rangle$ as:

$$|\Psi\rangle = \sum_{a_1, a_2, a_3 \dots a_L} A_{1; a_1}^{\sigma_1} A_{a_1; a_2}^{\sigma_2} A_{a_2; a_3}^{\sigma_3} \dots A_{a_{L-1}; 1}^{\sigma_L} |\sigma_1, \sigma_2, \dots, \sigma_L\rangle \quad (3.8)$$

The main property of tensors $A_{i-1; i}^{\sigma_i}$ is that they are left-normalized, i.e.:

$$\sum_{\sigma_i} (A^{\sigma_i})^\dagger A^{\sigma_i} = \mathbb{I} \quad (3.9)$$

3.2.2 Right-Canonical MPS

The procedure of generation of Right Canonical MPS (R-MPS) out of tensor $C_{\sigma_1; \sigma_2; \sigma_3 \dots \sigma_L}$ is similar to the generation procedure of L-MPS with a slight difference. The difference is that one should proceed from the right side of the chain, and reshape V^\dagger s as site matrices. So:

$$\begin{aligned} C_{\sigma_1; \sigma_2 \dots \sigma_{L-2}; \sigma_{L-1}; \sigma_L} &= K_{\sigma_1 * \sigma_2 \dots \sigma_{L-2} * \sigma_{L-1}; \sigma_L} = \\ &= \sum_{a_{L-1}} U_{\sigma_1 * \sigma_2 \dots \sigma_{L-2} * \sigma_{L-1}; a_{L-1}} S_{a_{L-1}; a_{L-1}} V_{a_{L-1}; \sigma_L}^\dagger = \sum_{a_{L-1}} C_{\sigma_1 * \sigma_2 \dots \sigma_{L-2} * \sigma_{L-1}; a_{L-1}}^{[2]} B_{a_{L-1}; 1}^{\sigma_{L-1}} \\ &= \sum_{a_{L-1}} K_{\sigma_1 * \sigma_2 \dots \sigma_{L-2}; \sigma_{L-1} * a_{L-1}}^{[2]} B_{a_{L-1}; 1}^{\sigma_{L-1}} = \\ &= \sum_{a_{L-1}, a_{L-2}} U_{\sigma_1 * \sigma_2 \dots \sigma_{L-2}; a_{L-2}} S_{a_{L-2}; a_{L-2}} V_{a_{L-2}; \sigma_{L-1} a_{L-1}}^\dagger B_{a_{L-1}; 1}^{\sigma_L} = \\ &= \sum_{a_{L-1}, a_{L-2}} C_{\sigma_1 * \sigma_2 \dots \sigma_{L-2}; a_{L-2}}^{[3]} B_{a_{L-2}; a_{L-1}}^{\sigma_{L-1}} B_{a_{L-1}; 1}^{\sigma_L} \end{aligned} \quad (3.10)$$

As one can see from equation (2.10) the logic behind of the procedure is the same as for L-MPS generation. At the end, one gets:

$$|\Psi\rangle = \sum_{a_1, a_2, a_3 \dots a_L} B_{1;a_1}^{\sigma_1} B_{a_1;a_2}^{\sigma_2} B_{a_2;a_3}^{\sigma_3} \dots B_{a_{L-2};a_{L-1}}^{\sigma_{L-1}} B_{a_{L-1};1}^{\sigma_L} |\sigma_1, \sigma_2, \dots, \sigma_L\rangle \quad (3.11)$$

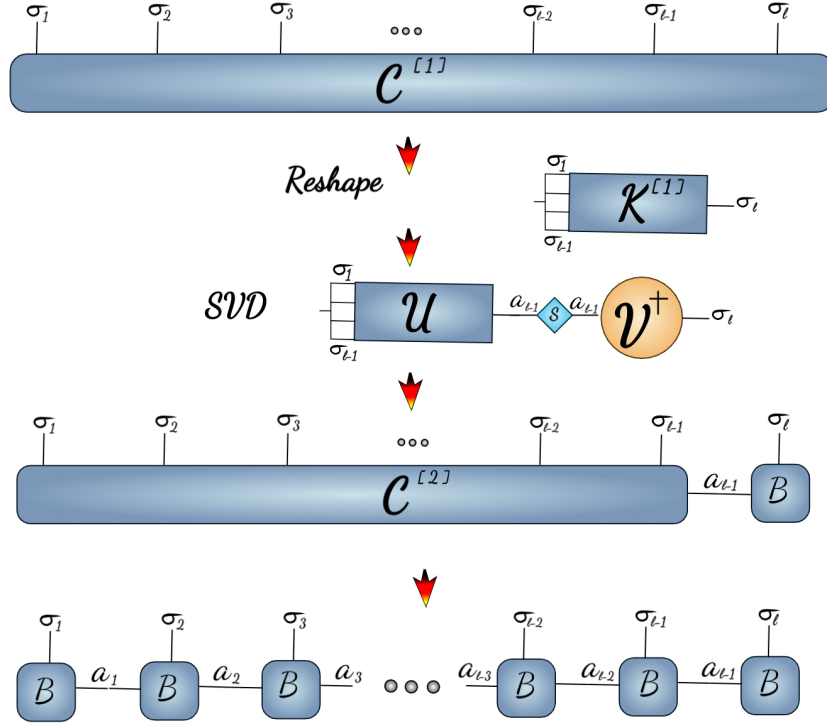


Figure 3.6: Diagrammatic representation of R-MPS generation process

The B tensors satisfy right-normalization condition, i.e

$$\sum_{\sigma_i} B^{\sigma_i} (B^{\sigma_i})^\dagger = \mathbb{I} \quad (3.12)$$

Now, for an arbitrary given quantum state of a chain of L sites we are able to get L-MPS and R-MPS representations.

3.2.3 Mixed-Canonical MPS

One can bipartite the chain of the length L to two parts from a given site $l < L$ and represent left side of the chain by L-MPS when right side with R-MPS. This is so called Mixed-Canonical MPS (M-MPS). Firstly, L - MPS up to site l can be obtained, i.e:

$$C_{\sigma_1; \sigma_2; \sigma_3 \dots \sigma_L} = \sum_{a_l} (A^{\sigma_1} A^{\sigma_2} \dots A^{\sigma_l})_{a_l} S_{a_l; a_l} V_{a_l; \sigma_{l+1} \dots \sigma_L}^\dagger \quad (3.13)$$

Now, we can reshape $V_{a_l; \sigma_{l+1} \dots \sigma_L}^\dagger$ to $K_{a_l \dots \sigma_{l+1} \dots \sigma_{L-1}; \sigma_L}$ so that it allows us to do R-MPS generation procedure and get a set of B tensors.

When the process is finished one gets:

$$C_{\sigma_1; \sigma_2; \sigma_3 \dots \sigma_L} = \sum_{a_l} (A^{\sigma_1} A^{\sigma_2} \dots A^{\sigma_l})_{1; a_l} S_{a_l; a_l} (B^{\sigma_{l+1}} B^{\sigma_{l+2}} \dots B^{\sigma_L})_{a_l; 1} \quad (3.14)$$

As an example, the diagrammatic M-MPS representation of the chain of $L = 6$ sites is show in the figure below.

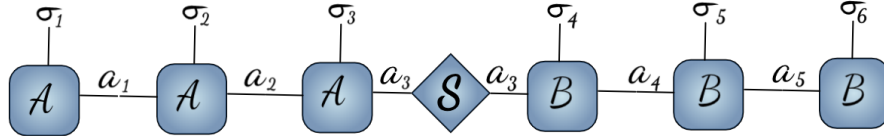


Figure 3.7: Diagrammatic M-MPS representation of a chain with $L = 6$ sites

Physical interpretation

At this point it is important to mention the physical meaning behind the Eq. 3.14. If we define new basis set by:

$$|a_l\rangle_A = \sum_{\sigma_1 \dots \sigma_l} (A^{\sigma_1} A^{\sigma_2} \dots A^{\sigma_l})_{1; a_l} |\sigma_1; \sigma_2; \sigma_3 \dots \sigma_l\rangle \quad (3.15)$$

$$|a_l\rangle_B = \sum_{\sigma_{l+1} \dots \sigma_L} (B^{\sigma_{l+1}} B^{\sigma_{l+2}} \dots B^{\sigma_L})_{a_l; 1} |\sigma_{l+1}; \sigma_{l+2}; \sigma_{l+3} \dots \sigma_L\rangle \quad (3.16)$$

Then, one can write Schmidt decomposition of bipartite chain as:

$$|\Psi\rangle = \sum_{a_l} s_a |a_l\rangle_A |a_l\rangle_B \quad (3.17)$$

Orthonormality of new basis sets is guaranteed by the properties of A and B tensors.

Assuming entanglement spectrum in the matrix s is sorted in descending order, one can judge about the entanglement character of the system, as it was discussed in Chapter 2.

3.2.4 Calculation of overlaps and expectation values

In this section, we discuss the wavefunction overlaps and calculating the general type of expectation values. As it was mentioned in Chapter 2, unlike standard DMRG algorithms, the procedure of calculating any type of correlators is a very easy job and can be numerically realized effectively.

We will calculating overlaps of the form: $\langle\psi|\phi\rangle$. We assume that for $|\psi\rangle$ MPS M and for $\langle\phi|$ MPS N are given. Then, their overlap can be calculated as:

$$\langle\psi|\phi\rangle = \sum_{\sigma_1, \sigma_2, \dots, \sigma_L} N^{\sigma_1\dagger} N^{\sigma_2\dagger} \dots N^{\sigma_L\dagger} M^{\sigma_1} M^{\sigma_2} \dots M^{\sigma_L} \quad (3.18)$$

Diagrammatically it has the following form:

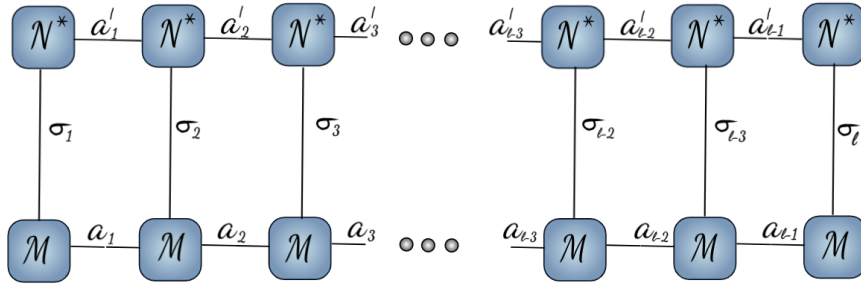


Figure 3.8: Diagrammatic representation of overlap calculation

Equation 3.18 can be regrouped as:

$$\langle \phi | \psi \rangle = \sum_{\sigma_L} N^{\sigma_L \dagger} (\dots (\sum_{\sigma_2} N^{\sigma_2 \dagger} (\sum_{\sigma_1} N^{\sigma_1 \dagger} M^{\sigma_1}) M^{\sigma_2})) M^{\sigma_L} \quad (3.19)$$

Obviously, it satisfies normalization condition $\langle \psi | \psi \rangle$ when MPS is left - normalized since, in every step of tensor contraction, one has identity matrices of the corresponding bond dimensions. As one can see, the calculation of overlaps leads to the tensor contractions.

Similarly, one can calculate the general type of expectation values with a slight difference.

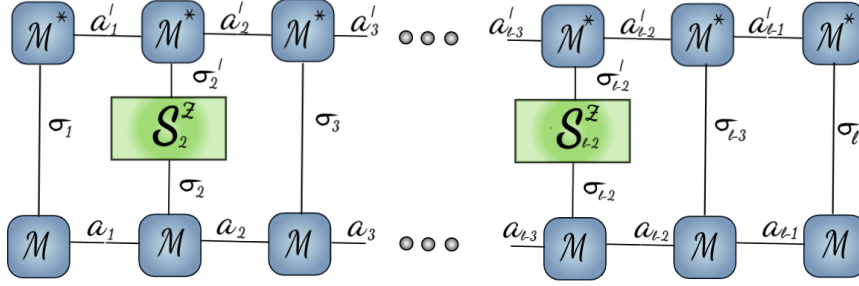


Figure 3.9: An example of MPS diagram for expectation value calculation

Suppose, for every site i an operator O_i is given. Then, one can easily calculate:

$$\langle \psi | O_1 O_2 \dots O_L | \psi \rangle = \sum_{\sigma_L, \sigma_{L'}} O^{\sigma_L, \sigma_{L'}} M^{\sigma_L \dagger} (\dots (\sum_{\sigma_2, \sigma_2'} O^{\sigma_2, \sigma_2'} M^{\sigma_2 \dagger} (\sum_{\sigma_1, \sigma_1'} O^{\sigma_1, \sigma_1'} M^{\sigma_1 \dagger} M^{\sigma_1'})) M^{\sigma_2'}) M^{\sigma_{L'}} \quad (3.20)$$

A general recipe for calculation of the correlators and overlap values is the following:

For calculating overlaps: calculate a set of matrices

$$C^{[l]} = \sum_{\sigma_l} M^{\sigma_l \dagger} C^{[l-1]} M^{\sigma_l} \quad (3.21)$$

iteratively, where $C^{[0]} = 1$ and the last matrix $C^{[L]}$ is the overlap to be calculated. For calculating of expectation values:

$$C^{[l]} = \sum_{\sigma_l, \sigma_{l'}} O^{\sigma_l, \sigma_{l'}} M^{\sigma_l \dagger} C^{[l-1]} M^{\sigma_{l'}} \quad (3.22)$$

where $C^{[L]}$ gives the expectation value for a given set of O 's (See also Fig. 3.11).

3.3 Matrix Product Operators

In this section, we show how operators can be written in MPS-like language, namely we introduce the concept of Matrix Product Operators (MPO). General representation of operator in the $|\sigma_1; \sigma_2; \sigma_3 \dots \sigma_L\rangle$ basis set is the following:

$$\hat{O} = \sum_{\sigma_1, \sigma_2, \dots, \sigma_L} \sum_{\sigma_1', \sigma_2', \dots, \sigma_L'} O^{\sigma_1 \sigma_1'; \sigma_2 \sigma_2'; \dots; \sigma_L \sigma_L'} |\sigma_1; \sigma_2; \sigma_3 \dots \sigma_L\rangle \langle \sigma_1', \sigma_2', \dots, \sigma_L'| \quad (3.23)$$

If any operator is given in a tensor form, it will have $2 * L$ legs and one needs to do SVD to get MPO. The diagrammatic form of arbitrary given MPO is shown in figure.

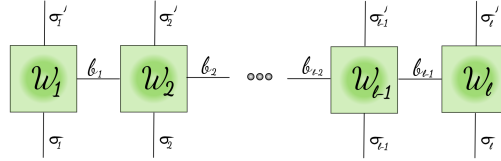


Figure 3.10: Diagrammatic representation of MPO

For every site, we have four-leg tensor W_i . As one can notice, similarly to the auxiliary bonds a_i of MPS, we have auxiliary bonds of MPO b_i . We rewrite (3.23) as:

$$\hat{O} = \sum_{\sigma_1, \sigma_2, \dots, \sigma_L} \sum_{\sigma_1', \sigma_2', \dots, \sigma_L'} \sum_{b_1, b_2, \dots, b_{L-1}} W_{1; b_1}^{\sigma_1 \sigma_1'} W_{b_1; b_2}^{\sigma_2 \sigma_2'} \dots W_{b_{L-1}; 1}^{\sigma_L \sigma_L'} |\sigma_1; \sigma_2; \sigma_3 \dots \sigma_L\rangle \langle \sigma_1', \sigma_2', \dots, \sigma_L'| \quad (3.24)$$

Expectation values $\langle \psi | \hat{O} | \psi \rangle$ can be diagrammatically represented as:

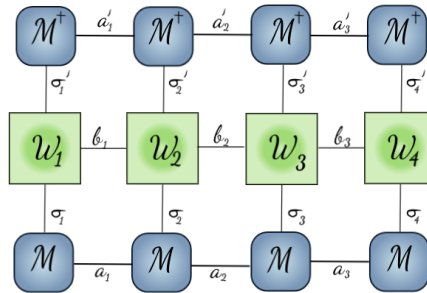


Figure 3.11: Diagrammatic representation of $\langle \psi | \hat{O} | \psi \rangle$

One can use the technique explained in the previous section, to calculate it.

3.3.1 Explicit form of MPO

Mostly, we are interested on construction of Hamiltonian MPOs for a chain of L sites with a given local operators h_i . As an example, we consider the following nearest-neighbor OBC Hamiltonian:

$$H = \sum_{i=1}^{L-1} h_i h_{i+1} \quad (3.25)$$

where local basis representation of h_i is assumed to be known. In tensor form, it can be written as:

$$\begin{aligned} H^{\sigma_1\sigma_1',\sigma_2\sigma_2',\dots,\sigma_L\sigma_L'} &= h_1^{\sigma_1\sigma_1'} \otimes h_2^{\sigma_2\sigma_2'} \otimes \mathbb{I}_3^{\sigma_3\sigma_3'} \otimes \dots \otimes \mathbb{I}_L^{\sigma_L\sigma_L'} + \\ &+ \mathbb{I}_1^{\sigma_1\sigma_1'} \otimes h_2^{\sigma_2\sigma_2'} \otimes h_3^{\sigma_3\sigma_3'} \otimes \mathbb{I}_4^{\sigma_4\sigma_4'} \otimes \dots \otimes \mathbb{I}_L^{\sigma_L\sigma_L'} + \\ &\dots \\ &+ \mathbb{I}_1^{\sigma_1\sigma_1'} \otimes \mathbb{I}_2^{\sigma_2\sigma_2'} \otimes \mathbb{I}_3^{\sigma_3\sigma_3'} \otimes \dots \otimes h_{L-1}^{\sigma_{L-1}\sigma_{L-1}'} \otimes h_L^{\sigma_L\sigma_L'} \end{aligned} \quad (3.26)$$

The equation above, can be written as MPO:

$$\begin{aligned} W_1^{\sigma_1\sigma_1'} &= \begin{bmatrix} \mathbb{I}^{\sigma_1\sigma_1'} & h_1^{\sigma_1\sigma_1'} & 0 \end{bmatrix} \\ W_i^{\sigma_i\sigma_i'} &= \begin{bmatrix} \mathbb{I}^{\sigma_i\sigma_i'} & h_i^{\sigma_i\sigma_i'} & 0 \\ 0 & 0 & h_i^{\sigma_i\sigma_i'} \\ 0 & 0 & \mathbb{I}^{\sigma_i\sigma_i'} \end{bmatrix} \\ W_L^{\sigma_L\sigma_L'} &= \begin{bmatrix} 0 \\ \mathbb{I}^{\sigma_L\sigma_L'} \\ h_L^{\sigma_L\sigma_L'} \end{bmatrix} \end{aligned} \quad (3.27)$$

One can check this result by the direct matrix multiplication and get the same result.

Similarly, one can get MPO for 1D Heisenberg Hamiltonian in a magnetic field with general spin value S which is defined as (XXX Heisenberg chain):

$$H = \sum_{i=1}^{L-1} J \vec{S}_i \vec{S}_{i+1} - h \sum_{i=1}^{L-1} S_i^z \quad (3.28)$$

$$\begin{aligned}
W_1^{\sigma_1\sigma_1'} &= \begin{bmatrix} \mathbb{I}^{\sigma_1\sigma_1'} & \frac{J}{2} [S^+]^{\sigma_1\sigma_1'} & \frac{J}{2} [S^-]^{\sigma_1\sigma_1'} & J [S^z]^{\sigma_1\sigma_1'} & -h [S^z]^{\sigma_1\sigma_1'} \end{bmatrix} \\
W_i^{\sigma_i\sigma_i'} &= \begin{bmatrix} \mathbb{I}^{\sigma_i\sigma_i'} & \frac{J}{2} [S^+]^{\sigma_i\sigma_i'} & \frac{J}{2} [S^-]^{\sigma_i\sigma_i'} & J [S^z]^{\sigma_i\sigma_i'} & -h [S^z]^{\sigma_i\sigma_i'} \\ 0 & 0 & 0 & 0 & [S^-]^{\sigma_i\sigma_i'} \\ 0 & 0 & 0 & 0 & [S^+]^{\sigma_i\sigma_i'} \\ 0 & 0 & 0 & 0 & [S^z]^{\sigma_i\sigma_i'} \\ 0 & 0 & 0 & 0 & [\mathbb{I}]^{\sigma_i\sigma_i'} \end{bmatrix} \\
W_L^{\sigma_L\sigma_L'} &= \begin{bmatrix} -h [S^z]^{\sigma_i\sigma_i'} \\ [S^-]^{\sigma_i\sigma_i'} \\ [S^+]^{\sigma_i\sigma_i'} \\ [S^z]^{\sigma_i\sigma_i'} \\ [\mathbb{I}]^{\sigma_i\sigma_i'} \end{bmatrix}
\end{aligned} \tag{3.29}$$

There are several analytical algorithms [31] which can be used to construct MPO for a given Hamiltonian of a general type, but this topic is the out of the scope of this thesis.

3.4 Variational MPS DMRG

Now, when MPS and MPO are introduced, we can formulate analog of Finite-size White's DMRG procedure in the language of MPS and MPOs. The idea is the same: by the procedure of sweeping one minimizes ground state energy E_{GS} .

Here, as an example, we will consider XXZ spin $S = \frac{1}{2}$ Heisenberg chain with L sites under the magnetic field and explain the main idea of the algorithm step by step.

1: Generate R-MPS One starts with creating Right-Normalized random MPS, which is assumed to be normalized. Since the auxiliary bond dimensions of

MPS grows fast, one needs to cut it whenever $a_l > \chi$. When $\langle \Psi_{rand} | H | \Psi_{rand} \rangle$ is calculated, it brings random number, since R-MPS is random. The idea behind the algorithms is to update the MPS site by site beginning from the first.

At this point it makes to grasping process easier if 'Right-Block' and 'Left-Block' tensors are introduced. By Right-Block $R_{a_j; b_j; a'_j}^{[j]}$ we mean the tensor of the rank 3, which holds all information about other part of the chain with $l > j$. Thus, in order to get $R^{[j]}$ one needs to contract all tensors which are in the right. Obviously, $R_{1;1;1}^{[L]} = 1$. In the figure below, as an example it is shown $R_{a_2; b_2; a'_2}^{[2]}$ of the chain of $L = 4$ sites. Similarly, the Left-Block $L_{a_{j-1}; b_{j-1}; a'_{j-1}}^{[j]}$ contains all information about from $l = 1$ to $j - 1$. Mathematically, they can be defined as:

$$R_{a_j, b_j, a'_j}^{[j]} = \sum_{\sigma_{[j+1:L]}; \sigma'_{[j+1:L]}} \sum_{a_{[j+1:L]}; a'_{[j+1:L]}} \sum_{b_{[j+1:L]}} \left(B_{a'_j; a'_{j+1}}^{* \sigma_{j+1}'} W_{b_j; b_{j+1}}^{\sigma_{j+1} \sigma'_{j+1}} B_{a_j; a_{j+1}}^{\sigma_{j+1}} \right) \times \dots$$

$$\dots \times B_{a'_{L-1}; 1}^{* \sigma_{L-1}'} W_{b_{L-1}; 1}^{\sigma_{L-1} \sigma'_{L-1}} B_{a_{L-1}; 1}^{\sigma_{L-1}}$$
(3.30)

. and for the Left - Block:

$$L_{a_{j-1}, b_{j-1}, a'_{j-1}}^{[j]} = \sum_{\sigma_{[1:j-1]}; \sigma'_{[1:j-1]}} \sum_{a_{[1:j-2]}; a'_{[1:j-2]}} \sum_{b_{[1:j-2]}} \left(A_{1; a'_1}^{* \sigma_1'} W_{1; b_1}^{\sigma_1 \sigma'_1} A_{1; a_1}^{\sigma_1'} \right) \times \dots$$

$$\dots \times A_{a'_{j-2}; a'_{j-1}}^{* \sigma_{j-1}'} W_{b_{j-2}; b_{j-1}}^{\sigma_{j-1} \sigma'_{j-1}} A_{a_{j-2}; a_{j-1}}^{\sigma_{j-1}}$$
(3.31)

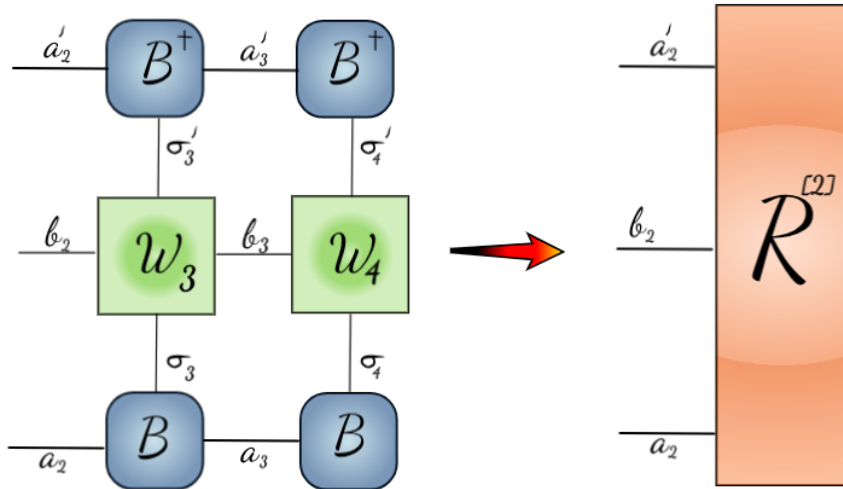


Figure 3.12: Right-Block R_2 tensor for $L = 4$

As one can see from the figure, if all necessary bonds are contracted only three legs will be remained: $[a_2; b_2; a'_2]$

Step 2: Generate Right-Blocks To find the most optimized MPS for the first site one needs to calculate $R^{[j]}$'s for all j 's. For our example with $L = 4$ one has to calculate $R^{[1,2,3,4]}$ tensors, where the last one is identity tensor of rank 3.

Step 3: Generate MPO for a given Hamiltonian Prepare MPO for a given Hamiltonian. In our XXZ Hamiltonian MPO is given by equation (3.29) , so that for L sites you have L 4-leg tensors of the form $W_{b_{j-1}, b_j}^{\sigma_j, \sigma'_j}$.

Step 4: Obtain Hamiltonian matrix At this point, we start to describe Right-sweeping on which we are going to optimize every site from $l = 1$ to $l = 4$. We start with optimizing the first site MPS. For this, one needs $R^{l=1}$ and $L^{l=1} = 1$. Contract $R_{a_1; b_1; a'_1}^{[1]}$ with $W_{b_0; b_1}^{\sigma_1, \sigma'_1}$. Then resulting 4-leg tensor $G_{\sigma_1; \sigma'_1; a_1; a'_1}$ can be contracted with $L_{a_0; b_0; a'_0}^{[1]}$, which should be reshaped to Hamiltonian $H_{\sigma_1 * a_0 * a_1; \sigma'_1 * a'_0 * a'_1}^{[1]}$. So for any given site j one can form Hamiltonian of the form:

$$H_{(\sigma_j * a_{j-1} * a_j); (\sigma'_j * a'_{j-1} * a'_j)}^{[j]} = \sum_{b_j; b_{j-1}} L_{a_j; b_{j-1}; a'_{j-1}}^{[j]} W_{b_{j-1}; b_j}^{\sigma_j, \sigma'_j} R_{a_j; b_j; a'_j}^{[j]} \quad (3.32)$$

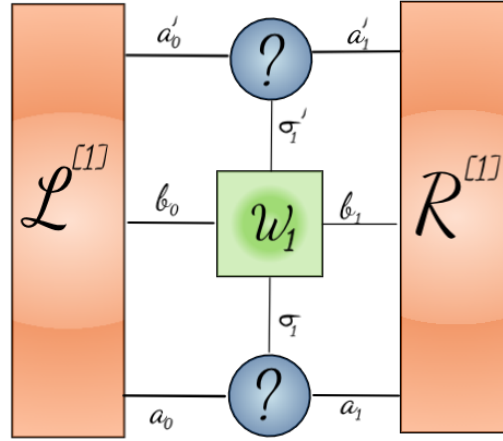


Figure 3.13: Tensor contractions to obtain Hamiltonian

Step 5: SVD of the GS wavefunction When Hamiltonian $H^{[1]}$ is obtained, one can get ground state by diagonalization of the matrix:

$$H^{[1]} |\psi\rangle = E_{GS} |\psi\rangle \quad (3.33)$$

Next step is one should do SVD of obtained $|\psi\rangle$ and reshape $U_{a_{j-1}^* \sigma; a_j}$ to a new site tensor $A_{a_{j-1}, a_j}^{\sigma_j}$. This step is needed to keep all left side tensors left normalized, so that after full right sweeping we have left normalized MPS. For our specific example, finally we have $A_{a_0, a_1}^{\sigma_1}$ and the ground state energy $E_{GS}^{[1]}$. One can use $s * V^\dagger$ as a guess when updating the next site

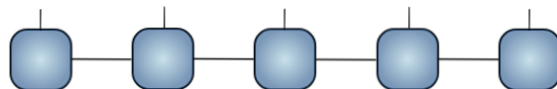
Step 6: Left-Block generation for $j = 2$ Now, when we have new $A^{[1]}$ tensor for site $j = 1$, we can generate Left-Block tensor $L^{[2]}$. Then, one can repeat step 4 to contract $L^{[2]} - W^{[2]} - R^{[2]}$ and to get new Hamiltonian and consequently get new left-normalized tensor for site $j = 2$ $A^{[2]}$ with $E_{GS}^{[2]}$. One needs to repeat the site update process until the end of the chain. At this point, right-sweeping process is finished. During the process, ground state energy should decrease by the value in every new site update, i.e $E_{GS}^{[1]} > E_{GS}^{[2]} > \dots > E_{GS}^{[L]}$.

Step 6: Left sweeping When full right sweeping is done, we have L-MPS with corresponding left blocks $L^{[1\dots L]}$. The process of left - sweeping is identical to the right sweeping one: one needs to generate new $B^{[l]}$ tensors for every site iteratively beginning from the end of the chain.

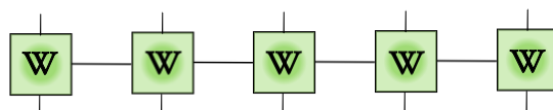
Algorithm 4 Variational MPS algorithm

- 1: Create random MPS. Right-Normalize it.
 - 2: Right Sweeping: Create right blocks R^j
 - 3: Generate MPO for a given analytic Hamiltonian.
 - 4: Form Hamiltonian Matrix out of Left-Block and Right-Blocks, and MPO and diagonalize it.
 - 5: Do SVD on obtained $|\psi\rangle$ and save U as the site MPS A . Multiply sV^\dagger and save it for next iteration wavefunction guess.
 - 6: Get Left-Block including new obtained site.
 - 7: Repeat the procedure until the last site is updated.
 - 8: Perform Left-sweeping.
 - 9: Perform Right-Left sweepings until the energy converged with a given accuracy
-

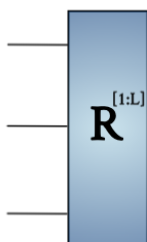
Step 1: Generate random R-MPS:



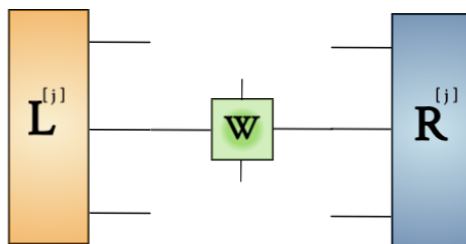
Step 2: Generate MPO:



Step 3: Generate right blocks $R^{[1:L]}$:



Step 4: Form Hamiltonian matrix:



Step 5: Do SVD of $|\Psi\rangle$

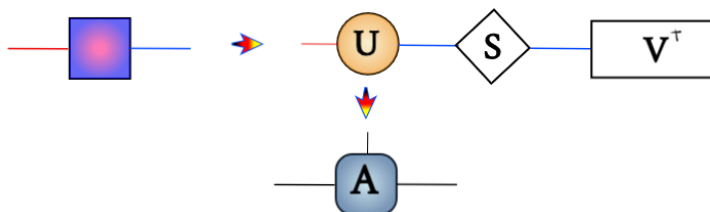
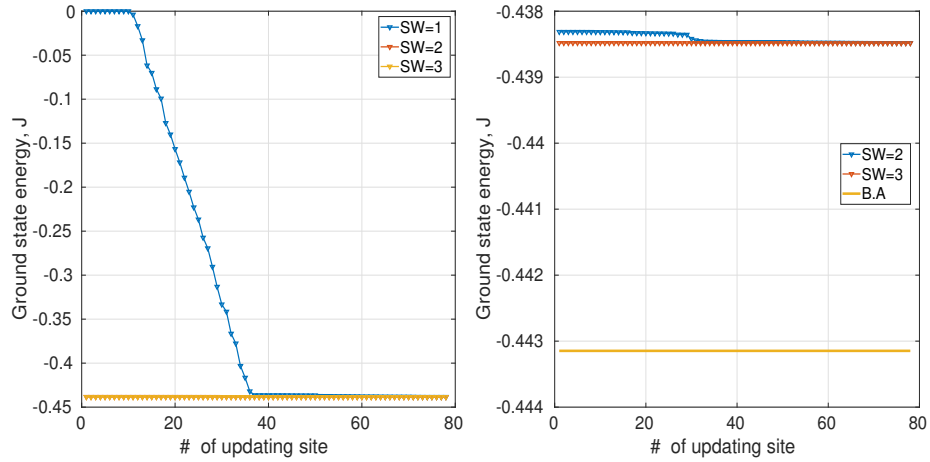


Figure 3.14: Variational MPS algorithm



(a) Convergence process of E_{GS} during sweeping process (b) Comparison of E_{GS} with Bethe-Ansatz solution

Figure 3.15: Ground state energy per site calculated using VMPS algorithm

3.4.1 Variational MPS for XXX Heisenberg chain

In this section, we check our implemented Variational MPS algorithm which is a part of BilkentDMRG program in the example of XXX Heisenberg chain with the following parameters:

- Model parameters: $J_x = J_y = J_z = 1$;
- DMRG parameters: $N = 100$; $\chi = 10$; $N_{sw} = 3$;

Ground state calculations

In the Figure 3.15 (a) one can see calculated $E_{GS}^{[j]}$ per site in every site update in every full sweepings. It has the value of $E_{GS} = 0$ in the beginning of the process, and converges to the value of $E_{GS} \approx -0.435J$ when first left sweeping is performed. Next sweepings results on change of the value to $E_{GS} = 0.4385J$ as it can be seen in Figure 3.15 (b). In the figure also the exact analytic Bethe Ansatz value in $E_{GS} = 1/4 - \ln(2) \approx -0.4431J$ thermodynamic limit is shown. Even if for a large number of sites E_{GS} are stable and well converged, the VMPS

algorithm fails when there are local minima around. These minima make VMPS gets stuck on them and as a result wrong $|\psi\rangle$ will be accepted as ground state wavefunction. The problem cannot be even solved when the number of sweepings increased. This is because our initial guess was a set of random matrices. As an example, the figure below shows the VMPS algorithm implemented for $L = 6$ site XXX Heisenberg chain. Even after 3 sweeps, energy is not well converged and has spike values in some site updates. This means to get correct value one needs good initial guess of the initial wavefunction. This can be obtained by infinite-size MPS DMRG algorithm.

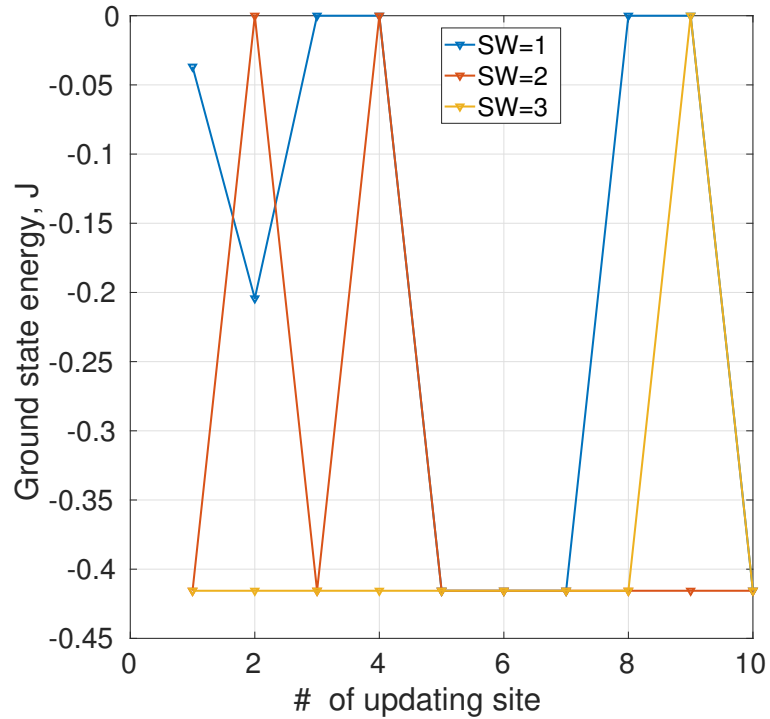


Figure 3.16: Ground state energy per site calculated using VMPS algorithm

3.5 Infinite-size MPS DMRG

In this part we are going to describe Infinite-size DMRG (iDMRG) [30] in terms of MPS. This algorithm provides a very good initial guess of the wavefunction so that VMPS can be implemented to make it precise ground state wavefunction.

Here we consider only two-site iDMRG, while it can be extended easily by following the logical path behind the method.

The algorithm is very similar to standard White's IDMRG and has the same idea behind it. Here we briefly explain the basic idea behind the algorithm.

Step 1 Get MPO for a given analytically defined Hamiltonian; This step is similar to one in VMPS algorithm.

Step 2 Make two identity left-block and right block tensors of the rank 3. That is $L_{a_0; b_0; a'_0}^{[1]}$ and $R_{a_L; b_L; a'_L}^{[L]}$ where all indexes are $a_0 = b_0 = a'_0 = a_L = b_L = a'_L = 1$.

Step 3 Contract the left-block tensor to the first site MPO $W_{b_0, b_1}^{\sigma_1 \sigma'_1}$ and the last site MPO $W_{b_{L-1}, b_L}^{\sigma_L \sigma'_L}$ with the right-block and then contract them together. Reshape the resulting tensor to get a Hamiltonian matrix.

Step 4 Diagonalize the Hamiltonian matrix. Perform SVD to the reshaped ground state $|\psi\rangle$. Save U as the first site tensor $A_{a_0; a_1}^{\sigma_1}$ and V^\dagger as the last site tensor $B_{a_{L-1}; a_L}^{\sigma_L}$.

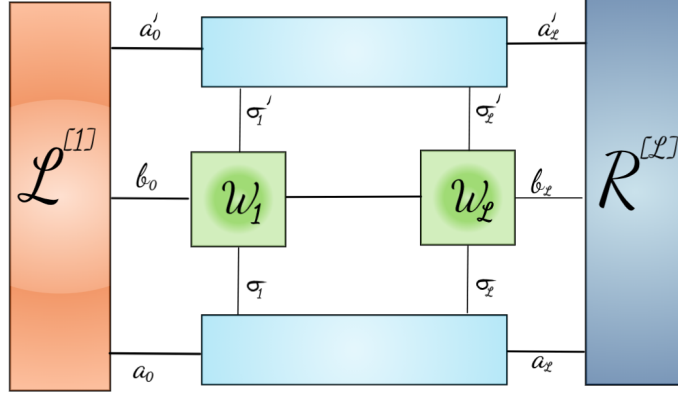


Figure 3.17: General iDMRG procedure: L-W-W-R contractions

Step 5 Enlarge the left - block contracting it with $A_{a_0; a_1}^{\sigma_1}$ tensor and the right- block with $B_{a_{L-1}; a_L}^{\sigma_L}$. Resulting tensors are $R_{a_{L-1}; b_{L-1}; a'_{L-1}}^{[L-1]}$ and $L_{a_1; b_1; a'_1}^{[2]}$.

Step 6 Repeat the process: contract two new $W_{b_1; b_2}^2$ and $W_{b_{L-2}; b_{L-1}}^{L-1}$ and then contract them with $R_{a_{L-1}; b_{L-1}; a'_{L-1}}^{[L-1]}$ and $L_{a_1; b_1; a'_1}^{[2]}$. Form new Hamiltonian and get the ground state tensor. Reshape it and do SVD. At this point it is important to mention that the auxiliary bond dimensions of $A_{a_{j-1}; a_j}^{\sigma_j}$ and $B_{a_{L-j+1}; a_{L-j}}^{\sigma_{L-j}}$ increases in every step. When it becomes larger than given χ , one needs to keep only χ vectors of U matrix and χ vectors of V^\dagger matrix, so that the resulting $a_j = a_{L-j+1} = \chi$.

As a result, one has M-MPS bipartited in the middle of the chain. Now, one can Right-Normalize M-MPS and perform VMPS.

Ground state energy E_{GS} calculation

For the famous XXX Heisenberg chain with a given set of parameters:

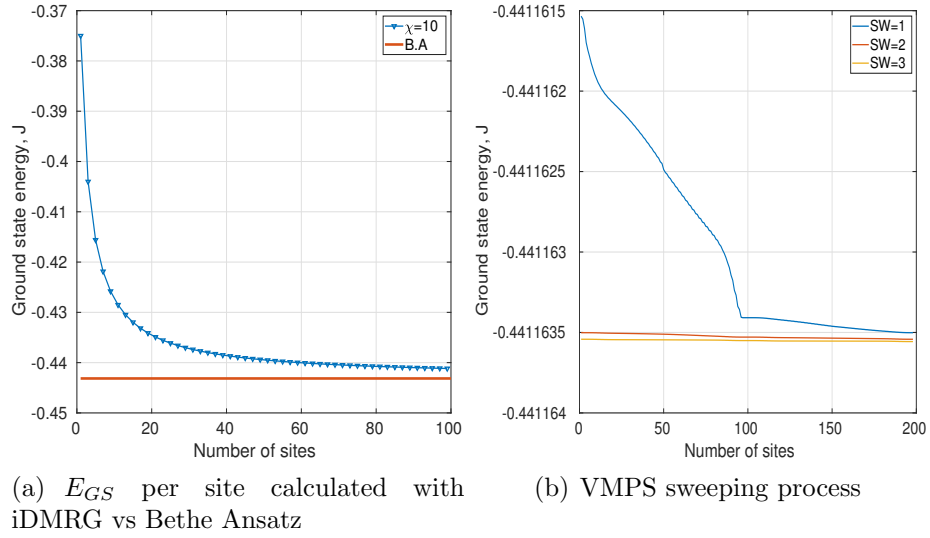


Figure 3.18: VMPS sweeping process

- Model parameters: $J_x = J_y = J_z = 1$;
- DMRG parameters: $N = [6 : 100]$; $\chi = 10$; $N_{sw} = 3$;

we performed iDMRG and following VMPS calculation of E_{GS} per site. As one has noticed, the converging process of iDMRG is similar to one in standard algorithm. Following 3 sweeps of VMPS calculation makes calculated energy per site to converge to the value $E_{GS} = -0.4411635J$.

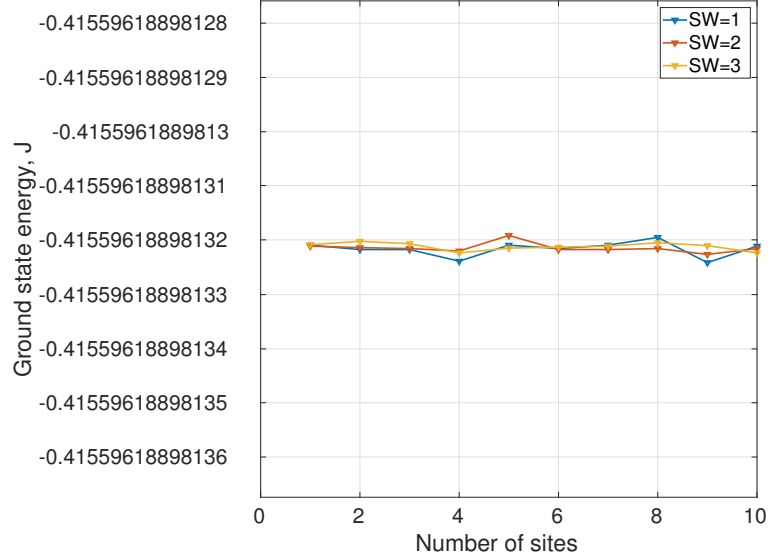


Figure 3.19: General iDMRG procedure: L-W-W-R contractions

Fig.3.19 shows E_{GS} values during 3 sweeping VMPS calculation of a chain with $L = 6$ sites. The guess wavefunction now is R-MPS which is obtained after the iDMRG procedure. As one can see, there are not any spikes, and the energy per site is well converged to the value $E_{GS} = -0.415596J$, which has an absolute error of the order 10^{-7} with respect to the exact diagonalization value. These good results suggest to perform iDMRG firstly and then do VMPS calculations to get well-converged ground state wavefunction.

Bond strength and Correlation functions

In this section, we show calculated physical properties of XXX chain of the length $L = 100$. The maximum auxiliary bond has a value of $\chi = 10$ and $N_{sw} = 3$. The bond strength is defined as $\langle \Psi | \vec{S}_i \vec{S}_{i+1} | \Psi \rangle$, as in the previous section. As one can see from Fig. 3.20 (a) bond strength averages to a value of E_{GS} per spin. Also one can notice that at the edges of the chain, oscillation amplitude is high due to finite size effects. This result matches with a result of White obtained in original paper [28].

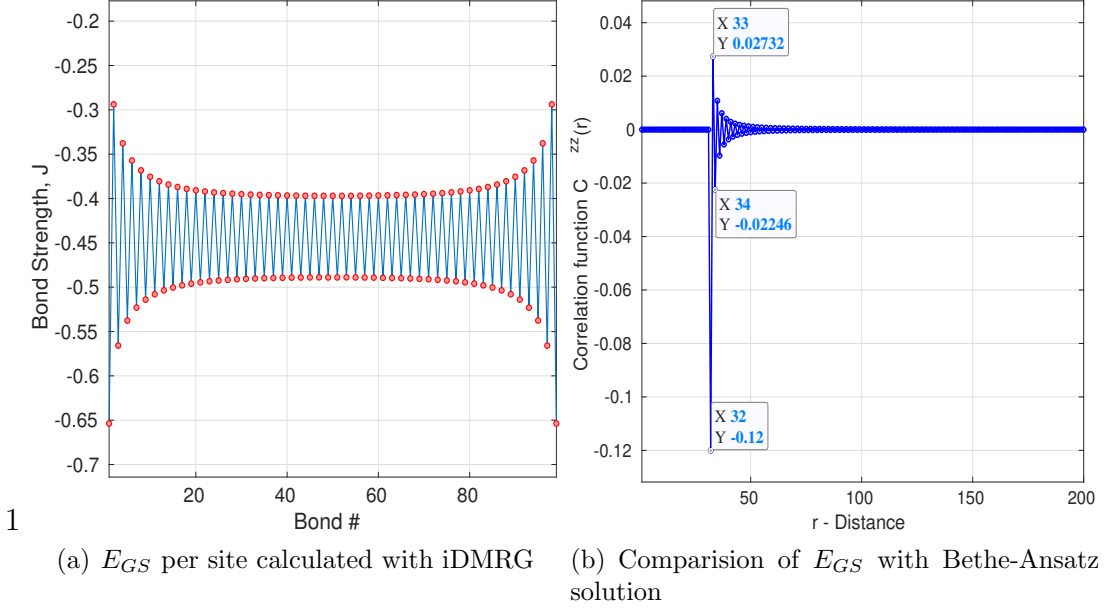


Figure 3.20: VMPS calculation followed after iDMRG procedure

Next, we calculated correlation function $C^{zz}(r)$ for XXZ model with $\Delta = \frac{1}{2}$ for longer chain with $N = 200$. It is an oscillating function in a distance and $|C^{zz}(r)|$ shows power-law decaying behavior. Numerical values for three nearest neighbors $C^{zz}(1) = -0.12$, $C^{zz}(2) = 0.0273$ and $C^{zz}(3) = -0.0224$ are in a good agreement with an exact theoretical values $C^{zz}(1) = -0.125$, $C^{zz}(2) = \frac{7}{256} \approx 0.0273$ and $C^{zz}(3) = \frac{401}{16384} \approx -0.0245$ [32]. These values can be calculated more accurately by an increase of auxiliary bonds of MPS χ .

Phases of XXZ chain

To check numerical stability and availability of phase transition detection, we use our package to identify 2 main phases of XXX chain under the magnetic field, namely the XY phase and Ferromagnetic phase [33]. Also, we will check the ground state phase of the XXZ chain with $\Delta = 2 \gg J_{x,y}$, which is known to be in the Neel phase.

We use standard correlation functions to identify Neel order (AF), Ferromagnetic

order which are defined as:

$$O^F = \lim_{r \rightarrow \infty} G_F^{zz}(r) = \lim_{r \rightarrow \infty} \langle \Psi | S_i^z S_{i+r}^z | \Psi \rangle \quad (3.34)$$

and for Neel order:

$$O^N = \lim_{r \rightarrow \infty} G_N^{zz}(r) = \lim_{r \rightarrow \infty} (-1)^{|i-r|} \langle \Psi | S_i^z S_{i+r}^z | \Psi \rangle \quad (3.35)$$

We used following parameters:

- Model parameters: $J_z = 2$; $J_x = J_y = 1$; $L = 160$;
- DMRG parameters: $\chi = 20$; $N_{sw} = 3$;

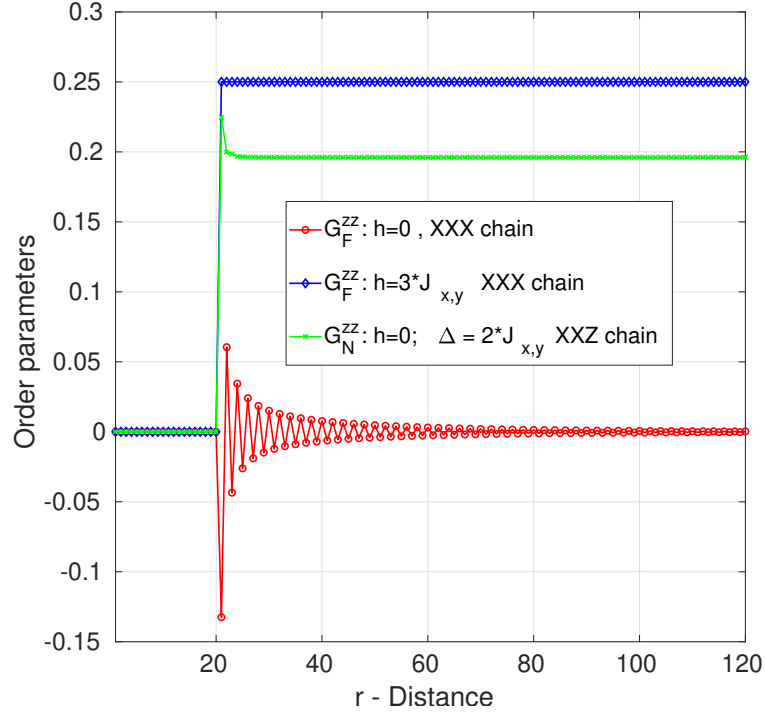


Figure 3.21: Two point correlators behavior in different XXZ chain phases

As one notices, XXX chain in the limit if big $h \gg J_{x,y} = 1$ has ferromagnetic phase, while in the absence of a magnetic field, the ground state is in disordered XY phase. Also, one can get Neel phase in the limit of big z-component anisotropy $\Delta \gg J_{x,y}$.

At this point, we conclude that in the numerical package BilkentDMRG is giving consistent results and can be used for research further.

Chapter 4

Bond-Alternating Heisenberg Chain

In this chapter, we consider our main model BAHC to study quantum trivial zero-temperature quantum phase transition under the magnetic field. Firstly, for this purpose, we use the Jordan-Wigner fermionization of the chain, which maps the model to a fermionic 1D chain. We calculate ground state energy per spin and also zero temperature magnetization and susceptibility for a corresponding fermionic model. To get a more intuitive picture of ground state phase, we calculate spin-spin correlation functions for every spin components both analytically and numerically. For numerical treatment, we use MPS-DMRG algorithms presented in the previous chapter.

4.1 Fermionization approach for quantum spin chains

While quantum many-body physics for fermions and bosons are well developed, for quantum spin chains it is not. The reason behind it is the more involved algebra, a rather standard Heisenberg-Weyl algebra which makes physics more

complicated. Thus, it is better to transform spin algebra to one of the previously mentioned algebra: for bosons or fermions.

From the perspective of mapping to bosons, the non-linear transformation of Holstein-Primakoff [34] can be used to map any spin S to a bosonic system by :

$$\begin{aligned} S_i^+ &= \sqrt{2S - a_i^\dagger a_i} a_i; \\ S_i^- &= a_i^\dagger \sqrt{2S - a_i^\dagger a_i} \\ S_i^z &= a_i^\dagger a_i - \frac{1}{2} \end{aligned} \tag{4.1}$$

However, it suffers from two major problems: Kinematic problem and non-linearity. The kinematic problem is related to the fact that the dimension of bosonic Hilbert space is infinity, while spin has a finite dimension of Hilbert space, meaning one needs to restrict the maximum number of bosons per site. While the second can be solved by expanding the non-linear term for large S , the first one hard to solve.

In any case, mapping to the bosonic system is not convenient for our purpose, since we have spin $S = 1/2$ system. Thus, in this work, instead of mapping to bosonic algebra, we use the Jordan-Wigner fermionization, which has more elegant form rather than bosonic projectors.

4.1.1 Jordan-Wigner transformation

The Jordan-Wigner transformation maps spin $S = \frac{1}{2}$ to fermions, by non-local transformation. To clarify the idea behind of Jordan-Wigner transformation (JWT), we start with commutation relations of spins and fermions.

Fermions obey to canonical anticommutation relation for the same site:

$$\{c_i^\dagger, c_i\} = \mathbb{I} \tag{4.2}$$

so for different sites $[i; j]$

$$\{c_i^\dagger, c_j\} = 0 \tag{4.3}$$

It is well known that spins on the different sites $[i; j]$ commute, while on the same site anticommute:

$$[S_i^+, S_j^-] = 2S_i^z \delta_{i,j}; \tag{4.4}$$

One can get anticommutation relations of spins:

$$\{S_i^+, S_j^-\} = [S_i^+, S_j^-] + 2S_j^- S_i^+ = 2S_i^z \delta_{i,j} + 2S_j^- S_i^+ \quad (4.5)$$

From equation above, one can derive that for the the same sites

$$\{S_i^+, S_i^-\} = \mathbb{I} \quad (4.6)$$

while for different sites i and j ,

$$\{S_i^+, S_j^-\} = 2S_j^- S_i^+ \quad (4.7)$$

By comparing anticommutation relations, one can see that anticommutation relation is similar to the fermionic one on the same sites, while for different sites it is different.

The question to which JWT answers is that whether spins anticommutation relations can be satisfied by using fermionic operators. Mathematically, can we find such operators consisting of fermionic operators such that they satisfy anticommutation relations of spins?

To do this, Jordan and Wigner [35] in 1932 proposed the following relations :

$$S_i^+ = c_i^\dagger e^{i\pi \sum_{k<i} c_k^\dagger c_k} \quad (4.8)$$

$$S_i^- = e^{-i\pi \sum_{k<i} c_k^\dagger c_k} c_i \quad (4.9)$$

$$S_i^z = c_i^\dagger c_i - 1/2 \quad (4.10)$$

The intuitive physical picture can be grasped from last equation: if there is no fermion at site i ($n_i = 0$), in equivalent spin chain at that site spin has $m_i^z = -\frac{1}{2}$. Obviously, $S_i^+ S_i^- = c_i^\dagger c_i$ and $S_i^- S_i^+ = c_i c_i^\dagger$. Thus, $[S_i^+, S_i^-] = (c_i^\dagger c_i - c_i c_i^\dagger) = (c_i^\dagger c_i - (1 - c_i^\dagger c_i)) = 2c_i^\dagger c_i - 1 = 2S_i^z$;

Also, anticommutation relation (4.6) on the same site is satisfied. Similarly, for $j > i$ one has:

$$S_i^+ S_j^- = c_i^\dagger e^{-i\pi \sum_{k=i}^{k=j-1} c_k^\dagger c_k} c_i = c_i^\dagger e^{-i\pi c_i^\dagger c_i} c_i e^{-i\pi \sum_{k=i+1}^{k=j-1} c_k^\dagger c_k} \quad (4.11)$$

Next, it is useful to simplify: $e^{-i\pi c_i^\dagger c_i} = e^{-i\pi \hat{n}_i}$:

$$e^{-i\pi \hat{n}_i} = \sum_{p=0}^{p=\infty} \frac{(-i\pi \hat{n}_i)^p}{p!} = \mathbb{I} + \hat{n}_i \sum_{p=1}^{p=\infty} \frac{(-i\pi)^p}{p!} = \mathbb{I} + \hat{n}_i (e^{-i\pi} - 1) = \mathbb{I} - 2\hat{n}_i \quad (4.12)$$

Similarly, $e^{i\pi\hat{n}_i} = \mathbb{I} - 2\hat{n}_i$. Using these relations, equation (4.11) can be written in the form:

$$S_i^+ S_j^- = c_i^\dagger e^{-i\pi c_i^\dagger c_i} c_j e^{-i\phi} = c_i^\dagger (\mathbb{I} - 2\hat{n}_i) c_j e^{-i\phi} = c_i^\dagger (\mathbb{I} - 2c_i^\dagger c_i) c_j e^{-i\phi} = c_i^\dagger c_j e^{-i\phi} \quad (4.13)$$

where

$$\phi = \pi \sum_{k=i+1}^{k=j-1} c_k^\dagger c_k \quad (4.14)$$

For $S_j^- S_i^+$ we have

$$\begin{aligned} S_j^- S_i^+ &= e^{-i\pi \sum_{k<j} c_k^\dagger c_k} c_j c_i^\dagger e^{i\pi \sum_{k<i} c_k^\dagger c_k} = c_j e^{-i\pi \sum_{k=i}^{k=j-1} c_k^\dagger c_k} c_i^\dagger = c_j (\mathbb{I} - 2c_i^\dagger c_i) c_i^\dagger e^{-i\phi} = \\ &= (c_j c_i^\dagger - 2c_j c_i^\dagger c_i c_i^\dagger) e^{-i\phi} = -c_j c_i^\dagger e^{-i\phi} = c_i^\dagger c_j e^{-i\phi} \end{aligned} \quad (4.15)$$

It is clear that commutation relationship (4.4) for different $[i; j]$ sites is satisfied.

4.1.2 Jordan-Wigner Transformation for XXZ model

One of the first application of JWT was for spin-1/2 XXZ model under the magnetic field B . One more time, XXZ Hamiltonian has the following form:

$$H = \sum_{i=1}^N J^z S_i^z S_{i+1}^z + \frac{J}{2} (S_i^+ S_{i+1}^- + S_i^- S_{i+1}^+) - B \sum_{i=1}^N S_i^z \quad (4.16)$$

The first and the last terms, transforms easily with equation (4.10) to:

$$\sum_{i=1}^N J^z S_i^z S_{i+1}^z = \sum_{i=1}^N J^z (c_i^\dagger c_i - 1/2)(c_{i+1}^\dagger c_{i+1} - 1/2) \quad (4.17)$$

$$-B \sum_{i=1}^N S_i^z = -B \sum_{i=1}^N (c_i^\dagger c_i - 1/2) \quad (4.18)$$

Since Hamiltonian has only nearest neighbors, the related phase (4.14) is $\phi = 0$, so that $S_i^+ S_{i+1}^- = c_i^\dagger c_{i+1}$. The second kinetic term $S_i^- S_{i+1}^+ = c_{i+1}^\dagger c_i$ can be obtained using equation (4.12). Thus, kinetic term of Hamiltonian can be written in the following form:

$$\sum_{i=1}^N \frac{J}{2} (S_i^+ S_{i+1}^- + S_i^- S_{i+1}^+) = \sum_{i=1}^N \frac{J}{2} (c_i^\dagger c_{i+1} + c_{i+1}^\dagger c_i) \quad (4.19)$$

So, summary Hamiltonian (4.16) can be written in the following form:

$$H = \sum_{i=1}^N J^z (\hat{n}_i - 1/2)(\hat{n}_{i+1} - 1/2) + \frac{J}{2} (c_i^\dagger c_{i+1} + c_{i+1}^\dagger c_i) - B \sum_{i=1}^N (\hat{n}_i - 1/2) \quad (4.20)$$

It should be noted, in the case of periodic boundary conditions (PBC) one needs to include boundary term to Hamiltonian. However, it has the order of $O(1/N)$ to physical quantities, so that when the number of sites is sufficiently large, one can neglect that terms.

This model equivalent to 1D interacting Hubbard model. Magnetic field B in this case plays as a role of chemical potential, so that one can manipulate Fermi level by changing B .

Hamiltonian (4.20) is exactly solvable, in the limit of $J^z = 0$. This is free fermionic 1D model, which has the dispersion $\epsilon(k) = J \cos(k) - B$. So, one can calculate physical properties of quantum chain by studying fermionic chain.

4.1.3 Jordan-Wigner Transformation of BAHC

In this section we perform JWT of our BAHC model.

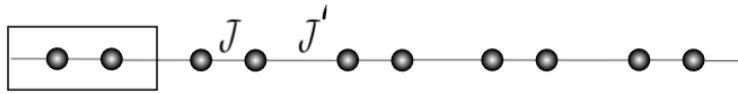


Figure 4.1: Bond-alternating Heisenberg chain

As one can see from the sketch above, the model has alternating values of spin couplings J and J' . The Hamiltonian of the model can be written in the following form:

$$H = J \sum_{i=1}^N \vec{S}_{2i-1} \cdot \vec{S}_{2i} + J' \sum_{i=1}^N \vec{S}_{2i} \cdot \vec{S}_{2i+1} \quad (4.21)$$

One can notice that it is similar to AFHC but with translation symmetry broken up to 2 spins. Thus, to see more clearly fermionization process we can rewrite

our Hamiltonian in the following form:

$$H = \sum_{i=1}^N J \vec{S}_i^a \cdot \vec{S}_i^b + J' \vec{S}_i^b \cdot \vec{S}_{i+1}^a \quad (4.22)$$

where by i we mean i -th unit cell. This notation makes fermionization procedure more clearer. We can write it as $H = H_1 + H_2$ where

$$H_1 = \sum_{i=1}^N J (S_i^{z(a)} S_i^{z(b)} + \frac{1}{2} (S_i^{+(a)} S_i^{-(b)} + S_i^{-(a)} S_i^{+(b)})) \quad (4.23)$$

and

$$H_2 = \sum_{i=1}^N J' (S_i^{z(b)} S_{i+1}^{z(a)} + \frac{1}{2} (S_i^{+(b)} S_{i+1}^{-(a)} + S_i^{-(b)} S_{i+1}^{+(a)})) \quad (4.24)$$

Firstly, to find JWT form for BAHC model, we rewrite anticommutation relations for our new notation :

$$\{S_i^{+(\alpha)}, S_j^{-(\beta)}\} = 2S_i^{z(\alpha)} \delta_{\alpha,\beta} \delta_{i,j} + 2S_j^{-(\beta)} S_i^{+(\alpha)} \quad (4.25)$$

So,

$$[S_i^{+(a)}, S_i^{-(b)}] = 0 \quad (4.26)$$

$$\{S_i^{+(a)}, S_i^{-(a)}\} = \mathbb{I} \quad (4.27)$$

$$[S_i^{+(a)}, S_j^{-(a,b)}] = 0, i \neq j \quad (4.28)$$

All these (anti)commutation relations are derived from standard (anti)commutation relations. One can show that following JWT fulfills all (anti)commutation relations above:

$$S_i^{+(a)} = a_i^\dagger e^{i\pi \sum_{k<i} (a_k^\dagger a_k + b_k^\dagger b_k)} \quad (4.29)$$

$$S_i^{+(b)} = b_i^\dagger e^{i\pi \sum_{k<i} (a_k^\dagger a_k + b_k^\dagger b_k + a_i^\dagger a_i)} \quad (4.30)$$

$$S_i^{z(a)} = a_i^\dagger a_i - 1/2 \quad (4.31)$$

Now, (anti)commutation relations above can be checked.

$$S_i^{+(a)} S_i^{-(a)} = a_i^\dagger e^{i\pi \sum_{k<i} (a_k^\dagger a_k + b_k^\dagger b_k)} e^{-i\pi \sum_{k<i} (a_k^\dagger a_k + b_k^\dagger b_k)} a_i = a_i^\dagger a_i \quad (4.32)$$

$$S_i^{-(a)} S_i^{+(a)} = e^{-i\pi \sum_{k<i} (a_k^\dagger a_k + b_k^\dagger b_k)} a_i a_i^\dagger e^{i\pi \sum_{k<i} (a_k^\dagger a_k + b_k^\dagger b_k)} = a_i a_i^\dagger = 1 - a_i^\dagger a_i \quad (4.33)$$

Thus, (4.27) is fulfilled. For 4.26:

$$\begin{aligned} S_i^{-(a)} S_i^{+(b)} &= e^{-i\pi \sum_{k<i} (a_k^\dagger a_k + b_k^\dagger b_k)} a_i^\dagger b_i^\dagger e^{i\pi \sum_{k<i} (a_k^\dagger a_k + b_k^\dagger b_k + a_i^\dagger a_i)} = \\ &= a_i^\dagger b_i^\dagger e^{i\pi a_i^\dagger a_i} = a_i^\dagger b_i^\dagger (1 - 2a_i^\dagger a_i) = -b_i^\dagger a_i (1 - 2a_i^\dagger a_i) = b_i^\dagger a_i \end{aligned} \quad (4.34)$$

$$\begin{aligned} S_i^{+(b)} S_i^{-(a)} &= b_i^\dagger e^{i\pi \sum_{k<i} (a_k^\dagger a_k + b_k^\dagger b_k + a_i^\dagger a_i)} e^{-i\pi \sum_{k<i} (a_k^\dagger a_k + b_k^\dagger b_k)} a_i = \\ &= b_i^\dagger e^{i\pi a_i^\dagger a_i} a_i = b_i^\dagger (1 - 2a_i^\dagger a_i) a_i = b_i^\dagger a_i \end{aligned} \quad (4.35)$$

Now, we will show commutation relationship (4.28):

$$\begin{aligned} S_i^{+(a)} S_j^{-(\gamma)} &= a_i^\dagger e^{i\pi \sum_{k<i} (a_k^\dagger a_k + b_k^\dagger b_k)} e^{-i\pi \sum_{k<j} (a_k^\dagger a_k + b_k^\dagger b_k) + \delta_{\gamma,b} a_j^\dagger a_j} \gamma_j = \\ &= a_i^\dagger e^{-i\pi (n_i^a + n_i^b + \delta_{\gamma,b} a_j^\dagger a_j)} \gamma_j e^{-i\pi \sum_{k=i+1}^{k=j-1} (a_k^\dagger a_k + b_k^\dagger b_k)} = \\ &= a_i^\dagger (1 - a_i^\dagger a_i) e^{-i\pi (n_i^b + \delta_{\gamma,b} a_j^\dagger a_j)} \gamma_j e^{-i\pi \phi} = a_i^\dagger e^{-i\pi (n_i^b + \delta_{\gamma,b} a_j^\dagger a_j)} \gamma_j e^{-i\phi} = \\ &= a_i^\dagger \gamma_j e^{-i\pi (\phi + n_i^b + \delta_{\gamma,b} a_j^\dagger a_j)} \end{aligned} \quad (4.36)$$

$$\begin{aligned} S_j^{-(\gamma)} S_i^{+(a)} &= e^{-i\pi \sum_{k<j} (a_k^\dagger a_k + b_k^\dagger b_k) + \delta_{\gamma,b} a_j^\dagger a_j} \gamma_j a_i^\dagger e^{i\pi \sum_{k<i} (a_k^\dagger a_k + b_k^\dagger b_k)} = \\ &= (1 - 2a_i^\dagger a_i) \gamma_j a_i^\dagger e^{-i\pi (\phi + n_i^b + \delta_{\gamma,b} a_j^\dagger a_j)} = -(1 - 2a_i^\dagger a_i) a_i^\dagger \gamma_j e^{-i\pi (\phi + n_i^b + \delta_{\gamma,b} a_j^\dagger a_j)} = \\ &= a_i^\dagger \gamma_j e^{-i\pi (\phi + n_i^b + \delta_{\gamma,b} a_j^\dagger a_j)} \end{aligned} \quad (4.37)$$

where $\phi = \sum_{k=i+1}^{k=j-1} (a_k^\dagger a_k + b_k^\dagger b_k)$. Thus, commutation relation (4.28) is satisfied for any $i \neq j$.

In the derivations above, we used the following (anti)commutation rules:

$$\left\{ a_i^\dagger, b_j \right\} = \left\{ b_i^\dagger, a_j \right\} = \left\{ b_i^\dagger, a_j^\dagger \right\} = 0; \forall i, j \quad (4.38)$$

At this point it is clear that JWT above gives correct (anti)commutation rules. Thus, we apply JWT to our Hamiltonian. For interaction parts of H we have:

- $J S_i^{z(a)} S_i^{z(b)} = J(a_i^\dagger a_i - 1/2)(b_i^\dagger b_i - 1/2)$
- $J' S_i^{z(b)} S_{i+1}^{z(a)} = J'(b_i^\dagger b_i - 1/2)(a_{i+1}^\dagger a_{i+1} - 1/2)$

Next, we see transformation of kinetic parts of H_1 :

$$H_1^k = \frac{J}{2} (S_i^{+(a)} S_i^{-(b)} + S_i^{-(a)} S_i^{+(b)}) \quad (4.39)$$

- $S_i^{+(a)} S_i^{-(b)} = a_i^\dagger e^{i\pi \sum_{k<i} (a_k^\dagger a_k + b_k^\dagger b_k)} e^{-i\pi \sum_{k<i} (a_k^\dagger a_k + b_k^\dagger b_k)} e^{-i\pi \hat{n}_i(a)} b_i = a_i^\dagger b_i$
- $S_i^{-(a)} S_i^{+(b)} = e^{-i\pi \sum_{k<i} (a_k^\dagger a_k + b_k^\dagger b_k)} a_i b_i^\dagger e^{i\pi \sum_{k<i} (a_k^\dagger a_k + b_k^\dagger b_k + a_i^\dagger a_i)} = -a_i b_i^\dagger = b_i^\dagger a_i$

Now, we consider kinetic part of H_2^k :

$$H_2^k = \frac{J'}{2} (S_i^{+(b)} S_{i+1}^{-(a)} + S_i^{-(b)} S_{i+1}^{+(a)}) \quad (4.40)$$

- $S_i^{+(b)} S_{i+1}^{-(a)} = b_i^\dagger e^{i\pi \sum_{k<i} (a_k^\dagger a_k + b_k^\dagger b_k + a_i^\dagger a_i)} e^{-i\pi \sum_{k<i+1} (a_k^\dagger a_k + b_k^\dagger b_k)} a_{i+1} = b_i^\dagger (1 - 2b_i^\dagger b_i) a_{i+1} = b_i^\dagger a_{i+1}$
- $S_i^{-(b)} S_{i+1}^{+(a)} = e^{-i\pi \sum_{k<i} (a_k^\dagger a_k + b_k^\dagger b_k + a_i^\dagger a_i)} b_i a_{i+1}^\dagger e^{i\pi \sum_{k<i+1} (a_k^\dagger a_k + b_k^\dagger b_k)} = b_i e^{-i\pi b_i^\dagger b_i} a_{i+1}^\dagger = b_i (1 - 2b_i^\dagger b_i) a_{i+1}^\dagger = -b_i a_{i+1}^\dagger = a_{i+1}^\dagger b_i$

At this point, we parametrise interaction of z-components with Δ and Δ' .

Thus, finally we have $H = H_1 + H_2$ with:

$$H_1 = \sum_{i=1}^N J \Delta (a_i^\dagger a_i - 1/2) (b_i^\dagger b_i - 1/2) + \frac{J}{2} (a_i^\dagger b_i + b_i^\dagger a_i) \quad (4.41)$$

$$H_2 = \sum_{i=1}^N J' \Delta' (b_i^\dagger b_i - 1/2) (a_{i+1}^\dagger a_{i+1} - 1/2) + \frac{J'}{2} (b_i^\dagger a_{i+1} + a_{i+1}^\dagger b_i) \quad (4.42)$$

If we put $\Delta' = \Delta = 0$, we get XX limit of BAHC and add magnetic field B in z-direction, Hamiltonian will have following form :

$$H_{xx} = \sum_{i=1}^N \frac{J}{2} (a_i^\dagger b_i + b_i^\dagger a_i) + \frac{J'}{2} (b_i^\dagger a_{i+1} + a_{i+1}^\dagger b_i) - B ((a_i^\dagger a_i - 1/2) + (b_i^\dagger b_i - 1/2)) \quad (4.43)$$

As one can notice, this is non-interacting Su-Schrieffer-Heeger (SSH) model [36]. Our model is more general since the values of J and J' can be positive or negative, when in SSH usually both of them are counted positive or negative. Also, we neglect boundary terms appearing due to PBC, assuming that the chain is

long enough for terms to be neglected.

In next section, we will zero temperature properties of the model under the magnetic field.

4.2 Zero-temperature properties of XX BAHC model

By using JWT, the study of zero-temperature properties of BAHC model in XX limit is transformed to study of ground state properties of generalized non-interacting SSH model.

We assign new parameters and perform Fourier transform of the model:

- $t = \frac{J}{2}$; $t' = \frac{J'}{2}$

$$a_i^\dagger = \frac{1}{\sqrt{N}} \sum_{k \in BZ} e^{-ikR_i} a_k^\dagger \quad (4.44)$$

$$a_i = \frac{1}{\sqrt{N}} \sum_{k \in BZ} e^{ikR_i} a_k \quad (4.45)$$

The first term of Hamiltonian transforms as:

$$\begin{aligned} H_{xx}^1 &= \sum_{i=1}^N t(a_i^\dagger b_i + b_i^\dagger a_i) = \frac{1}{N} \sum_{i=1}^N \sum_{k, q \in BZ} t(e^{-ikR_{ai}} e^{iqR_{bi}} a_k^\dagger b_q + e^{-iqR_{bi}} e^{ikR_{ai}} b_q^\dagger a_k) = \\ &= \sum_{q \in BZ} t(e^{iq(R_{bi}-R_{ai})} a_q^\dagger b_q + e^{-iq(R_{bi}-R_{ai})} b_q^\dagger a_q) = \sum_{q \in BZ} t(e^{i\frac{q}{2}} a_q^\dagger b_q + e^{-i\frac{q}{2}} b_q^\dagger a_q) \end{aligned} \quad (4.46)$$

For the second term we have:

$$H_{xx}^2 = \sum_{i=1}^N t'(b_i^\dagger a_{i+1} + a_{i+1}^\dagger b_i) = \sum_{q \in BZ} t'(e^{i\frac{q}{2}} b_q^\dagger a_q + e^{-i\frac{q}{2}} a_q^\dagger b_q) \quad (4.47)$$

Thus, the final form of k-space Hamiltonian can be written as:

$$H_{xx} = \sum_{q \in BZ} (t' e^{i\frac{q}{2}} + t e^{-i\frac{q}{2}}) b_q^\dagger a_q + (e^{-i\frac{q}{2}} t' + e^{i\frac{q}{2}} t) a_q^\dagger b_q - B(b_q^\dagger b_q + a_q^\dagger a_q) - BN \quad (4.48)$$

In the matrix form $H_K = H_{xx} + BN$ can be written as:

$$H_K = \begin{bmatrix} a_q^\dagger & b_q^\dagger \end{bmatrix} \begin{bmatrix} -B & (e^{-i\frac{q}{2}}t' + e^{i\frac{q}{2}}t) \\ (t'e^{i\frac{q}{2}} + te^{-i\frac{q}{2}}) & -B \end{bmatrix} \begin{bmatrix} a_q \\ b_q \end{bmatrix} \quad (4.49)$$

Thus, one needs to diagonalize kernel of H_k matrix. It is convenient to kernel $h(k)$ as:

$$h(k) = \mathbf{G}^\mu \sigma_\mu \quad (4.50)$$

where $G^0 = -B$, $G^x = (t + t') \cos(\frac{q}{2})$ and $G^y = (t - t') \sin(\frac{q}{2})$. Eigenvectors can be found as:

$$|\psi\rangle^{+,-} = \frac{1}{\sqrt{2|G|(|G| \mp G^3)}} \begin{pmatrix} G^1 - iG^2 \\ \pm|G| - G^3 \end{pmatrix} \quad (4.51)$$

when eigenvalues are defined as:

$$E^{+,-} = G^0 \pm |G| \quad (4.52)$$

Using $|G| = \sqrt{t'^2 + 2tt' \cos(q) + t^2}$ brings:

$$E^{[+,-]}(q) = -B \pm \sqrt{t'^2 + 2tt' \cos(q) + t^2} \quad (4.53)$$

Thus, Hamiltonian can be written in the following form:

$$H_{xx} = \sum_{q \in BZ} (E^-(q) \alpha_q^\dagger \alpha_q + E^+(q) \beta_q^\dagger \beta_q) - BN \quad (4.54)$$

Finally, due to particle hole symmetry, one can show that equation (4.54) can be written as:

$$H_{xx} = \sum_{q \in BZ} (E^-(q) (\alpha_q^\dagger \alpha_q - \frac{1}{2}) + E^+(q) (\beta_q^\dagger \beta_q - \frac{1}{2})) \quad (4.55)$$

Eigenvectors have the following form:

$$v_{1,2} = \frac{1}{\sqrt{2}} \begin{pmatrix} \pm \frac{E^+(q)}{e^{i\frac{q}{2}}t' + e^{-i\frac{q}{2}}t} \\ 1 \end{pmatrix} \quad (4.56)$$

4.2.1 Spectrum and ground state energy

We note that, in contrast to the standard SSH model, fermionic hopping parameters t and t' in our model are extended and can have negative values also. The

spectrum of the Hamiltonian at $B = 0$ is shown in the figure below, when intercell hopping is kept, $t' = 1$. We changed intracell hopping in a range $t \in [-2, 2]$. It should be noted, that negative hopping in the fermionic model, corresponds to ferromagnetic coupling in our XX spin chain, while a positive one corresponds to antiferromagnetic interaction of spins.

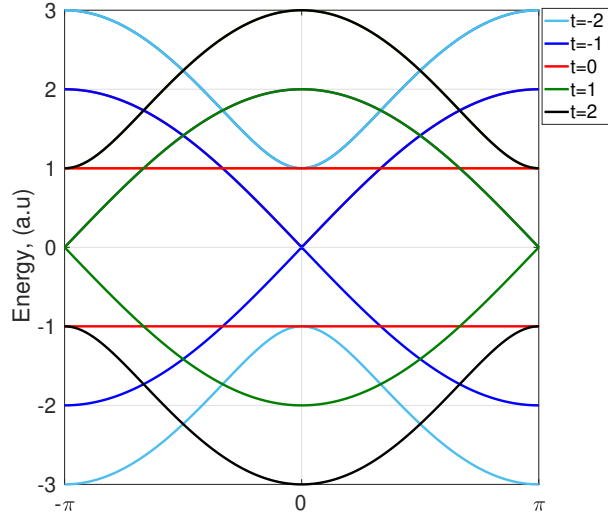


Figure 4.2: Energy spectrum of the model for $t' = 1$

As one can notice, when $t < 0$ and $|t| > t'$ there is a gap in the spectrum. For $t = -2$, the minimum gap of $e_g = 2$ is reached in $k = 0$, while it reaches maximum value of $e_g = 6$ in $k = \pm\pi$. The gap closures, when at $t = -1$, i.e. $|t| = t'$. The gap closure occurs at $k = 0$ point. This signals about topological quantum phase transition, as it was mentioned in Chapter 1. Next increasing of t opens a gap, making the band flatter. At $t = 0$ complete dimerized limit is obtained. A further increment of t deforms the bands and makes two new Dirac cones touching at $t = \pm\pi$. This is another QPT point. And finally, when the t is further increased, the gap opens again.

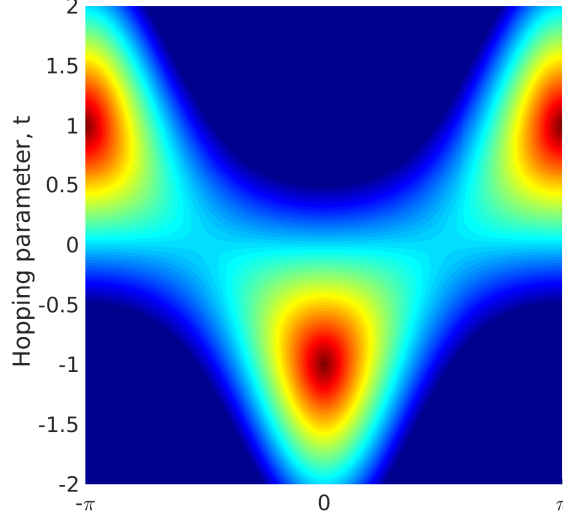


Figure 4.3: Gap closure in QPT points

Fig. (4.3) shows in which points gap closures occur based on the formation of Dirac cones. One can clearly see that at the points $t = -1$ and at $t = 1$ the gap closures occur. We will discuss these signals about the QPT in the next section.

Ground state energy

The energy per site can be calculated from a dispersion.

$$\epsilon_G = \frac{E_G}{N} = \frac{1}{4\pi} \int_{-\pi}^{\pi} E^-(q) dq \quad (4.57)$$

where addition $\frac{1}{2}$ comes due to 2 sites per effective unit cell.

$$\begin{aligned} \epsilon_G &= \frac{E_G}{N} = -\frac{1}{4\pi} \int_{-\pi}^{\pi} \sqrt{t'^2 + 2tt' \cos(q) + t^2} dq = \\ &= -\frac{1}{2\pi} \int_0^{\pi} \sqrt{(t+t')^2 - 4tt' \sin^2(\frac{q}{2})} dq = -\frac{|t+t'|}{2\pi} \int_0^{\pi} \sqrt{1 - \frac{4tt'}{(t+t')^2} \sin^2(\frac{q}{2})} dq = \\ &= -\frac{|t+t'|}{\pi} \int_0^{\frac{\pi}{2}} \sqrt{1 - \frac{4tt'}{(t+t')^2} \sin^2(\frac{q}{2})} d(\frac{q}{2}) = -\frac{|t+t'|}{\pi} E\left(\frac{4tt'}{(t+t')^2}\right) \end{aligned} \quad (4.58)$$

where $E(x)$ is the complete elliptic integral of the second kind. One can notice that in dimerized limit $t' = 0$ and

$$\epsilon_{G-dimer} = -\frac{1}{\pi}|t|E(0) = -\frac{|t|}{2} \quad (4.59)$$

which is the energy of a singlet. For an insulating phase $t = 1$ and $t' = 2$ we have :

$$\epsilon_G = -\frac{1}{\pi}|t|E(0) = -\frac{3}{\pi}E\left(\frac{8}{9}\right) \approx -1.06354 \quad (4.60)$$

In the figure below we show calculated ground state energy per site using i-DMRG method. The model parameters were: $J = 2$; $J' = 4$; $\chi = 10$

Blue dashed line represents analytical result (4.58). As one can see, the results are matching precisely.

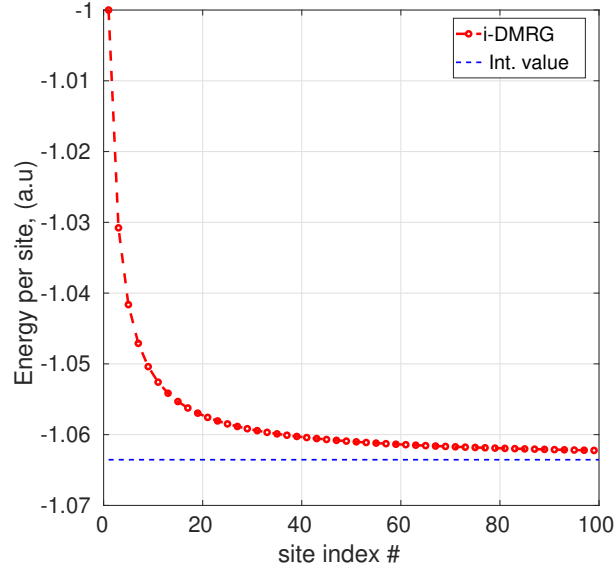


Figure 4.4: Energy per site calculated via i-DMRG for $N = 100$.

4.2.2 Zero - temperature quantum phase transition under the magnetic field

Here we will study quantum phase transition of BAHC under magnetic field B . In the model, mainly there are 3 main situations:

- F -AF limit: $t < 0$ while $t' > 0$.
- AF-AF limit: $t > 0$ and $t' > 0$.
- Critical point: in a flat band regime and in Dirac cone, i.e $t < 0$ and $|t| = t'$

As we will see from algebra below, the two first cases have the same physics under the magnetic field. We will consider only them.

F - AF and AF-AF limits

In F - AF limit we have $t < 0$ while $t' > 0$, so that inside the unit cell spins are coupling ferromagnetically, while intercell couplings are antiferromagnetic. In this limit, we have the following dispersion relation:

$$E^{[+,-]}(q) = -B \pm \sqrt{t'^2 - 2|t||t'| \cos(q) + t^2} \quad (4.61)$$

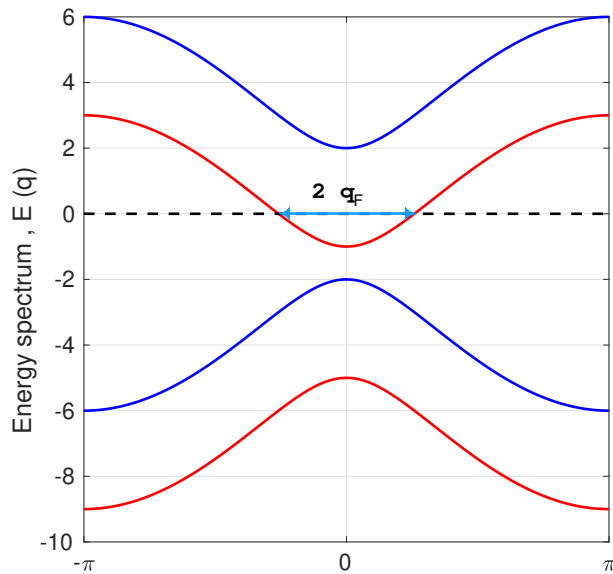


Figure 4.5: Spectrum in F-AF limit under the magnetic field $B=[0,3]$ for $t = -4$ and $t' = 2$

When there is no magnetic field, the spectrum is gapped, and the fermionic chain is an insulator. One can show that the value of the maximum gap is $E_{gap} = 2(|t'| - |t|)$ which occurs at $q = 0$ for F-AF and $q = \pm\pi$ for AF-AF limits. When a magnetic field is applied, the reference energy (Fermi energy) E_F starts shifting, so that after critical value B_{c1} it touches one of the bands, depending on the direction of B . Due to the presence of particle-hole symmetry, the magnetization curve should be a symmetric function of B . The value of B_{c1} obviously depends on the value of the gap. For F-AF and AF-AF limits with the same magnitudes of parameters, one has the same E_{gap} , thus B_{c1} is the same for both systems. At this critical point, a magnetization of the chain starts. The fermionic chain becomes metallic - 1D Luttinger liquid. Further increasing of B leads to the second critical point B_{c2} , in which all spins become fully polarized, i.e $m_c = \frac{1}{2}$. The dynamics of magnetization is determined by excitation around Fermi level in the metallic phase. To study it, we define a Fermi vector q_F which determines the properties of the metallic fermionic system. The magnitude of q_F for F-AF limit can be found as:

$$q_F = \arccos\left(\frac{t^2 - t'^2 - B^2}{2|t||t'|}\right) \quad (4.62)$$

The part of the band which is below the Fermi level is occupied, i.e :

$$n_q \in \left[-q_F, q_F\right] = 1 \quad (4.63)$$

We can find the density :

$$n = 1 + \frac{q_F}{\pi} \quad (4.64)$$

Since JWT defines $S^z = \hat{n} - \frac{1}{2}$, similarly magnetization can be defined in the same way:

$$m = \frac{n - 1}{2} = \frac{q_F}{2\pi} \quad (4.65)$$

Thus, magnetic susceptibility is $\chi_S = \frac{\partial m}{\partial B}$:

$$\chi_S = \frac{\partial m}{\partial q_F} \frac{\partial q_F}{\partial B} = \frac{B}{2\pi|t||t'| \sqrt{1 - \frac{(t^2 + t'^2 - B^2)^2}{4t^2 t'^2}}} \quad (4.66)$$

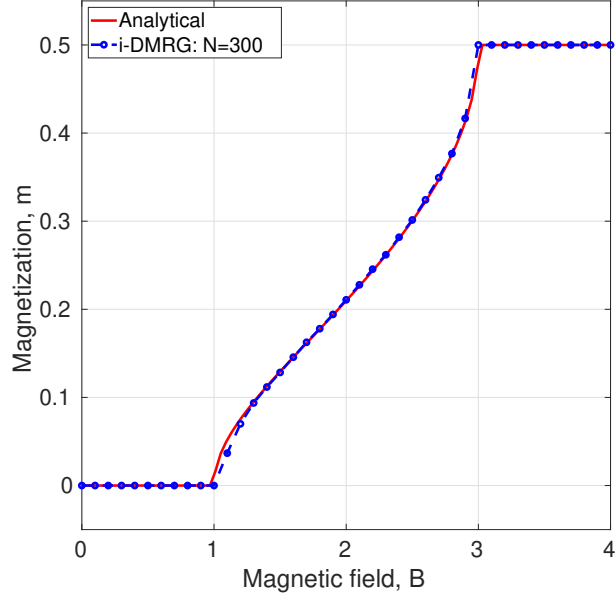


Figure 4.6: Magnetization curve for F-AF limit

While the algebra is done for F-AF mode, for AF-AF limit the physics is the same. This is because the bands of F-AF mode is just shifted bands of AF-AF limit by $q = \frac{\pi}{2}$. Figure 4.6 shows magnetization curve for $t = 1$ and $t' = \pm 2$ calculated using i-DMRG for $N=300$ with the maximum bond dimension $\chi = 10$. The result is matching well with analytical solution (4.65), except the critical point at $B = 1$ in which more bond dimension is needed to calculate m accurately.

4.2.3 Spin-Spin correlation functions

Using (4.56) one can write a_q and b_q in terms of α_q and β_q operators:

$$\alpha_q = \frac{1}{\sqrt{2}}(-A_q a_q + b_q) \quad (4.67)$$

$$\beta_q = \frac{1}{\sqrt{2}}(A_q a_q + b_q) \quad (4.68)$$

where

$$A_q = \frac{E^+(2q)}{e^{iqt'} + e^{-iqt}} \quad (4.69)$$

Thus,

$$a_q = \frac{1}{\sqrt{2}A_q}(\beta_q - \alpha_q) \quad (4.70)$$

$$b_q = \frac{1}{\sqrt{2}}(\alpha_q + \beta_q) \quad (4.71)$$

The quasiparticle vacuum is defined as:

$$\begin{aligned} \alpha_q^\dagger |0\rangle &= 0 \\ \beta_q |0\rangle &= 0; \forall q \end{aligned} \quad (4.72)$$

From this definition of vacuum one can get following relationships:

$$\langle b_k^\dagger a_q \rangle = -\frac{\delta_{q,k}}{2A_k} \quad (4.73)$$

$$\langle a_k^\dagger b_q \rangle = -\frac{\delta_{q,k}}{2A_k^*} \quad (4.74)$$

One can show that,

$$\langle a_k^\dagger a_q \rangle = \langle b_k^\dagger b_q \rangle = \frac{\delta_{q,k}}{2} \quad (4.75)$$

Using anticommutation relations one can get a remained matrix elements. Obviously, for even $n - m$ correlation functions $\langle a_m^\dagger a_n \rangle = \langle b_m^\dagger b_n \rangle$ vanish :

$$\langle a_m^\dagger a_n \rangle = \langle b_m^\dagger b_n \rangle = \frac{\sin\left(\frac{\pi(n-m)}{2}\right)}{\pi(n-m)} = 0 \quad (4.76)$$

Here, indexes do not correspond to the effective unit cell, but to a site, thus we will work in a 'reduced Brillouin zone'.

Next, we evaluate non-vanishing correlation functions $\langle a_m^\dagger b_n \rangle$; Further, we assume $n > m$.

$$W_{m,n} = \langle a_m^\dagger b_n \rangle = -\frac{1}{\pi} \int_{-\frac{\pi}{2}}^{\frac{\pi}{2}} \frac{e^{-ik(n-m)}}{2A_k^*} dk = -\frac{1}{2\pi} \int_{-\frac{\pi}{2}}^{\frac{\pi}{2}} \frac{e^{-ik(n-m)}(e^{ikt} + e^{-ikt})}{\sqrt{t'^2 + 2tt' \cos(2k) + t^2}} dk \quad (4.77)$$

Another non-vanishing correlator is:

$$Z_{m,n} = \langle b_m^\dagger a_n \rangle = -\frac{1}{\pi} \int_{-\frac{\pi}{2}}^{\frac{\pi}{2}} \frac{e^{-ik(n-m)}}{2A_k} dk = -\frac{1}{2\pi} \int_{-\frac{\pi}{2}}^{\frac{\pi}{2}} \frac{e^{-ik(n-m)}(e^{ikt'} + e^{-ikt'})}{\sqrt{t'^2 + 2tt' \cos(2k) + t^2}} dk \quad (4.78)$$

It is can be noticed that $W_{n,m} = Z_{m,n}$ and $Z_{n,m} = W_{m,n}$. Integrals above for nearest neighbors (i.e $|n - m| = 1$) are the linear composition of $K(t, t')$ and $E(t, t')$ which are elliptic integrals of the first and the second kinds. For remaining distances, the analytical solution is involved and the integration consists other terms.

Correlation function for x - component of spins: $C_{n,m}^{xx}$

We consider correlation function of x - components of spin, i.e $\langle S_m^{(a)x} S_n^{(b)x} \rangle$, where indexes correspond to a site.

$$C_{m,n}^{xx(a)} = \langle S_m^{(a)x} S_n^{(b)x} \rangle = \frac{1}{4} \langle (S_m^{(a)+} + S_m^{(a)-})(S_n^{(b)+} + S_n^{(b)-}) \rangle \quad (4.79)$$

Index a in $C_{m,n}^{xx(a)}$ shows that we look the correlation of a spin with others and it is not equal to $C_{m,n}^{xx(b)}$ unless $t = t'$. In fermionic representation it has the following form:

$$\begin{aligned} C_{m,n}^{xx(a)} &= \frac{1}{4} \left\langle a_m^\dagger e^{i\pi \sum_{k<m} (\hat{n}_k^{(a,b)})} + e^{-i\pi \sum_{k<m} (\hat{n}_k^{(a,b)})} a_m \right\rangle (b_n^\dagger e^{i\pi \sum_{k<n} (\hat{n}_k^{(a,b)})} + e^{-i\pi \sum_{k<n} (\hat{n}_k^{(a,b)})} b_n) \rangle = \\ &= \frac{1}{4} \left\langle (a_m^\dagger + a_m) e^{i\pi \sum_{k=m}^{k=n-1} (\hat{n}_k^{(a,b)})} (b_n^\dagger + b_n) \right\rangle \end{aligned} \quad (4.80)$$

Since $(a_m^\dagger + a_m) e^{i\pi a_m^\dagger a_m} = (a_m^\dagger - a_m)$ the equation above can be written as:

$$C_{m,n}^{xx(a)} = \frac{1}{4} \left\langle (a_m^\dagger - a_m) e^{i\pi \sum_{k=m+1}^{k=n-1} (\hat{n}_k^{(a,b)})} (b_n^\dagger + b_n) \right\rangle \quad (4.81)$$

Thus, we have for every site one has exponential string operator:

$$e^{i\pi p_k^\dagger p_k} = (1 - 2p_k^\dagger p_k) = (p_k^\dagger + p_k)(p_k^\dagger - p_k) \quad (4.82)$$

where $p = a, b$ is fermionic operator. We introduce the following operators to have convenient notation:

$$A_m = (a_m^\dagger - a_m) \quad (4.83)$$

$$B_m = (a_m^\dagger + a_m) \quad (4.84)$$

$$C_m = (b_m^\dagger - b_m) \quad (4.85)$$

$$D_m = (b_m^\dagger + b_m) \quad (4.86)$$

It is straightforward to derive anticommutation relations of the pairs for mentioned operators :

$$\{A_m, A_n\} = \{C_m, C_n\} = -2\delta_{m,n} \quad (4.87)$$

$$\{B_m, B_n\} = \{D_m, D_n\} = 2\delta_{m,n} \quad (4.88)$$

While for any other pair N and M from the set above, we have:

$$\{M_m, N_n\} = 0 \quad (4.89)$$

Then, equation (4.81) can be written as:

$$C_{m,n}^{xx(a)} = \frac{1}{4} \langle A_m D_{m+1} C_{m+1} B_{m+2} A_{m+2} \dots B_{n-1} A_{n-1} D_n \rangle \quad (4.90)$$

One can evaluate this correlation function using Wick theorem, since operators anticommute. Thus, we firstly evaluate expectation values of the form $\langle N_m M_n \rangle$ where N and M belong to a set of operators defined in (4.83- 4.86).

Using (4.76) it can be shown that for different sites $\langle N_m N_n \rangle = 0$ for any N . Furthermore, $\langle A_m B_n \rangle = \langle C_m D_n \rangle = 0$. For different pair of operators it is generally non-zero:

$$\langle A_m C_n \rangle = \langle b_n^\dagger a_m - a_m^\dagger b_n \rangle \quad (4.91)$$

However, from symmetry of integrals $W_{m,n}$ and $Z_{m,n}$, it is clear that $\langle A_m C_n \rangle = 0$ also vanishes. Similarly, $\langle B_m D_n \rangle$ vanishes, i.e

$$\langle B_m D_n \rangle = \langle -b_n^\dagger a_m + a_m^\dagger b_n \rangle = 0 \quad (4.92)$$

A non-zero elements are:

$$\langle A_m D_n \rangle = \langle b_n^\dagger a_m + a_m^\dagger b_n \rangle = 2 \langle a_m^\dagger b_n \rangle = 2W_{m,n} \quad (4.93)$$

$$\langle C_m B_n \rangle = \langle b_m^\dagger a_n + a_n^\dagger b_m \rangle = 2 \langle b_m^\dagger a_n \rangle = 2Z_{m,n} \quad (4.94)$$

One also can show that

$$\langle A_n D_m \rangle = 2 \langle b_m^\dagger a_n \rangle = 2Z_{m,n} \quad (4.95)$$

while

$$\langle C_n B_m \rangle = -2 \langle a_m^\dagger b_n \rangle = -2W_{m,n} \quad (4.96)$$

At this point, this information is enough to evaluate expression (4.90) using Wick theorem. Theorem states that:

$$\langle \Psi | O_1 O_2 \dots O_{2k} | \Psi \rangle = \sum_{\text{all pairings}} (-1)^p \prod_{\text{all pairs}} (\text{contraction of pair}) \quad (4.97)$$

Now, we know all contractions vanish except of (4.95-4.96). This makes our calculation of (3.89) more easier.

One starts with following product of pairings :

$$\langle A_m D_{m+1} \rangle \langle C_{m+1} B_{m+2} \rangle \langle A_{m+2} D_{m+3} \rangle \dots \langle A_{n-1} D_n \rangle \quad (4.98)$$

Obviously, this product is not vanishing. Then one needs to consider all other not vanishing contractions with the corresponding permutation signature p . A little math brings to the following result:

$$C_{1,n}^{xx(a)} = \frac{1}{4} \det \begin{vmatrix} 2W_{1,2} & 0 & 2W_{1,4} & 0 & \dots & 2W_{1,n} \\ 0 & 2Z_{2,3} & 0 & 2Z_{2,5} & \dots & 0 \\ 2W_{3,2} & 0 & 2W_{3,4} & 0 & \dots & 2W_{3,n} \\ 0 & 2Z_{4,3} & 0 & 2Z_{4,5} & \dots & 0 \\ \dots & \dots & \dots & \dots & \dots & \dots \end{vmatrix} \quad (4.99)$$

where matrix elements of C^{xx} for odd rows is defined by $W_{m,n}$ elements, while for even rows by $Z_{m,n}$. While for the standard XY model [37] [38] the matrix $C_{m,n}^{xx}$ is a well studied Toeplitz matrix and approximate behavior of correlation function can be derived analytically, in our case the matrix is a broken Toeplitz matrix, where diagonal elements oscillate between two values.

It is clear that $C_{1,2}^{xx(a)} = \frac{1}{2}W_{1,2}$, while for $C_{1,2}^{xx(a)} = W_{1,2}Z_{2,3}$. For further distance, one can get calculating determinants of the matrix (4.99).

Obviously, $C_{m,n}^{xx(b)} \neq C_{m,n}^{xx(a)}$. One can get equivalent matrix as (4.99) for the case $C_{m,n}^{xx(b)}$ by changing $W_{n,m} \rightarrow Z_{n,m}$ so that $C_{1,2}^{xx(b)} = \frac{1}{2}Z_{1,2}$. Since the model is isotropic, the the correlation function for y - component behaves in the same ways.

Correlation function for z - component of spins: $C_{n,m}^{zz}$

Calculation of $C_{m,n}^{zz}$ is more straightforward. We firstly consider $\langle S_m^{(a)z} S_n^{(b)z} \rangle$ case, i.e odd distances from a-sites:

$$C_{m,n}^{zz(a)} = \langle S_m^{(a)z} S_n^{(b)z} \rangle = -\frac{1}{4} \langle e^{i\pi S_m^{(a)z}} e^{i\pi S_n^{(b)z}} \rangle = -\frac{1}{4} \langle e^{i\pi a_m^\dagger a_m} e^{i\pi b_n^\dagger b_n} \rangle \quad (4.100)$$

where we have used $e^{i\pi S^z} = \frac{S^z}{2i}$. Using (4.82) the equation above can be written as:

$$C_{m,n}^{zz(a)} = -\frac{1}{4} \langle B_m A_m D_n C_n \rangle \quad (4.101)$$

The only non-zero contraction with $p = 1$ is:

$$\langle B_m C_n \rangle \langle D_n A_m \rangle \quad (4.102)$$

Thus,

$$C_{m,n}^{zz(a)} = \frac{1}{4} \langle B_m C_n \rangle \langle D_n A_m \rangle = -\frac{1}{4} \langle B_m C_n \rangle \langle A_m D_n \rangle = -(W_{n,m})^2 \quad (4.103)$$

Interestingly, the z -component correlation function for odd distances from a-sites is just proportional to $W_{n,m}$.

For z -component of $b - a$ spins it can be shown in a similar way that:

$$C_{m,n}^{zz(b)} = \langle S_m^{(b)z} S_n^{(a)z} \rangle = -(Z_{n,m})^2 \quad (4.104)$$

For even distances, $C_{m,n}^{zz(a,b)}$ vanishes, due to the fact that all contractions of the same type of fermions (i.e consisting only a 's or b 's) vanish in any permutations.

Results

Here we performed comparison of numerical DMRG results and analytically obtained results for $C_{m,n}^{xx(a,b)}$ and $C_{m,n}^{zz(a,b)}$. For $t = 2$ and $t' = 1$, we numerically evaluated matrix elements $Z_{n,m}$ and $W_{n,m}$. Next, we obtained matrix (4.99) and calculated subdeterminants of the matrix to get correlation function $C_{1,n}^{xx(a)}$. Similarly, $C_{m,n}^{xx(b)}$ is obtained by calculating of subdeterminants of corresponding matrix. We calculated $C_{m,n}^{zz(a,b)}$ as given in (4.103-4.104).

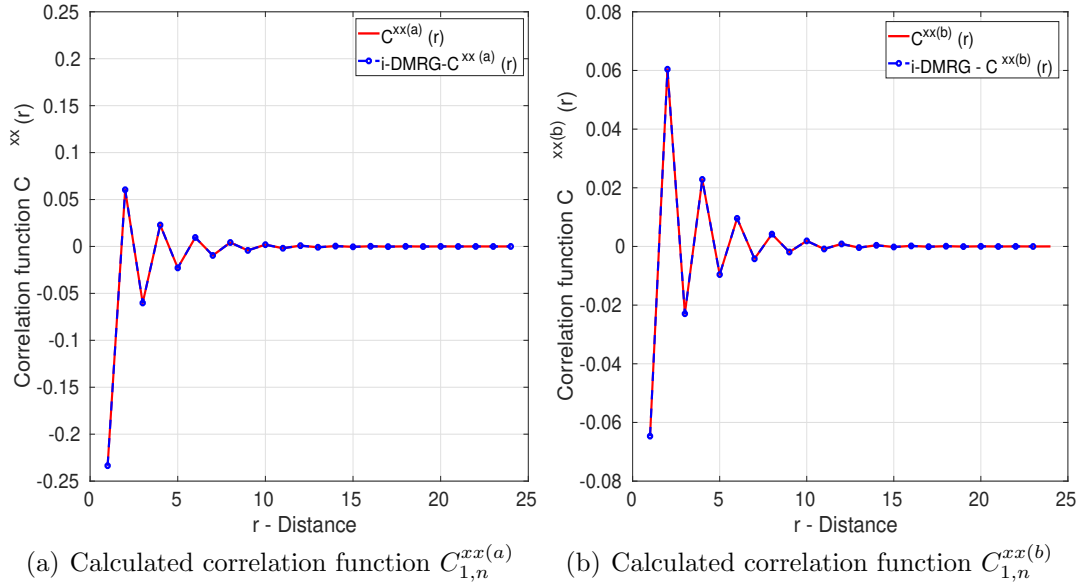


Figure 4.7: Comparison of analytical and numerical i-DMRG results of $C_{1,n}^{xx(a,b)}$

For a given spin chain of length $N = 100$ with $J = 4$ and $J' = 2$ we performed i-DMRG with following $N_{SW} = 3$ sweepings. Maximum bond dimension was $\chi = 12$.

Before discussing results, we will discuss some basic properties of the system. We start from limiting case: $t' = 0$. In this limit, we have dimerized spins in every unit cell. Wavefunction can be written in the following form depending on the sign of the spin coupling within the unit cell t :

$$|\Psi\rangle = \prod_{i=1}^{\frac{L}{2}} \frac{(|\uparrow\downarrow\rangle \pm |\downarrow\uparrow\rangle)}{\sqrt{2}} \quad (4.105)$$

where i runs through the all unit cells and by product sign we mean tensor product of the local unit cell wave-functions. The singlet state in the unit cell corresponds to $t > 0$ while triplet state to $t < 0$. Obviously, unit cell wavefunctions are not entangled at all, while within the unit cell the spins are maximally entangled.

One can easily show that $C^{zz} = \langle S^{z(a)} S^{z(b)} \rangle = -\frac{1}{4}$ for both cases $C^{xx} = \langle S^{x(a)} S^{x(b)} \rangle = \langle S^{y(a)} S^{y(b)} \rangle = \pm\frac{1}{4}$. At this point, we consider AF mode, i.e $t > 0$. When we turn on intercell coupling, i.e $t' > 0$, the singlet states becomes 'perturbed'. In Fig. (4.7) , we plotted the correlation function of x -component of spins for given above parameters. As we can see, in contrast to dimerized limit,

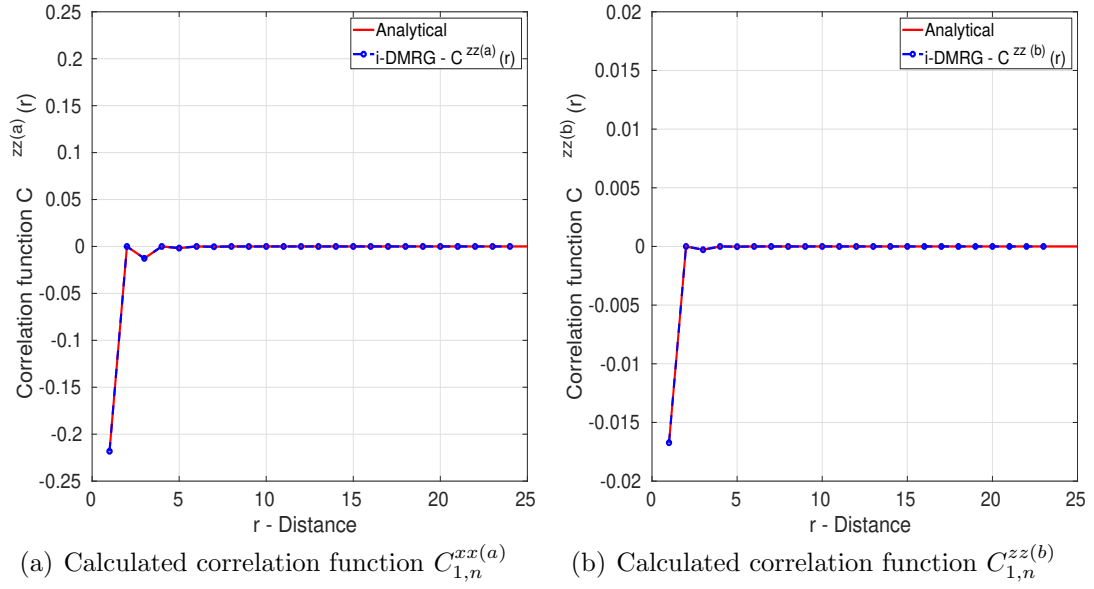


Figure 4.8: Comparison of analytical and numerical i-DMRG results of $C_{1,n}^{zz(a,b)}$

$C^{xx(a)} \neq -\frac{1}{4}$. The value of $C^{xx(a)}$ with the nearest neighbor (with the spin on the same unit cell) decreases with the increment of t' , however the $C^{xx(a)}$ with other spins become non-zero, and starts oscillate with a distance. Also the second spin in the unit cell starts to interact with the next spins, i.e $C^{xx(b)} \neq 0$ for any $t' \neq 0$. Because the system is 'insulator', the modulus of amplitude exponentially decrease and one can extract easily correlation length if needed. When $t = t'$, the system becomes spin liquid and all correlation functions, including C^{xx} , decay by power law.

In the similar form behaves $C^{zz(a)}$ and $C^{zz(b)}$. Obviously, for even distances $C^{zz} = 0$ and exponentially decreases with every next odd distance.

In Fig.(4.10 (a)) we have plot $C^{xx(a)}$ for all $\frac{t}{t'}$ values. For $\frac{t}{t'} \ll 0 (t < 0)$ we have triplet with total spin $S = 1$. Thus, all spins within the unit cell are coupled purely ferromagnetically with $C^{xx(a)} = \frac{1}{2}$, as described before. This means that correlation function $C^{(a)xx}$ within the unit cell is positive and exponentially decreases with a distance. When t' starts to compete with t , correlation length increases. It should be noted that correlation with next unit cell spins $C^{(a)xx} < 0$, since unit cells are coupled antiferromagnetically with each other. This explains the 'block' like behavior of $C^{(a)xx}$ for $t < 0$.

For $\frac{t}{t'} \gg 0$, within the unit cell $C^{xx(a)} \approx -\frac{1}{4}$ and decreases exponentially with a distance. In competing region, $t \approx t'$, we have quite noticeable interaction with spins in another unit cells. Since we have antiferromagnetic coupling with all spins, we have oscillating behavior for $C^{(a)xx}$ with the corresponding sign change.

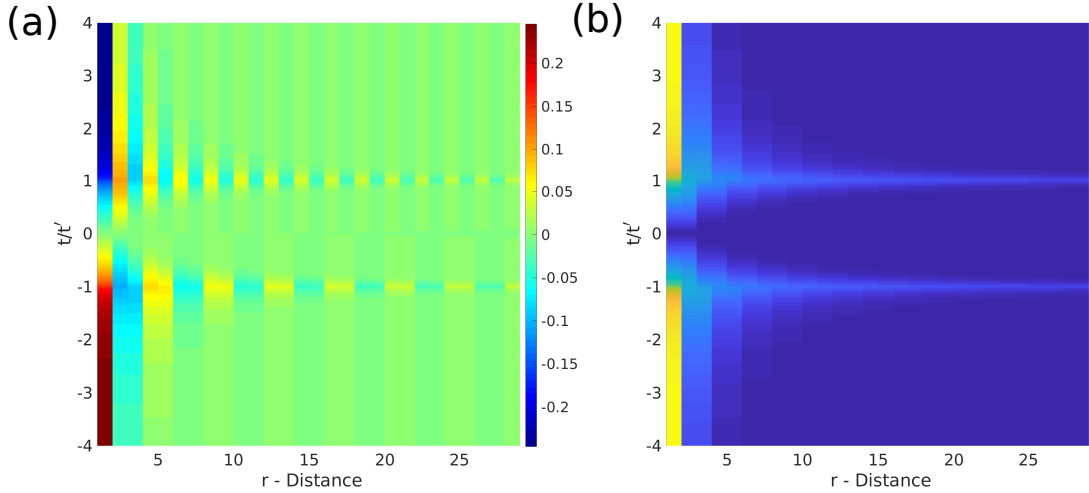


Figure 4.9: The behavior of $C^{xx(a)}$ (a) and its absolute value (b) for all $\frac{t}{t'}$ range

For the case $|\frac{t}{t'}| \approx 1$ we have power-law decrease of correlation function C^{xx} . In fact, C^{zz} also has the same behavior. This can be seen clearly in Fig. (4.9 (b)). The power-law decrease of correlation functions that there is quasi-long-range order, not pure long-range order. This is because, in 1D, any order is destroyed by quantum fluctuations. Furthermore, as we know from the previous Chapter, the t/t' points in which power-law is observed, corresponds to a gap closure in the system. In fact, this gap closure corresponds to the topological phase transition as we will see in the next chapter.

Summary, conducted research in the current chapter gives an intuitive understanding of the system. In the next chapter, we are going to study the properties of the Haldane phase of the current model.

Chapter 5

Haldane phase in the BAHC

We start this chapter by studying topological quantum phase transition in our bond-alternating fermionic chain in the non-interacting limit. Firstly, we calculate the topological winding number, which is a standard order parameter for 1D exactly solvable fermionic chains. Secondly, we will show that it is possible to use string order parameter to identify topological phases in the model under consideration. Using MPS-DMRG numerically we show emerging edge states and doubly degenerate character of entanglement spectrum in Haldane phase of the model.

In the second part of the chapter, by the use of MPS-DMRG, we determine Haldane phase boundary for non-zero z -component anisotropy Δ values in anti-ferromagnetic XXZ model (1.1).

5.1 Winding number

To identify the topological phase, namely Haldane phase in our spin model (in XX limit), by calculating winding number of corresponding non-interacting fermionic chain (4.55). One can use the integral form to calculate the winding number, but we will show graphically as in Ref. [39]. To do this, redefining Fourier transform

for unit cell, we rewrite our Hamiltonian (in the absence of magnetic field B) in the following form:

$$H_K = \begin{bmatrix} a_k^\dagger & b_k^\dagger \end{bmatrix} \begin{bmatrix} 0 & (e^{-ik}t' + t) \\ (t'e^{ik} + t) & 0 \end{bmatrix} \begin{bmatrix} a_k \\ b_k \end{bmatrix} \quad (5.1)$$

We rewrite kernel $h(k)$ as:

$$h(k) = h_x(k)\sigma_x + h_y(k)\sigma_y \quad (5.2)$$

where

$$h_x(k) = t + t'\cos(k) \quad (5.3)$$

and

$$h_y(k) = t'\sin(k) \quad (5.4)$$

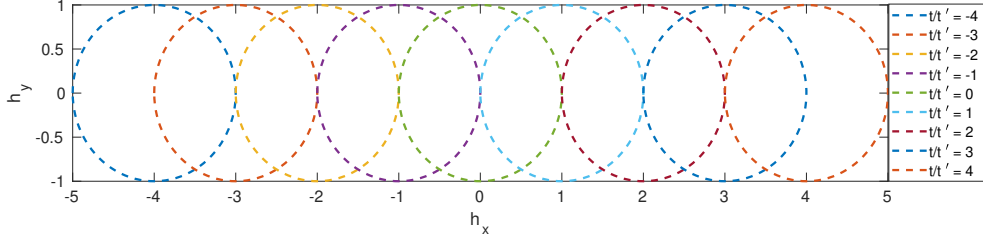


Figure 5.1: Graphical representation of winding number

To calculate the winding number, one needs to plot $h_x(k)$ vs $h_y(k)$ and see how many times it crosses the origin of the plane. This is a procedure which was done in [39] for SSH model. Our model has the only difference which is the sign of hopping parameters t and t' . As one can see from the figure above, when parameter $\frac{t}{t'} \in [-4 : 4]$ is changed, the circle may consist origin of coordinate system on it or may not. In the region $|\frac{t}{t'}| > 1$ the circle doesn't consist zero point ($\nu = 0$), while for $|\frac{t}{t'}| < 1$ the point inside the circle, thus winding number is unity ($\nu = 1$). In QPT point, $|\frac{t}{t'}| = 1$, the winding number is not defined and the point lies on the circle line.

Thus, one can come to the conclusion that for $|\frac{t}{t'}| < 1$ we have topological insulator (which is Haldane phase in corresponding spin chain) and for $|\frac{t}{t'}| > 1$ we have trivial insulator.

5.2 String order parameter

In this part, we will calculate the string order parameter for our fermionic model. As mentioned in Chapter 1, it has been used as a topological order parameter for spin systems. Here we convert it into a fermionic version by the use of JWT. String order parameter for our model can be defined as [10]:

$$O^S = O^z(|n - m| \rightarrow \infty) \Rightarrow O_{m,n}^z = -4 \left\langle S_m^{z(b)} e^{i\pi(S_{m+1}^{z(a)} + S_{m+2}^{z(b)} + \dots + S_{n-1}^{z(b)})} S_n^{z(a)} \right\rangle \quad (5.5)$$

Here, prefactor -4 is used to normalize, so that in the dimerized topological limit $t/t' = 0$ it brings $O_{m,n}^z = 1$. Using $e^{i\pi S^z} = \frac{S^z}{2i}$ Eq. (5.5) can be written as:

$$O_{m,n}^z = \left\langle e^{i\pi(S_m^{z(b)} + S_{m+1}^{z(a)} + S_{m+2}^{z(b)} + \dots + S_{n-1}^{z(b)} S_n^{z(a)})} \right\rangle \quad (5.6)$$

By the use of JWT, we convert string order parameter for spins to fermionic string order parameter:

$$O_{m,n}^z = \left\langle e^{i\pi(b_m^\dagger b_m + a_{m+1}^\dagger a_{m+1} + \dots + a_n^\dagger a_n)} \right\rangle \quad (5.7)$$

which is obtained using the fact that the number of operators in exponent always even. Using Eq.(4.82) it can be converted to a product of $A - B - C - D$ operators defined in (4.83-4.86):

$$O_{m,n}^z = \langle D_m C_m B_{m+1} A_{m+1} \dots D_{n-1} C_{n-1} B_n A_n \rangle \quad (5.8)$$

Using Wick theorem, following the path from the previous chapter and including only non-zero contractions, we get the following result:

$$O^S = O^z(|m - n| \rightarrow \infty) \Rightarrow O_{1,n}^z = \det(K_{n-1 \times n-1}) \quad (5.9)$$

where by site $m = 1$ we mean any chosen b site as reference and n any chosen site a which follows b . Matrix elements $K_{m,n}$ are defined as:

$$K_{m,n} = \frac{1}{2\pi} \int_0^{2\pi} \frac{e^{-ik(n-m)}(e^{-2ikt} + t')}{\sqrt{t^2 + t'^2 + 2tt' \cos(2k)}} dk \quad (5.10)$$

Interestingly, matrix K is a Toeplitz matrix, i.e any chosen diagonal has the constant value. Even if attempts to find an approximate value of their determinant

in large $n \rightarrow \infty$ limit were done long time ago [40], their properties were well studied after their application on statistical mechanics [41, 38, 42].

Generating function $g(k)$ of our Toeplitz matrix is defined as:

$$g(k) = \frac{(e^{-2ik}t + t')}{\sqrt{t^2 + t'^2 + 2tt' \cos(2k)}} \quad (5.11)$$

Finally, string order parameter can be evaluated as the determinant of the Toeplitz matrix in the large distance limit,

$$O^S = \lim_{n \rightarrow \infty} \det(K_{n-1 \times n-1}) \quad (5.12)$$

Szegő theorem to evaluate String order parameter

To find the value of convergence in big distance limit O^S , we will use Szegő theorem [40]. Exact formulation of it can be found in Appendix A.

To apply Szegő theorem, a generating function shouldn't have any zeros in interval $[0 : 2\pi)$ and should be smooth. The generating function (5.11) doesn't have any zeros for any $|\frac{t}{t'}| < 1$, i.e in topological phase. Thus, we can use the theorem only in this limit. In trivial insulator phase, $O^S = 0$ and one can use the Fisher-Hartwig [42] conjecture to show this.

The edge limit is to set $t = 0$, i.e $|\frac{t}{t'}| = 0$. In this case, generating function $g(k) = 1$. When intracell hopping t is turned on, the $g(k)$ starts oscillating around 1, finally transforming to $g(k) = |\cos(k)|$ at $\frac{t}{t'} = 1$ and $g(k) = |\sin(k)|$ at $\frac{t}{t'} = -1$. Thus, Szegő theorem is not applicable in these critical points.

The logarithm of the generating function $V(k) = \ln(g(k))$ in the topological dimerized limit $|\frac{t}{t'}| = 0$ is obviously vanishes. Thus, all Fourier coefficients also vanish. Therefore,

$$O^S = E e^{LV_0} = 1, L \rightarrow \infty \quad (5.13)$$

where

$$E = e^{\sum_{r=1}^{\infty} V_r V_{-r}} \quad (5.14)$$

and V_r are the Fourier coefficients of our $V(k)$ function. In non-zero intracell hopping term t , imaginary part of $V(k)$ is non-zero with a period of $T = 2\pi$.

Thus, still zeroth Fourier coefficient is $V_0 = 0$:

$$V_0 = \frac{1}{2\pi} \int_0^{2\pi} V(k) dk = 0 \quad (5.15)$$

From this equation, one can see that in expression (5.13) even if E is finite, $e^{V_0 L} = 1$. Thus, we come to the conclusion that string order parameter O^S doesn't have exponential decay behavior, but has a finite value depending on the Fourier coefficients of $V(k)$.

Keeping $|\frac{t}{t'}|^2 \approx 0$ and expanding the denominator leads to the following $g(k)$:

$$g(k) \approx 1 - i \frac{t}{t'} \sin(2k); \quad (5.16)$$

and $V(k)$:

$$V(k) \approx \ln(1 - i \frac{t}{t'} \sin(2k)) \approx -i \frac{t}{t'} \sin(2k) \quad (5.17)$$

Thus, the Fourier coefficients can be written as:

$$V_r = \frac{-it}{2\pi t'} \int_0^{2\pi} e^{-ikr} \sin(2k) = \frac{-t\delta_{r,2}}{2t'} \quad (5.18)$$

Finally, we can write string order parameter in the mentioned limit as:

$$O^S \approx e^{-\frac{t^2}{4t'^2}}; \left| \frac{t}{t'} \right|^2 \approx 0 \quad (5.19)$$

In conclusion, we have seen that in the fully dimerized topological limit, string order parameter is unity, and when intracell hopping t is turned on, O^S starts to decrease. In Fig. (5.2) above string order parameter O^S calculated using Szegő theorem (circle markers) and also numerically estimated Toeplitz determinants (solid lines) are shown. As one can see, the values of determinants converge to the value predicted with the Szegő theorem, except points around QPT, in which zeros of $g(k)$ starts to appear. In Fig. (5.2. b) we show our calculation of $O^S(\frac{t}{t'})$ using i-DMRG and numerically estimated Toeplitz determinants. For i-DMRG calculations, we used the bond dimensions of MPS $\chi = 12$ and $L = 200$. The chain is taken sufficiently long since near QPT point $O_{m,n}$ decreases by a power law.

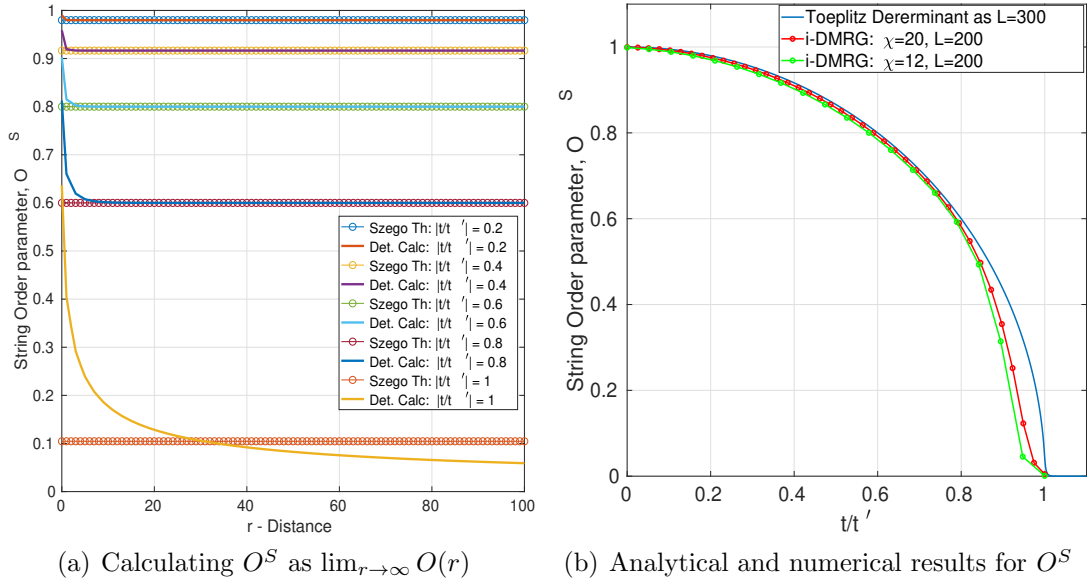


Figure 5.2: Calculation of string order parameter

String order parameter in trivial insulating phase Analytically, as it was mentioned before, in trivial insulating phase, i.e. $|\frac{t}{t'}| > 1$ our $g(k)$ will have zeros, thus Szegő theorem is not applicable. In any case, we can numerically evaluate the Toeplitz determinant in this limit also.

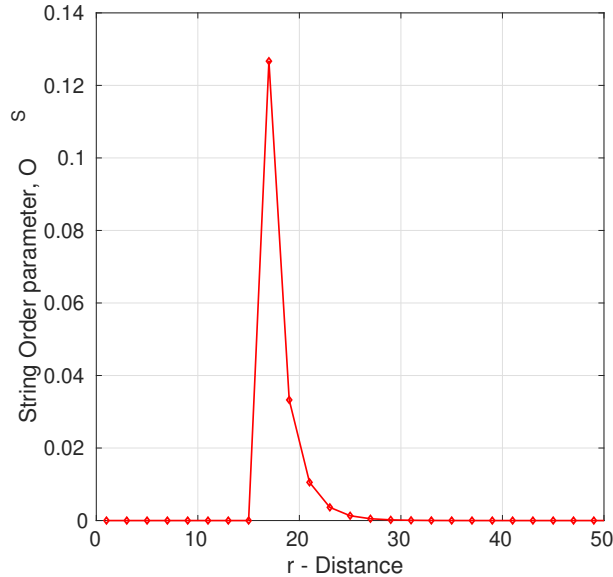


Figure 5.3: O^S in the trivial insulating phase $t/t' = 1.5$

In Fig. (5.3) i-DMRG results' plot of $O_{m,n}$ is shown for $\frac{t}{t'} = 1.5$. As one notices, $O_{m,n}$ decreases exponentially. Thus, $O_S = 0$.

Finally, we present phase diagram of our model based on O^S as a function $\frac{t}{t'}$.

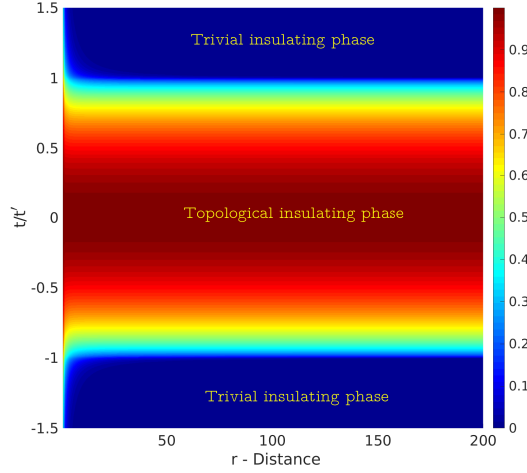


Figure 5.4: O^S based phase diagram of non-interacting model

5.3 Edge states as an order parameter

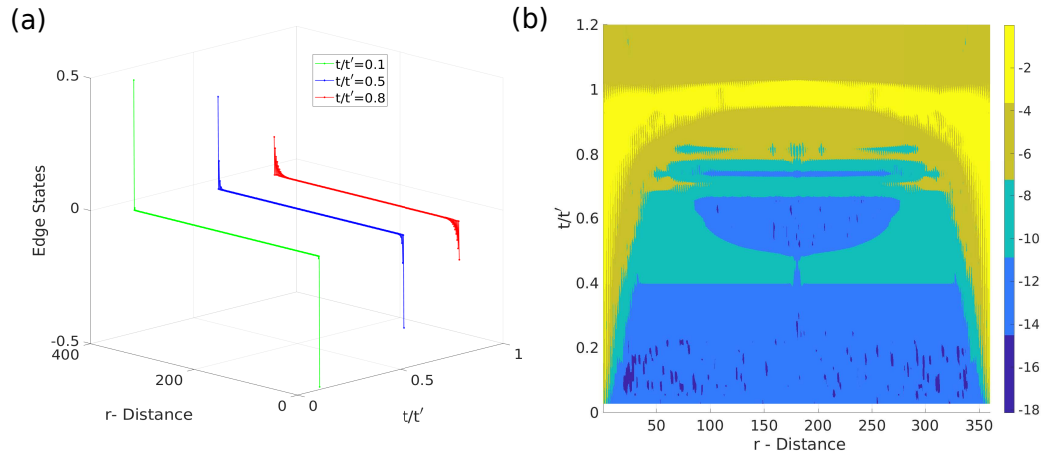


Figure 5.5: Topological Edge states in the Haldane phase

As it was mentioned in Chapter 1, edge states are one of the most important characteristics of topological phases. In this section, using i-DMRG we will show the existence of edge states in the topological phase of the model under consideration. We used $N = 200$, $\chi = 15$ and calculated S^z for every site. Since the fermionic model is half-filled, a local magnetization of the corresponding spin chain should be $m_i^z = \langle S_i^z \rangle = 0$.

However, in the topological phase at the edges of the chain fluctuations of S^z can be observed. In the language of fermions, it means the occupation number of fermions in the edge sites are not half-filled ($n \neq \frac{1}{2}$).

In Fig. 5.5 (a) we presented local magnetization m_i^z in Haldane phase for different values of t/t' . One can see that in the fully dimerized Haldane limit ($t/t' = 0$) we have free edge spins with $m_{1,N}^z = \pm \frac{1}{2}$. When an intracell hopping t is turned on, the m^z oscillates at the edges. One can notice that $m_{1,N}^z$ decreases also, with the increment of t/t' . In fact, this behavior conserved up to the QPT point $t/t' = 1$. In Fig.5.5 (b) the logarithm of the local magnetization is shown. For convenience, we redefined $\tilde{m}^z = 2m^z$, so that at the maximum edge state amplitude $m^z = \frac{1}{2}$ it becomes $\tilde{m}^z = 1$.

5.4 Entanglement spectrum as an order parameter

As it was mentioned in Chapter 1, entanglement spectrum in the gapped symmetry - protected topological phase is doubly degenerate, when in trivial phase it is not. In this section, we calculate a bipartite entanglement spectrum for a chain of $N = 400$ with the bond dimension $\chi = 20$ for $t/t' \in [0 : 1]$. Doubly degenerate behavior of all spectrum values can be observed in Fig.5.6 (a) for all $t/t' < 1$, while around QPT point the degeneracy is lifted and for trivial phase we don't have doubly degenerate behavior.

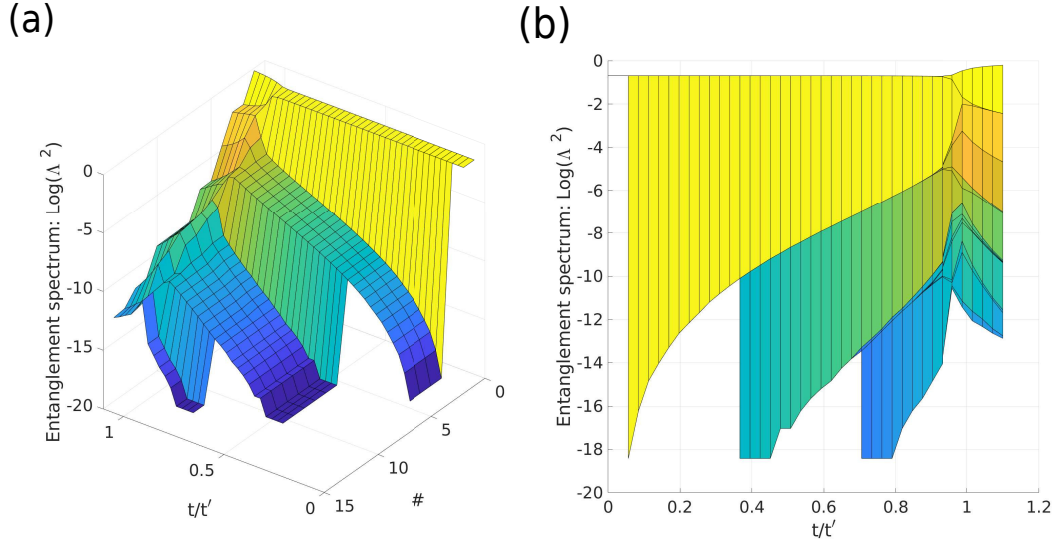


Figure 5.6: Entanglement Spectrum in the XX limit

5.5 When does the order parameters work?

When Hamiltonian has additional terms like an interacting part of Eq.(4.41) or terms like Dzyaloshinskiy - Moriya interaction, not all the order parameters mentioned previously are able to identify the Haldane phase. The winding number is a very general tool to identify non-trivial phases, however, the usage is limited due to the fact that not all Hamiltonians are exactly solvable. The string order parameter is able to identify the Haldane phase, which is protected by D_2 symmetry, while it cannot identify when it is protected by other symmetries [43]. In contrast, the degeneracy of the entanglement spectrum which is discussed above can be applied to identify the Haldane phase for a general Hamiltonian. Thus we can further use it as an order parameter for our interacting model.

5.6 Haldane phase of bond-alternating XXZ model

In this section, we use MPS-DMRG to identify the Haldane phase in our general bond-alternating XXZ model (1.1) $H = H_1 + H_2$:

$$H_1 = J \sum_{i=1}^N (\Delta S_{2i-1}^z S_{2i}^z + S_{2i-1}^x S_{2i}^x + S_{2i-1}^y S_{2i}^y) \quad (5.20)$$

$$H_2 = J' \sum_{i=1}^N (\Delta' S_{2i}^z S_{2i+1}^z + S_{2i}^x S_{2i+1}^x + S_{2i}^y S_{2i+1}^y) \quad (5.21)$$

In this study, we set $\Delta = \Delta'$, so that the anisotropy fraction is the same. We set also $J' = 1$. Our model parameters were: $N = 360$, $\chi = 20$. We varied the z -component anisotropy Δ and found in which value of Δ Haldane phase \rightarrow Neel phase transition occurs for every value of J/J' .

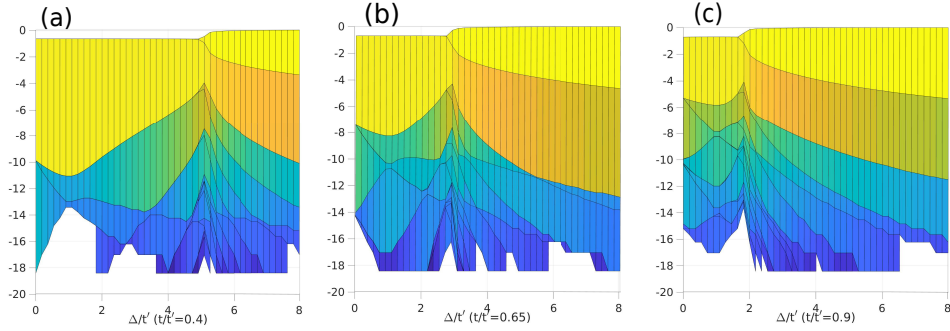


Figure 5.7: Entanglement spectrum character for XXZ model

From Fig. (5.7 (a) - (c)) one can see evolution of the entanglement spectrum character for the values $J/J' = 0.4, 0.65, 0.9$, when z -component anisotropy Δ is varied. It is clear that, for small values of J/J' one needs relatively big values of Δ . For $J/J' = 0.4$, the Haldane phase \rightarrow Neel phase transition occurs at $\Delta \approx 4.8$, while for $J/J' = 0.9$ this transition occurs at $\Delta \approx 1.63$. Clearly, in the pure XXZ limit (i.e $J/J' = 1$), Neel order is reached for $\Delta \approx 1$.

While the degeneracy of the entanglement spectrum predicts the phase transi-

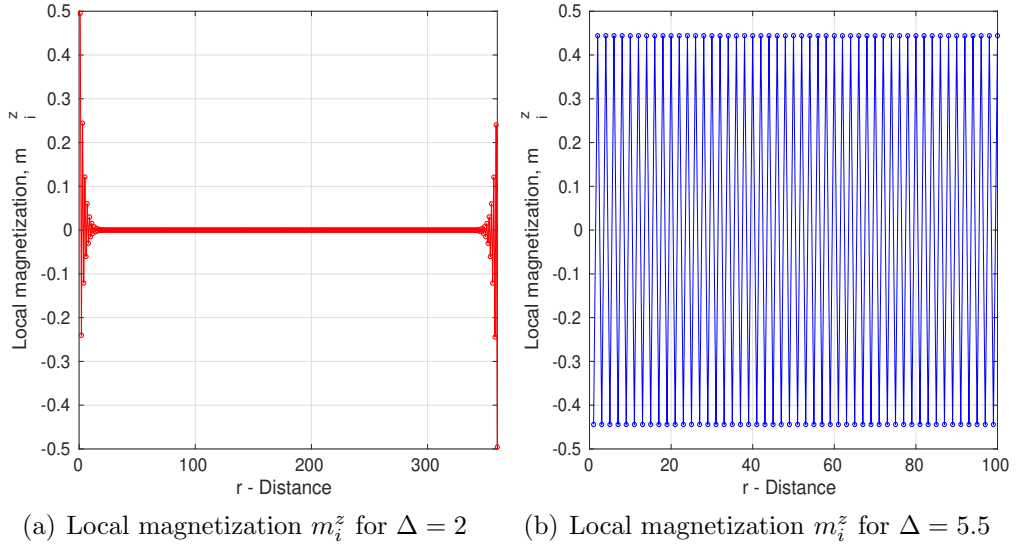


Figure 5.8: Local magnetization in two different phases of the model

tion points accurately, it doesn't tell anything about the nature of the transition. To confirm the phase transition to be from the Haldane phase to the Neel phase, we calculated local magnetization and plotted in Fig. (5.7) for $J/J' = 0.4$ with $\Delta = 2$ and $\Delta = 5.5$. As one can see for $\Delta = 2$ one has a net bulk magnetization of $\langle M^z \rangle = 0$, while at the edges we have localized topological states. However, for $\Delta = 5.5$, we have Neel-ordered phase, as it is shown in Fig. (5.7 (b)).

Finally, we present the phase diagram for bond-alternating XXZ model. It should be mentioned, that for $J/J' > 1$, one has gapped spin chain and the phase diagram looks like exactly the same as Fig. (5.8) when it is drawn for J'/J .

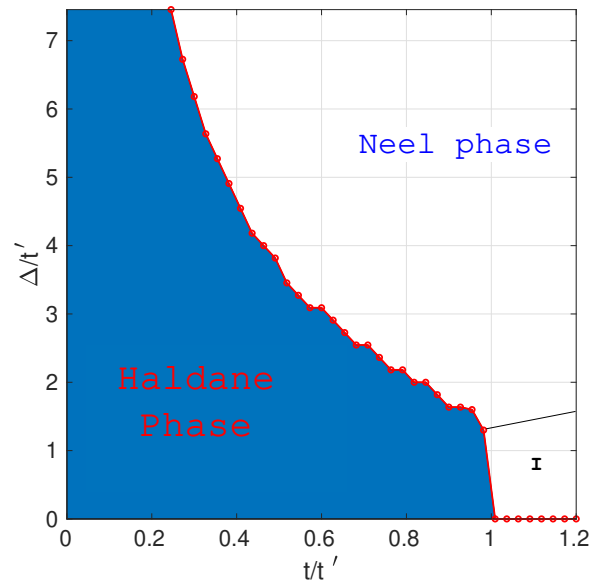


Figure 5.9: Phase diagram of bond-alternating XXZ model

Chapter 6

Conclusions

In this thesis, we have studied the bond-alternating XXZ model (1.1) analytically and numerically. All considered problems are solved. Namely,

- I. By the use of the JWT we studied zero-temperature properties of the model (1.1) in XX limit.
- (a) Quantum phase transition of the XX model (1.1) is studied under the magnetic field.
- (b) Zero-temperature static correlation functions for bond-alternating XX chain analytically derived and numerically checked.
- II (a) Trivial insulating \rightarrow topological phase transition is studied using fermionization of String order parameter in the XX limit.
- (b) Topological QPT Haldane phase \rightarrow Neel phase is numerically studied by using MPS-DMRG

For further perspectives we propose the following tasks:

- By the use of bosonization treat interacting fermionic models exactly.

Bibliography

- [1] X. Chen, Z.-C. Gu, Z.-X. Liu, and X.-G. Wen, “Symmetry-protected topological orders in interacting bosonic systems,” *Science*, vol. 338, no. 6114, pp. 1604–1606, 2012.
- [2] X.-G. Wen, “Symmetry-protected topological phases in noninteracting fermion systems,” *Physical Review B*, vol. 85, no. 8, p. 085103, 2012.
- [3] Z.-C. Gu and X.-G. Wen, “Symmetry-protected topological orders for interacting fermions: Fermionic topological nonlinear σ models and a special group supercohomology theory,” *Physical Review B*, vol. 90, no. 11, p. 115141, 2014.
- [4] F. D. M. Haldane, “Continuum dynamics of the 1-d heisenberg antiferromagnet: Identification with the $o(3)$ nonlinear sigma model,” *Physics Letters A*, vol. 93, no. 9, pp. 464–468, 1983.
- [5] F. D. M. Haldane, “Nonlinear field theory of large-spin heisenberg antiferromagnets: semiclassically quantized solitons of the one-dimensional easy-axis n el state,” *Physical Review Letters*, vol. 50, no. 15, p. 1153, 1983.
- [6] I. Affleck, T. Kennedy, E. H. Lieb, and H. Tasaki, “Valence bond ground states in isotropic quantum antiferromagnets,” in *Condensed matter physics and exactly soluble models*, pp. 253–304, Springer, 1988.
- [7] F. Pollmann, E. Berg, A. M. Turner, and M. Oshikawa, “Symmetry protection of topological phases in one-dimensional quantum spin systems,” *Physical review b*, vol. 85, no. 7, p. 075125, 2012.

- [8] K. Hida, “Haldane gap in the spin-1/2 double chain heisenberg antiferromagnet-numerical diagonalization and projector monte carlo study,” *Journal of the Physical Society of Japan*, vol. 60, no. 4, pp. 1347–1354, 1991.
- [9] T. Kennedy, “Exact diagonalisations of open spin-1 chains,” *Journal of Physics: Condensed Matter*, vol. 2, no. 26, p. 5737, 1990.
- [10] K. Hida, “Crossover between the haldane-gap phase and the dimer phase in the spin-1/2 alternating heisenberg chain,” *Physical Review B*, vol. 45, no. 5, p. 2207, 1992.
- [11] K. Hida, “Ground-state phase diagram of the spin-1/2 ferromagnetic-antiferromagnetic alternating heisenberg chain with anisotropy,” *Physical Review B*, vol. 46, no. 13, p. 8268, 1992.
- [12] T. Hirano, H. Katsura, and Y. Hatsugai, “Topological classification of gapped spin chains: Quantized berry phase as a local order parameter,” *Physical review B*, vol. 77, no. 9, p. 094431, 2008.
- [13] I. Maruyama, T. Hirano, and Y. Hatsugai, “Topological identification of a spin-1 2 two-leg ladder with four-spin ring exchange,” *Physical review B*, vol. 79, no. 11, p. 115107, 2009.
- [14] F. Anfuso and A. Rosch, “String order and adiabatic continuity of haldane chains and band insulators,” *Physical Review B*, vol. 75, no. 14, p. 144420, 2007.
- [15] F. Pollmann, A. M. Turner, E. Berg, and M. Oshikawa, “Entanglement spectrum of a topological phase in one dimension,” *Physical review b*, vol. 81, no. 6, p. 064439, 2010.
- [16] W. L. Buyers, R. Morra, R. Armstrong, M. Hogan, P. Gerlach, Hirakawa, and K, “Experimental evidence for the haldane gap in a spin-1 nearly isotropic, antiferromagnetic chain,” *Physical review letters*, vol. 56, no. 4, p. 371, 1986.

- [17] J. Renard, M. Verdaguer, L. Regnault, W. Erkelens, J. Rossat-Mignod, and W. Stirling, “Presumption for a quantum energy gap in the quasi-one-dimensional $s=1$ heisenberg antiferromagnet $\text{Ni}(\text{C}_2\text{H}_8\text{N}_2)_2\text{NO}_2(\text{ClO}_4)$,” *EPL (Europhysics Letters)*, vol. 3, no. 8, p. 945, 1987.
- [18] G. Xu, J. DiTusa, T. Ito, K. Oka, H. Takagi, C. Broholm, and G. Aeppli, “ Y_2BaNiO_5 : A nearly ideal realization of the $s=1$ heisenberg chain with antiferromagnetic interactions,” *Physical Review B*, vol. 54, no. 10, p. R6827, 1996.
- [19] K. Kodama, H. Harashina, H. Sasaki, M. Kato, M. Sato, K. Kakurai, and M. Nishi, “Neutron scattering study on the quasi-one-dimensional spin-gap system CuNb_2O_6 ,” *Journal of the Physical Society of Japan*, vol. 68, no. 1, pp. 237–241, 1999.
- [20] H. Manaka, I. Yamada, Z. Honda, H. Aruga Katori, and K. Katsumata, “Field-induced magnetic long-range order in the ferromagnetic-antiferromagnetic alternating heisenberg chain system $(\text{CH}_3)_2\text{CHNH}_3\text{CuCl}_3$ observed by specific heat measurements,” *Journal of the Physical Society of Japan*, vol. 67, no. 11, pp. 3913–3917, 1998.
- [21] H. Yamaguchi, Y. Shinpuku, T. Shimokawa, K. Iwase, T. Ono, Y. Kono, S. Kittaka, T. Sakakibara, and Y. Hosokoshi, “ $S=1/2$ ferromagnetic-antiferromagnetic alternating heisenberg chain in a zinc-verdazyl complex,” *Physical Review B*, vol. 91, no. 8, p. 085117, 2015.
- [22] H. Bethe, “H. bethe, z. phys. 71, 205 (1931).,” *Z. phys.*, vol. 71, p. 205, 1931.
- [23] M. den Nijs and K. Rommelse, “Preroughening transitions in crystal surfaces and valence-bond phases in quantum spin chains,” *Physical Review B*, vol. 40, no. 7, p. 4709, 1989.
- [24] C. K. Majumdar and D. K. Ghosh, “On next-nearest-neighbor interaction in linear chain. i,” *Journal of Mathematical Physics*, vol. 10, no. 8, pp. 1388–1398, 1969.

- [25] M. Oshikawa, “Hidden $z_2^* z_2$ symmetry in quantum spin chains with arbitrary integer spin,” *Journal of Physics: Condensed Matter*, vol. 4, no. 36, p. 7469, 1992.
- [26] R. Haghshenas, A. Langari, and A. Reza khani, “Symmetry fractionalization: symmetry-protected topological phases of the bond-alternating spin-1/2 heisenberg chain,” *Journal of Physics: Condensed Matter*, vol. 26, no. 45, p. 456001, 2014.
- [27] H. Krishna-Murthy, J. Wilkins, and K. Wilson, “Renormalization-group approach to the anderson model of dilute magnetic alloys. i. static properties for the symmetric case,” *Physical Review B*, vol. 21, no. 3, p. 1003, 1980.
- [28] S. R. White, “Density matrix formulation for quantum renormalization groups,” *Physical review letters*, vol. 69, no. 19, p. 2863, 1992.
- [29] S. R. White, “Density-matrix algorithms for quantum renormalization groups,” *Physical Review B*, vol. 48, no. 14, p. 10345, 1993.
- [30] U. Schollwöck, “The density-matrix renormalization group in the age of matrix product states,” *Annals of Physics*, vol. 326, no. 1, pp. 96–192, 2011.
- [31] G. M. Crosswhite, A. C. Doherty, and G. Vidal, “Applying matrix product operators to model systems with long-range interactions,” *Physical Review B*, vol. 78, no. 3, p. 035116, 2008.
- [32] M. Shiroishi and M. Takahashi, “Exact calculation of correlation functions for spin-1/2 heisenberg chain,” *Journal of the Physical Society of Japan*, vol. 74, no. Suppl, pp. 47–52, 2005.
- [33] H.-J. Mikeska and A. K. Kolezhuk, “One-dimensional magnetism,” in *Quantum magnetism*, pp. 1–83, Springer, 2004.
- [34] H. Primakoff and T. Holstein, “Many-body interactions in atomic and nuclear systems,” *Physical Review*, vol. 55, no. 12, p. 1218, 1939.
- [35] P. Jordan and E. P. Wigner, “About the pauli exclusion principle,” *Z. Phys.*, vol. 47, pp. 631–651, 1928.

- [36] W.-P. Su, J. Schrieffer, and A. Heeger, “Soliton excitations in polyacetylene,” *Physical Review B*, vol. 22, no. 4, p. 2099, 1980.
- [37] E. Lieb, T. Schultz, and D. Mattis, “Two soluble models of an antiferromagnetic chain,” *Annals of Physics*, vol. 16, no. 3, pp. 407–466, 1961.
- [38] B. M. McCoy and T. T. Wu, “Theory of toeplitz determinants and the spin correlations of the two-dimensional ising model. iv,” *Physical Review*, vol. 162, no. 2, p. 436, 1967.
- [39] J. K. Asbóth, L. Oroszlány, and A. Pályi, “The su-schrieffer-heeger (ssh) model,” in *A Short Course on Topological Insulators*, pp. 1–22, Springer, 2016.
- [40] G. Szegő, “Ein grenzwertsatz über die toeplitzschen determinanten einer reellen positiven funktion,” *Mathematische Annalen*, vol. 76, no. 4, pp. 490–503, 1915.
- [41] H. Widom, “Toeplitz determinants with singular generating functions,” *American Journal of Mathematics*, vol. 95, no. 2, pp. 333–383, 1973.
- [42] M. E. Fisher and R. E. Hartwig, “Toeplitz determinants: some applications, theorems, and conjectures,” *Advances in Chemical Physics: Stochastic processes in chemical physics*, pp. 333–353, 1969.
- [43] F. Pollmann, A. M. Turner, E. Berg, and M. Oshikawa, “Entanglement spectrum of a topological phase in one dimension,” *Physical review b*, vol. 81, no. 6, p. 064439, 2010.

Appendix A

Szegö theorem

Suppose that the generation function $\phi(\theta)$ satisfies the conditions,

- $\phi(\theta) \neq 0$ for all $\theta \in [0; 2\pi)$
- $\sum_{k=-\infty}^{k=\infty} |V_k| + \sum_{k=-\infty}^{k=\infty} |k||V_k|^2 < \infty$, where V_k are Fourier coefficients of the following function:

$$V(\theta) = \ln(\phi(\theta)); \tag{A.1}$$

Then, in the limit $L \rightarrow \infty$, the determinant of Toeplitz matrix with the generating function $\phi(\theta)$

$$D[\phi] = E_{SZ} e^{V_0 L} \tag{A.2}$$

where

$$E_{SZ} = e^{\sum_{k=1}^{k=\infty} k V_k V_{-k}} \tag{A.3}$$